MEASURING THE FRACTURE ENERGY OF BED BREAKAGE USING A SHORT IMPACT LOAD CELL

By

Thobile Thenjiwe Dube

Thesis submitted to the Faculty of Engineering and the Built Environment, University of Cape Town, in fulfilment of the requirements for the degree of Master of Science in Engineering

June 2017

DECLARATION

1. I know the meaning of plagiarism and declare that all the work in the document, save for that which is properly acknowledged, is my own. This thesis/dissertation has been submitted to the Turnitin module (or equivalent similarity and originality checking software) and I confirm that my supervisor has seen my report and any concerns revealed by such have been resolved with my supervisor.

2. I have used the Harvard-UCT 2015 convention for citation and referencing. Each contribution to, and quotation in, this report from the works of other people has been attributed, and has been cited and referenced.

Signature 

Date_____17__June 2017_____

ACKNOWLEDGEMENTS

First I would like to thank God, my first hero, for His abundant grace and mercy throughout the duration of my studies. Thank you for moving mountains for me Daddy.

A huge thank you goes to Dr Lawrence Bbosa for the supervision and guidance that led to the completion of this work. I cannot thank you enough for your patience, time and intense coaching; I wouldn't have made it without your assistance.

Thank you to UCT Centre for Minerals Research (CMR) for the funding that made it possible for me to complete this work.

To Mr Kenneth Maseko, Mr Monde Bekaphi and Mr Gilmour Zimri of the UCT CMR, I really appreciate the laboratory assistance with my experimental work.

Zethu Dlamini, Lungile Khoza and Lerato Mopeli, I am so blessed to have strong, brave and intelligent women like you in my life. Thanks for the continuous motivation and for inspiring me daily through your own lives.

To my prayer warriors Sithembile Nkambule and Nanji Sheni, a million thank yous go out to you ladies. Your prayers kept me sane and enabled me to walk through fires unscathed.

Tiisetso Moimane, I cannot thank you enough for being my voice of reason, for always being a shoulder to lean on and for keeping me grounded. Thanks for all your patience and assistance and for reminding me that I am more than a conqueror.

Thokozani Malinga, the yin to my yang, my gift from God. Thanks for the laughs, the motivation and for walking through every single day of my MSc with me. Alfred Waligo, my ninja, my person, my confidant. I cannot express how much I value our friendship, thank you for the continuous support and for constantly reminding me that I too, am a ninja!

Jane Phumzile Simelane-Dube: My mum, my twin soul, my prayer warrior, my best friend. You have been the constant in my life through all the ups and downs. Thanks for loving me unconditionally, believing in me and for always giving me the best. Because of you, I know there is no greater gift than a mother's love and that there are few things more powerful than the prayers of a righteous mother. Ngiyabonga Mnguni lomuhle. I love you mum.

SYNOPSIS

Particle fracture is the elementary process that governs comminution. In industrial machines particle breakage occurs mainly through three mechanisms: impact, abrasion and attrition. Of these mechanisms, impact breakage is known to be the most basic form of particle size reduction. Comminution devices are highly inefficient, as the energy used for particle breakage relative to that consumed by the equipment is low and reported to be between 1-2 %. As such, understanding the fundamentals of particle fracture is crucial for the development of energy efficient particle size reduction methods. Research done towards investigating particle fracture under impact loading has led to the development of several devices which include the twin pendulum device, drop weight tester, Split Hopkinson Pressure Bar, Rotary Breakage Tester and the Short Impact Load Cell.

In this study the Short Impact Load Cell (SILC) was used to conduct bed breakage experiments on partially confined particles. Breakage tests using this device were conducted by vertically releasing a steel ball of known mass onto a bed of particles from a known height. The bed rested on a steel rod which was fitted with strain gauges to measure the particle response to impact loading. Tests were conducted on two ores, blue stone and UG2, to investigate the effect of three variables: steel ball mass, drop height and bed depth on the breakage behaviour of particles. The effect of each variable was investigated by evaluating the peak forces obtained, the particle fracture energy and the degree of particle breakage attained.

For both ores it was found that the peak force increased linearly with increasing steel ball mass and drop height, and it was found that the drop height had a greater effect on the peak force than the steel ball mass. The maximum peak forces were obtained at one layer of particles and increasing the bed depth generally led to a reduction in the peak force. An exponential relationship was found between the peak force and bed depth, where the peak force decreased with increasing bed depth.

It was found that the blue stone particles did not break at the range of input energies used in this work, therefore no fracture energy results were reported for blue stone. The fracture energy values for UG2 were low, where the maximum energy used for particle fracture was 2.7 % of the input energy. There was no direct correlation between the fracture energy and the steel ball mass, drop height and bed depth; however it was found that the bed depth had a larger effect on the fracture energy compared to both the steel ball mass and drop height. The greatest amount of energy used for fracture was generally obtained at the largest input energies using the 357 and 510 g balls. The optimum drop height which resulted in the highest fracture energy was generally found to be either 240 or 300 mm. A bed depth of five layers was found to be the optimum bed depth that allowed for the highest amount of energy to be utilized for breakage.

No breakage results were obtained for blue stone due to the hardness and stiffness of the ore. For UG2, tests conducted at the same bed depth showed a trend in which the breakage initially increased greatly with increasing input energy; however at larger input energies the breakage obtained approached a constant value. Although the input energy was varied by changing both the

steel ball mass and the drop height, the results showed that the degree of breakage was more dependent on the steel ball mass compared to the drop height. For all tests conducted, the maximum breakage was obtained at one layer of particles and increasing the bed depth led to a decrease in the breakage obtained. The results showed that the fracture energy and the degree of breakage were not directly related. It was found that there is an optimum amount of energy utilized for fracture that leads to the greatest breakage, where an in increase in the energy beyond the optimum point does not significantly affect the breakage obtained.

LIST OF ABBREVIATIONS AND NOMENCLATURE

SILC: Short Impact Load Cell

SHPB: Split Hopkinson Pressure Bar

RBT: Rotary Breakage Tester

UG2: Upper Group 2

PGMs: Platinum group metals

UCS: Ultimate compressive stress

DEM: Discrete Element Method

UCT: University of Cape Town

E_{cs}: Specific input energy

t_{10}: The percentage of progeny particles passing through a screen whose aperture size is $\frac{1}{10}$ of the initial mean particle size.

t_2: The percentage of progeny particles passing through a screen whose aperture size is $\frac{1}{2}$ of the initial mean particle size.

σ: Stress applied to the steel rod (N/m^2)

K: A calibration constant used to relate the measured voltage to the stress (N/Vm^2)

V: Measured voltage (V)

F: Force applied to the particle sample (N)

A_{rod}: Cross sectional area of the steel rod (m^2)

E_{strain}: Strain energy on the rod (J)

C: Pulse speed through the rod (m/s)

ρ: Density (kg/m^3)

m_{sb}: Mass of the steel ball (kg)

g: Acceleration due to gravity (m/s^2)

h_0: Initial height of the steel ball before it is released (m)

E: Young's modulus (N/m^2)

v_b: Steel ball velocity (m/s)

L: Length of the rod (m)

V_{avg}: Maximum average velocity obtained for a breakage test (V)

A: Amplifier gain

B: Bridge factor

F: Gauge factor

TABLE OF CONTENTS

LIST OF FIGURES

LIST OF TABLES

1. INTRODUCTION

1.1. Background to the research

Particle fracture is the fundamental process that governs comminution (Tavares & King, 1998). Within comminution circuits, ore particles are reduced in size through crushing and grinding operations. In industrial machines such as crushers and mills, particle breakage is known to occur through several mechanisms, namely impact, abrasion and attrition. Of the three mechanisms, impact breakage has been identified as the most basic form of particle size reduction (Schönert, 1991; Moothedath & Ahluwalia, 1992). Comminution devices are energy intensive and their efficiency, defined as the energy used for particle breakage relative to that consumed by the equipment, is low and reported to be between 1-2 % (Tromans, 2008). As such, understanding the principles behind particle fracture is essential for the development of energy efficient particle size reduction techniques.

Comminution research is mainly based on quantifying the product size distribution which results from the application of energy to a particular feed size. More specifically, particle breakage characterization aims to relate the specific input energy to the resultant product size through a type of laboratory test on a given ore (Napier-Munn et al., 1996). The results obtained from breakage characterization tests may be used to determine the hardness or strength parameters of the ore, or link the level of size reduction to the applied energy. The outcomes of breakage characterization are useful in the specification of comminution equipment, circuit design, machine modelling and process optimization (Shi et al., 2009). One of the main challenges associated with comminution studies has been quantifying the energy utilization of impact breakage.

Studies dedicated to investigating particle fracture under impact loading have led to the development of several devices used to conduct standard breakage characterization tests. These devices include the twin pendulum device, drop weight tester, Split Hopkinson Pressure Bar (SHPB), Rotary Breakage Tester (RBT) and the Short Impact Load Cell (SILC) (Napier-Munn et al., 1996; Bourgeois & Banini, 2002, Shi et al., 2009).

Of the mentioned devices, the Short Impact Load Cell is used to conduct breakage tests in this study. It is a drop weight device in which a steel ball of known mass falls vertically under gravity on an ore sample from a known height. The ore sample rests on a steel rod which is fitted with strain gauges to indirectly measure the response of the ore to impact loading. The SILC is the most suitable for this work as it can be used to conduct bed breakage experiments and to determine properties such as the ultimate strength and fracture energy of particles (Bourgeois & Banini, 2002; Tavares, 2007).

A considerable amount of experimental techniques and research exists that allows understanding of single particle response to stressing (Narayanan, 1987; Kapur et al., 1997; Tavares & King, 1998; Genc et al., 2004; Tavares, 2007). Comparatively, there is currently little research available on the bed breakage characterization of particles (Barrios et al, 2011).

Stress can be applied to a bed of particles in either confined or unconfined conditions (Tang et al., 2001) In confined conditions, the movement of particles is restricted whereas in unconfined conditions particles are free to move and get repositioned within the bed. Particles under stress in fully confined conditions have been used to investigate inter-particle breakage within the bed (Schonert, 1996 and Tang et al., 2001). However, the fully confined particle bed arrangement does not occur in comminution practice (Nguyen et al., 2002), and researchers such as Oettel & Husemann (2004) and Barrios et al (2011) have investigated the application of stress to particles in unconfined conditions. In this work the breakage behaviour of particles under partial confinement is investigated; in which particles are contained in a material that offers some resistance to their movement but allows for repositioning of the particles within the bed.

In this study two ore types are used for breakage experiments, blue stone and Upper Group 2 (UG2) chromitite ore. Blue stone is igneous rock which is commonly used as an aggregate in construction. This ore is used as a base case because it is homogenous and is expected to yield consistent breakage results (Bbosa et al., 2006). UG2 chromitite ore forms one of three layers of the South African reserves of platinum group metals (PGMs) found in the Bushveld Complex (McLaren & De Villiers, 1982). In this work UG2 is used to investigate the breakage behaviour of industrial ores. Breakage tests are conducted on particles of geometric mean size 4.73 and 4.74 mm which form a bed of a 20 mm radius. Steel balls with diameters which range from 24.5 - 50.0 mm are used to conduct experiments.

1.2. Objectives of the study

The objectives of the study are to:

- Conduct bed breakage experiments using the Short Impact Load Cell altering the three variables:
    - Steel ball mass
    - Drop height
    - Bed depth of particles

- Use SILC data to evaluate the peak forces obtained for tests conducted at each configuration of the three variables and compare the effect that changing each variable has on the peak force
- Use data collected from experiments to calculate the particle fracture energy for each configuration of the three variables and compare how altering each variable affects the particle fracture energy
- Use experimental data to evaluate the degree of particle breakage for each variable configuration and compare how changing each variable affects the breakage obtained
- Compare the degree of breakage obtained for each configuration of the variables to the particle fracture energy

1.3. Scope of the study

The study focuses on the bed breakage behaviour of partially confined fine particles. Of the three breakage mechanisms, only impact breakage is investigated as it considered to be the most elementary form of particle breakage. Thus this breakage mechanism is the most important to understand for long term gains in comminution advancements.

Due to the limited amount of research that currently exists on the bed breakage characterization of particles, investigating this area is of interest in this work. This study will also include extending the methodology which currently exists for characterizing the breakage behaviour of coarse particles to one that can be used for finer particles.

Only two ore types are used for breakage experiments. Also, the study is limited to obtaining experimental data using the SILC as this device can be used to determine the parameters of interest to this study. The effects of only three variables: steel ball mass, drop height and bed depth on the breakage behaviour of particles are investigated. The steel ball mass and drop height are of interest as they are used to vary the input energy. Bed breakage of particles is investigated as it closely resembles the conditions in industrial comminution machines.

The study investigates the effects of spherical strikers; other striker geometries such as cubes are not considered. Spherical strikers are used as they closely resemble the steel balls used for impact breakage in industrial ball mills.

1.4. Plan of development

Chapter 1- Introduction:

The background to the project, as well as the objectives and scope of the study are provided in this chapter.

Chapter 2 - Literature review:

This chapter provides a background to comminution studies, a discussion of the fundamentals of particle breakage, a review of various impact breakage devices and a discussion of the effects of various factors on the breakage behaviour of particles. The hypotheses and research questions are then given, based on the review of the literature.

Chapter 3 - Experimental programme:

This chapter presents details of the calibration done prior to conducting breakage tests on the SILC, the sample preparation done on the ores used, the experimental matrix and procedure used to conduct breakage tests, and the screening done for the determination of the particle size classes resulting from the breakage tests conducted.

Chapter 4 - Blue stone results:

In this chapter the peak force results obtained for tests conducted on blue stone are presented.

Chapter 5 - UG2 results:

The peak force, particle fracture energy and breakage results obtained for tests conducted on UG2 are presented in this chapter.

Chapter 6 - Discussion of the results obtained for blue stone and UG2

The blue stone peak force results presented in Chapter 4 are discussed, along with the peak force, particle fracture energy and breakage results presented for UG2 in Chapter 5

Chapter 7 - Conclusions and Recommendations:

In this chapter the conclusions made from the work done in this study are provided, along with recommendations for future work.

2. LITERATURE REVIEW

Overview

This chapter is a review of the literature that pertains to this study. A brief background to comminution operations is given, followed by the principles which govern particle breakage. Techniques and devices used for particle breakage characterization are reviewed and the effects of various factors on particle breakage are discussed. The hypotheses and research questions, which are based on the review of the literature done, are given at the end of the chapter.

2.1. Background to comminution operations

In comminution processes ore size is reduced in order to increase the likelihood of mineral liberation in subsequent stages of processing (Towler & Sinnott, 2013). Particle size reduction occurs through three mechanisms which depend on the magnitude of the applied stress and characteristics of the ore (Potapov & Campbell, 2001). In industrial comminution devices the main mechanisms which result in particle breakage have been identified as:

- *Impact:* Particle breakage occurs through impacting the ore with a rigid object, causing the ore particles to fracture. This mechanism of particle breakage occurs mainly through two modes: In the first mode, the ore is placed on a rigid anvil and is impacted by a rigid object, compressing the ore and leading to breakage. In the second case, the ore is launched at a rigid target, resulting in breakage (Austin, 2002).
- *Attrition:* Occurs when smaller particles become finer due to being grinded against larger particles.
- *Abrasion*: Occurs as a result of similar sized particles grinding against each other, resulting in more rounded particles. Abrasion occurs when the applied stresses are not large enough to break the particle, thus it remains intact but undergoes gradual wearing of its surface (Hogg, 1999).

In minerals processing, comminution occurs in a sequence of crushing and grinding operations. Crushing is used for initial reduction of ore size and is followed by grinding to obtain smaller particle sizes required for mineral beneficiation. Crushing is attained by compression or impact of the ore against rigid surfaces in a controlled motion path (Gupta & Suri, 1993). The various crushers available include jaw, cone, gyratory, roll and impact crushers (Darling, 2011). Grinding is accomplished through abrasion and impact of the ore by free the motion of grinding media such as balls, rods or pebbles (Kumar, 2011).

The crushing and grinding operations in comminution are estimated to consume approximately 3-4 % of the total electrical energy expended worldwide (Pokrajcic, 2008). Additionally, comminution processes are estimated to account for 40% of the total energy used and 30-50 % of the total costs in minerals processing operations (Radziszewski, 2000).

Industrial comminution processes are inefficient in their use of energy as considerably more energy is consumed by the equipment than is used for particle breakage (Tavares & King, 1998). The inefficiency of comminution devices is due to large amounts of the input energy being dissipated as heat instead of being used for particle breakage. It is estimated that grinding operations are between 1-2 % efficient and crushing efficiencies range from 3-4 %. Overall, comminution operations are approximately 1-2 % efficient (Sadrai et al., 2006).

Figure 2.1 shows an indication of how energy is typically distributed in comminution processes, and shows that approximately 99 % of the input energy is lost and is not used for particle breakage.

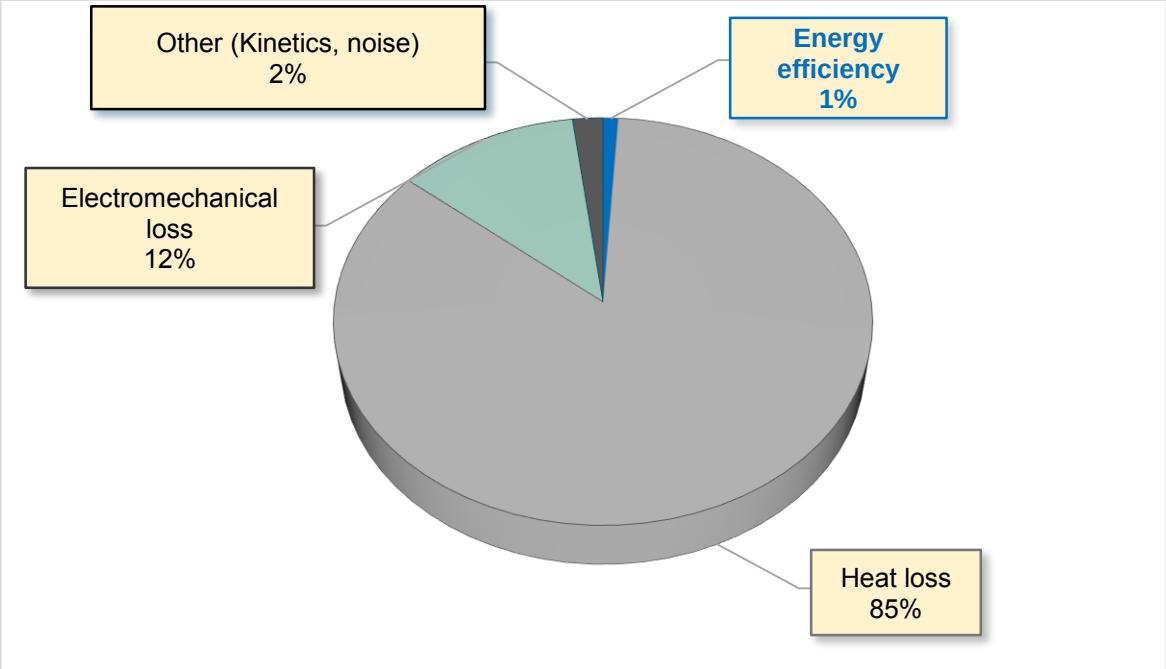

Figure 2.1: Energy distribution in comminution operations (Adapted from Sadrai et al., 2006)

From Figure 2.1 it can be seen that approximately 85 % of the input energy is lost as heat generated within the ore, 12 % is dissipated through the equipment as electromechanical losses, 2 % is lost as noise and kinetic energy and only about 1 % of the total input energy is utilized for particle breakage.

The comminution of particles by impact loading is one of the elementary mechanisms of size reduction in media mills (Kapur et al., 1997). As such, many researchers have studied the breakage of particles under impact for greater understanding of this mode of fracture in order

to improve the energy efficiency of comminution operations (King & Bourgeois, 1993; Narayanan & Whiten, 1988; Pauw & Maré, 1988; Tavares & King, 2004).

Technologies have evolved over the years in an effort to reduce power requirements and production costs. Crushers and grinding devices have increased in size and newer comminution circuits are replacing classic crushing/rod mill/ball mill operations with crushing/semi-autogenous grinding (SAG)/ball milling to enable the processing of larger tonnage rates (Darling, 2011). In some instances, plants have installed high pressure grinding rolls (HPGR)/ball mill circuits because they require less energy per ton of ore processed (Runge et al., 2013).

2.2. The elementary principles of particle breakage

Particle fracture may be defined as the breaking of a particle into two or more pieces due to the initiation and propagation of cracks caused by the application of stress to the solid (Broek, 1986). The fracture of particles is influenced by factors such as the particle shape and size, material properties such as the elasticity of the particle, the homogeneity and flaws of the particle, and the type of stress applied (Bernotat & Schönert, 1988). Stress can be applied to a particle in one of three different modes:

- Compressive: The applied load acts to reduce the length of the material.
- Tensile: The applied load acts to elongate the material.
- Shear: Opposing forces act along parallel lines of action on the material.

Particles which contain a greater number of flaws are more susceptible to breakage because it is easier for cracks to spread within them, resulting in breakage of the solid. When a particle fractures, the number and size of progeny particles formed depends on the size and position of the cracks within the initial particle before it is broken (Brown & Jones, 1996).

Potapov & Campbell (2001) investigated the breakage pattern observed in a solid particle subjected to impact. A simulation snapshot of the tensile stresses which result in breakage of the particle is shown in Figure 2.2 (a). Figure 2.2 (b) shows the resulting crack pattern which begins to develop the instant impact occurs.

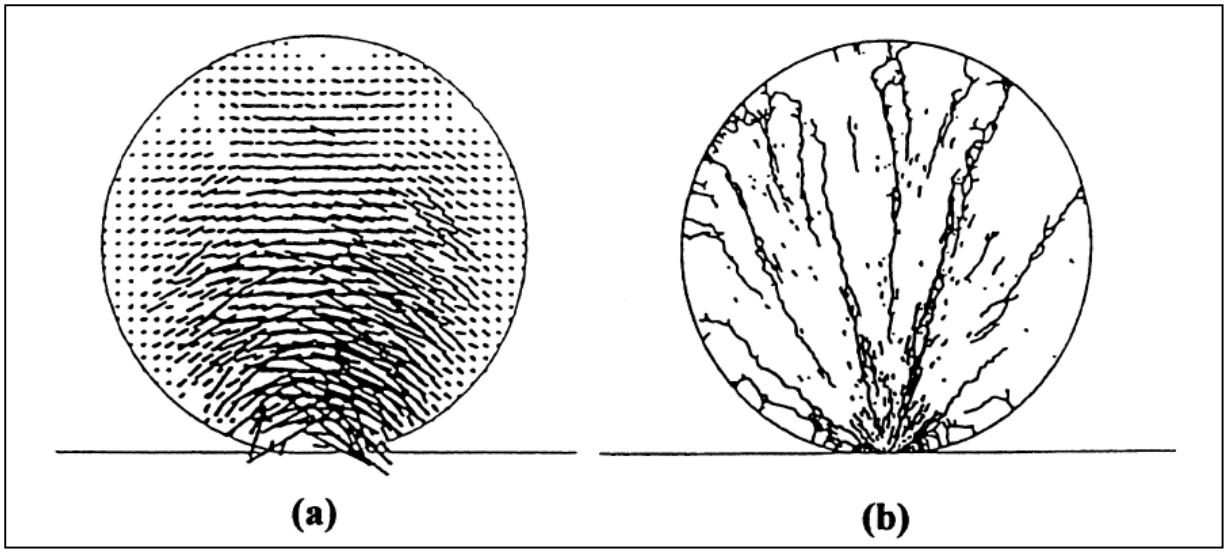

Figure 2.2: (a) The tensile stresses which are generated in a solid particle subjected to impact. (b) The crack pattern formed as a result of the stresses in the particle (Potapov & Campbell, 2001)

The length and direction of each line shown in Figure 2.2 (a) indicates the magnitude and direction of the stresses generated in the particle when impact occurs. The breakage pattern shown in Figure 2.2 (b) indicates that impact forces result in the formation of a fan-like pattern of cracks which extend from the contact point to the far edges of the particle.

Erdogan (2000) states that studying the fracture of particles is highly complex, as broadly diverse factors such as the microscopic and macroscopic phenomena and the solid geometry have to be considered. Due to the complicated nature of particle fracture, there is currently no single theory which covers all the aspects pertaining to it. Particle fracture under impact is investigated from one of two different viewpoints: microscopic (fracture mechanics) or macroscopic (rock mechanics).

2.2.1. Fracture mechanics

Continuum damage mechanics (CDM) is a branch of fracture mechanics which is concerned with representation of damage in materials that is suitable for making engineering predictions about the initiation and propagation of cracks resulting in fracture (Chaboche, 1988). In CDM the effect of damage on the stress-strain behaviour of materials is investigated. Damage can be defined as any change which impairs the microstructural properties of a material and hence decreases its strength and ultimately results in component failure (Kachanov, 1986). The work done in CDM uses mechanical variables such as stiffness and crack density to represent the influence of damage on the remaining life of the material (Krajcinovic & Mastilovic, 1995).

Common types of material damage include (Anderson, 2005):

- Creep: Occurs in metals and alloys as a result of exposure to stress at high temperatures.
- Fatigue: Gradual deterioration of a material due to the initiation and enlargement of cracks when it is subjected to loading.
- Fracture: The breaking of a material due to the nucleation and growth of cracks when it is subjected to loading.

2.2.2. Rock mechanics

The fundamentals of the rock mechanics field consist of solid mechanics subject matters: stress, strain, elasticity, plastic deformation and elastic wave propagation (Jaeger et al., 2009). A stress/strain curve, shown in Figure 2.3, is used to define the response of a material under loading. Stress is defined as ratio of the applied force to the cross sectional area of the material and strain is defined as extension per unit length (Courtney, 2005).

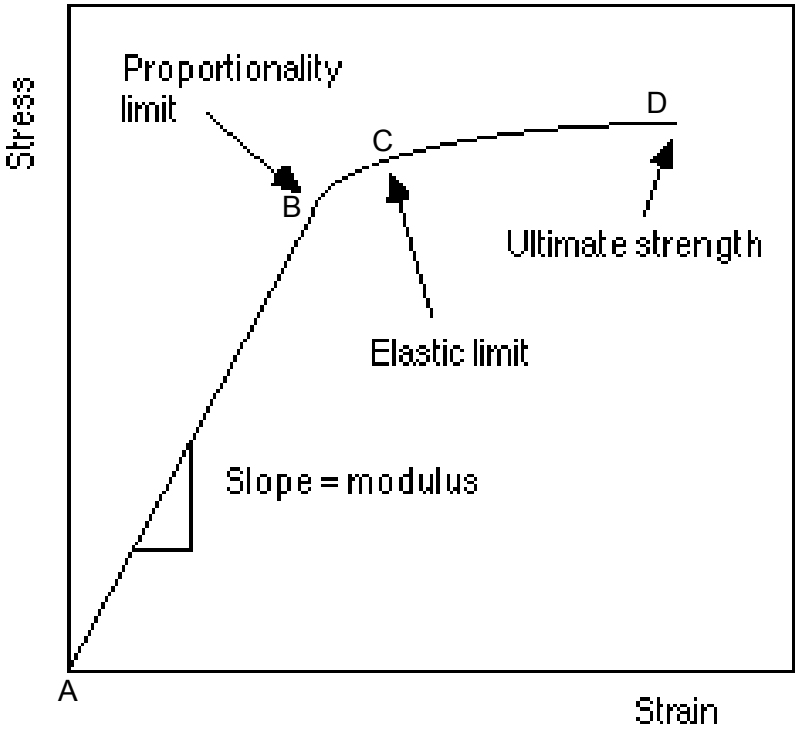

Figure 2.3: Typical stress/strain curve used in rock mechanics (Harrison & Hudson, 2000)

Region AB in Figure 2.3 indicates the elastic region of the material. In this region the material undergoes elastic deformation with increasing stress, where it is capable of sustaining stress without deforming permanently. Hooke's Law, which states that strain is proportional to stress, is obeyed in the elastic region with Young's modulus being the constant of proportionality (Young & Budynas, 2002). As the stress is increased in region BC the maximum stress that can be applied to the material without producing permanent deformation is reached at point

C, which is referred to as the elastic limit. The material starts to undergo plastic deformation after point C and as the stress is further increased, the critical strength value at point D is reached. The stress at this point is referred to as the Ultimate Compressive Stress (UCS), and is defined as the maximum stress a material can undergo before complete failure (Harrison & Hudson, 2000).

Other than Young's modulus of elasticity and UCS, another commonly quoted value relating to the compressional properties of rock is Poisson's ratio. This is determined as the ratio of the lateral strain to the longitudinal strain on the rock material (Napier-Munn et al., 1996).

2.3. Standard breakage characterization procedures

The size and energy consumption of comminution machines is dependent on feed rate and desired product size as well as the hardness of the ore. Various laboratory characterization procedures have been developed for investigating how materials break in comminution machines and the results have been used to design these industrial devices. Breakage characterization techniques can be classified into three different classes (Napier-Munn, et al., 1996):

- Conventional rock and fracture mechanics measurements
- Standard grindability tests
- Single particle characterization tests

Each of these is discussed in the sections that follow.

2.3.1. Conventional rock and fracture mechanics measurements

As mentioned in Section 2.2, rock exhibits macro and micro response under an applied load.

Macro measures of response:

- Compressive loading: UCS, Young's modulus and Poisson's ratio are the properties used to describe the rock's response to an applied load (Section 2.2). Young's modulus and Poisson's ratio can be used to determine a material's stiffness, defined as the extent to which it resists deformation in response to an applied load (Pharr et al., 1992).
- Tensile loading: The tensile strength of a rock controls its breakage, hence understanding this mode of failure is important in comminution research. The measurement of tensile strength is determined through an indirect measure known as the Brazilian test which relies on the diametral compression of a rock disk. In this test,

the centre of the disk is put into tension and a crack initiates at the centre and propagates outwards (Rocco et al., 1999).

Micro fracture mechanisms:

The mechanism by which rock responds to an applied load and hence the macroscale mechanical properties it has are controlled by its microscale features (Landis, 1999). Fracture toughness, defined as the rock resistance to crack propagation, is an intrinsic material property which indicates how rock behaves under loading (Napier-Munn, et al., 1996). Fracture toughness has been identified as a useful parameter in comminution studies as it can be correlated with cone crusher performance (Brown & Reddish, 1997).

2.3.2. Standard grindability tests

It is necessary to determine the energy requirements of a comminution process in order to size crushing and grinding devices and to specify motor sizes for the equipment. Impact breakage research is used to relate the power draw of comminution devices to the energy transferred to the ore to obtain breakage. An example of a method used to do this is the determination of the standard ore hardness characterization parameter known as the Bond work index; with hardness defined as an ore's resistance to break under loading.

The Bond work index is defined as the power required to reduce a material from an infinite size to 80% by mass of the original material passing through a screen of size matching the desired product size. According to the method published by Fred Bond in 1952, the work input is proportional to the feed and product size of an ore through a material specific constant called its work index (Lynch & Rowland, 2005).

The work index can be related to the feed and product size by the relationship in Equation 2.1 (Bond, 1952):

$$W = 10W_i\left(\frac{1}{\sqrt{P_{80}}} - \frac{1}{\sqrt{F_{80}}}\right) \qquad \text{Equation 2.1}$$

Where:

W: Work input (kWh/t)

W_i: Bond work index (kWh/t)

P_{80}: Size at which 80% of the product passes (μm)

F_{80}: Size at which 80% of the feed passes (μm)

Grinding power for rod and ball mills determined using work indices from Bond grindability tests has been found to correlate well with the relationship shown in Equation 2.1, which can be corrected to calculate indices under other conditions. Equation 2.1 is also useful for the calculation of an 'operating work index' which is used for feed ore type comparison and assessing crushing and grinding performance (Napier-Munn et al., 1996; Ozkahraman, 2005).

As a basic measure of rock hardness, the Bond work index has been found to be broadly related to the UCS (Section 2.2.2). Table 2.1 shows the ore hardness relationship between the two parameters.

Table 2.1: Relationship between UCS and the Bond Work Index (Napier-Munn et al., 1996)

Parameter	Soft	Medium	Hard	Very hard
UCS (MPa)	50 - 100	100 - 150	150 - 250	>250
Bond work index (kWh/t)	7 - 9	9 - 14	14 - 20	>20

Breakage models which incorporate ore hardness represent a relationship between the input energy and the progeny particle size. The standard t_{10}-E_{cs} function proposed by the Julius Kruttschnitt Mineral Research Centre (JKMRC) at the University of Queensland in Australia has been used in breakage modelling (Shi & Kojovic, 2007):

$$t_{10} = A(1 - e^{-b.Ecs}) \qquad \text{Equation 2.2}$$

Where:

t_{10}: A progeny particle fineness indicator defined as the percentage of progeny particles passing through a screen whose aperture size is a tenth of the initial mean particle size.

Ecs: Specific comminution energy (kWh/t)

A & b: Impact breakage parameters of the ore

The hardness of an ore affects its breakage characteristics (Wills, 2011). Axb values are commonly used as an indicator of ore hardness. A lower Axb value indicates that the ore has a higher resistance to breakage and a greater Axb value is an indication of a 'softer' ore which fractures more easily.

2.3.3. Single particle breakage characterization tests

Single particle impact breakage testing is a valuable tool for characterizing ore hardness and determining ore parameters that are applied in breakage modelling and simulation in

comminution research (Napier-Munn et al., 1996). Ore characterization tests are useful for measuring the ore-specific energy/size-reduction behaviour. Several devices have been developed for the controlled breakage of single particles under impact loading in order to determine comminution parameters. These devices include the twin pendulum device, drop weight tester, Split Hopkinson Pressure Bar, Rotary Breakage Tester, and the Short Impact Load Cell. The devices are discussed in the following section.

2.4. Impact breakage devices

Comminution of particles by impact is the main mechanism of size reduction in industrial devices, where particle fracture occurs as a result of falling media. Thus, the breakage of particles subjected to impact has been investigated as a means to gain better understanding of this breakage mechanism (Kapur et al., 1997).

2.4.1. Twin pendulum device

The twin pendulum device was the first single particle breakage testing instrument to be developed at the JKMRC. The single particle breakage results obtained using twin pendulum tests can be used to determine the energy used by the particle for breakage and the resultant product size distribution (Napier-Munn et al., 1996).

The device consists of two pendulums, namely the impact and rebound pendulums, which are suspended on a firm frame as shown in the schematic in Figure 2.4.

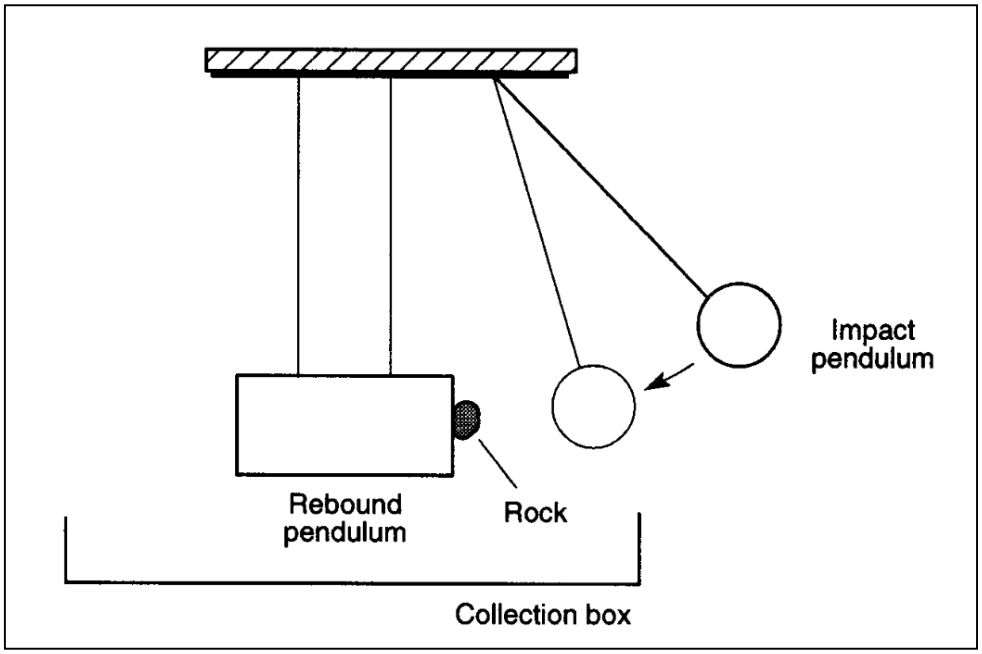

Figure 2.4: Schematic of the twin pendulum device indicating the impact and rebound pendulums, and the positioning of the rock specimen when a breakage test is conducted (Napier-Munn et al., 1996)

When a breakage test is conducted, a particle of known mass is attached to the rebound pendulum and the impact pendulum is drawn back to a known height and released to collide with and break the particle. After impact, the rebound pendulum swings and passes through a laser beam and the time taken to complete oscillations is measured and recorded on a computer to determine the period (Weedon & Wilson, 2000).

After a breakage test, the energy transmitted to the rebound pendulum is determined using Equation 2.3 (Napier-Munn, et al., 1996):

$$E_t = M_r(L - L\cos\theta) \qquad \text{Equation 2.3}$$

Where:

E_t: Energy transmitted to the rebound pendulum (J)

M_r: Rebound pendulum mass (kg)

L: Length of the pendulum (m)

$\boldsymbol{\theta}$: Angle of displacement of the rebound pendulum from its equilibrium position (rad)

The residual energy (Er) of the impact pendulum is computed by determining its velocity after impact with the rebound pendulum. The energy used by the particle for breakage can be determined from an energy balance during collision of the input pendulum with the particle attached to the rebound pendulum using Equation 2.4 (Napier-Munn, et al., 1996):

$$E_c = E_i - E_t - E_r \qquad \text{Equation 2.4}$$

Where:

E_c: Energy used by the particle for breakage (J)

E_i: Input energy (J)

E_t: Energy transmitted to the rebound pendulum upon impact (J)

E_r: Residual energy of the impact pendulum after impact (J)

The specific comminution energy Ecs (kWh/t) which is defined as the energy used for particle breakage per unit mass can be determined by using the Ec values obtained using Equation 2.4.

The use of the twin pendulum device is advantageous because it is a simple tool to use to determine the fraction of the input energy that is used by the particle for breakage through measurement of the residual energy of the pendulums. However, disadvantages associated with using twin pendulum testing are that carrying out a breakage test is time consuming and it can only be used in restricted energy and particle size ranges (Salman et al, 2007). Additionally, secondary motion of the rebound pendulum can result in imprecise calculation of the energy used by the particle for breakage.

Due to the limitations associated with twin pendulum devices, drop weight tests are more commonly used for conducting breakage tests. Drop weight tests are discussed in the following section.

2.4.2. Drop weight tester

The drop weight tester was developed at the JKMRC as a replacement of the Twin pendulum device for particle breakage characterization tests (Napier-Munn et al., 1996). The drop weight device is built on a steel frame which is mounted onto a concrete block and it is comprised of a steel drop weight which is mounted on two guide rails and typically enclosed in perspex. An electromagnetic system, or a system of pulleys and strings, is used to raise the steel weight to the desired drop height. A pneumatic switch is used to release the weight which falls onto a particle placed onto an anvil. The input energy is altered by varying the drop height and the mass of the drop weight used (Genc et al., 2004). A schematic of the drop weight tester is shown in Figure 2.5.

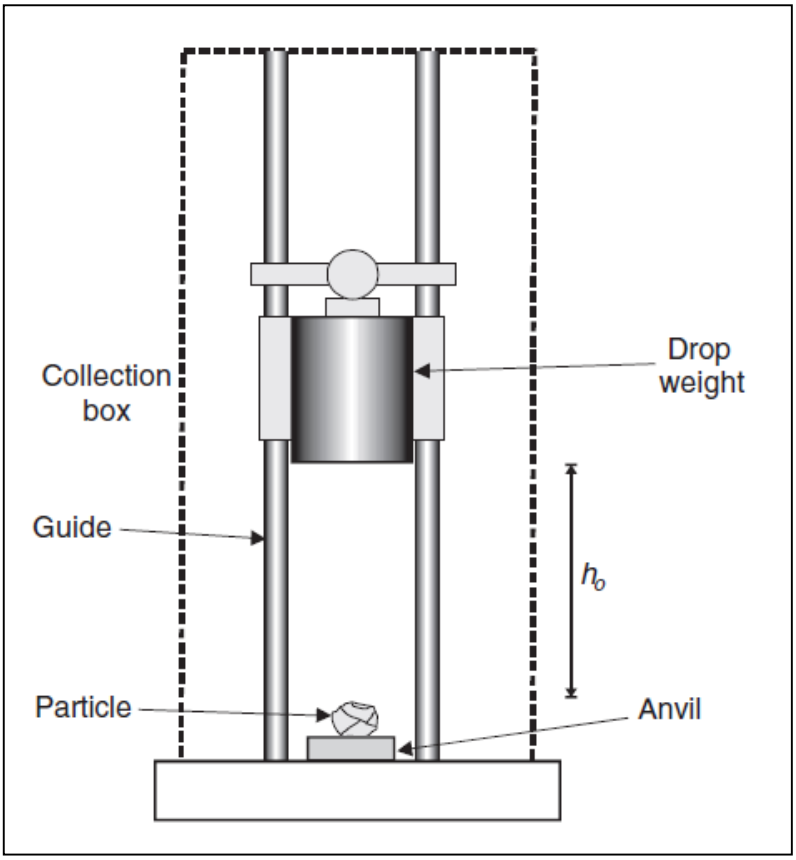

Figure 2.5: Schematic of the drop weight testing device showing the drop weight at its initial drop height h_0 and the particle specimen before a breakage test is conducted (Salman et al., 2007)

When a breakage test is conducted using the drop weight tester, it is assumed that the potential energy of the drop weight before release is converted to its kinetic energy when it impacts the particle sample. Sample preparation involves screening particles to narrow size ranges, from which the mean mass $(\bar{m})$ of particles to be broken is computed.

The required drop height depends on the specific input energy for each breakage tests and is calculated using Equation 2.5 (Napier-Munn, et al., 1996):

$$h_i = \frac{\bar{m}\, E_{cs}}{0.0272 M_d} \qquad \text{Equation 2.5}$$

Where:

H_i: Required drop height from which drop weight is released (cm)

$\bar{m}$: Mean mass of particles to be broken (kg)

E_{cs}: Specific input energy (kWh/t)

M_d: Mass of the drop weight (kg)

An additional 10 cm is usually added to the calculated drop height to allow for the fact that the drop weight rests at some height above the anvil because of the crushed particle after a breakage test is conducted. The height added to the calculated drop height ensures that the final specific comminution energy (energy available to cause fracture per mass present, Ecs) obtained is correct.

The offset in height (h_f) can be measured for each breakage test and is used to compute the actual input energy according to Equation 2.6:

$$E_{is} = \frac{0.0272\, M_d\, (h_i - h_f)}{\bar{m}} \qquad \text{Equation 2.6}$$

One of the advantages associated with using drop weight testing devices is that a wider input energy range is generated in comparison to that generated by pendulum devices (Napier-Munn et al., 1996). Also, drop weight tests are helpful in the investigation of the relationship between input energy and the product size distribution. Additionally, they are useful for the validation of breakage models (Salman et al, 2007).

One of the shortcomings of using drop weight devices is that they do not allow direct measurement of the actual energy used by a particle for breakage (Tavares, 1999). Another limitation of the device is that it is only suitable for conducting breakage tests on brittle ores which do not undergo much plastic deformation before they break. The device cannot be used to reliably characterize the breakage of ores which experience a substantial amount of plastic deformation such as those with high clay content. Also, the size of particles which can be tested using the drop weight testing device is limited to smaller particles; results of larger particles have to be extrapolated from those of the smaller sizes tested (JKTech, n.d.).

2.4.3. Split Hopkinson Pressure Bar (SHPB)

The Hopkinson bar technique was originally devised by John Hopkinson in 1872 to perform stress wave experiments on iron wires. In 1914 his son, Bertram Hopkinson, developed the pressure bar technique to determine the pressure produced by explosives (Gama et al., 2004). In 1949, H Kolsky made use of the pressure bar technique for the determination of the dynamic compression stress-strain data for various materials (Ramesh & Narasimhan, 1996).

To date there have been many modifications made of the original SHPB or Kolsky Bar, however the various devices essentially operate in a similar manner (Gray & Blumenthal, 2000). The SHPB technique has been used by many researchers to determine dynamic compression properties of solid materials at high strain rates. The SHPB is useful for determining the failure properties of ductile materials such as metals (Frew et al., 2001).

A conventional SHPB device consists of striker, incident and transmission bars. A sample of the material whose compression properties are being investigated is placed between the incident and transmission bars. The striker bar is launched at the incident bar using a launching mechanism (such as a gas gun, coiled spring or rail gun), causing the transmission of an elastic compression wave from the incident bar to the sample upon impact. An elastic tensile wave is reflected into the incident bar and an elastic compression wave is transmitted into the transmission bar when the impedance of the sample is less than that of the bars. The incident and transmission bars are equipped with strain gauges which measure the strain and the generated data can be used to determine the response of the sample upon impact (Song and Chen, 2005). A schematic of a conventional SHPB is shown in Figure 2.6.

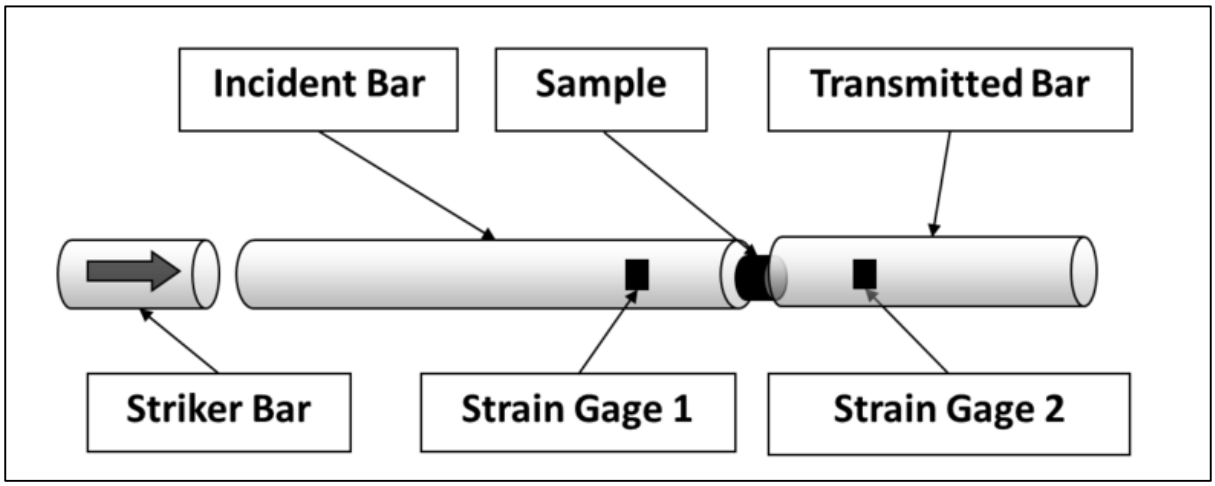

Figure 2.6: Schematic of the Split Hopkinson Pressure Bar indicating the incident and transmitter bars, strain gauges and sample positioning in the device (Adapted from Song & Chen, 2005)

As long as the pressures in the bars remain within their elastic limits, the force vs time histories recorded from the impact can be used to determine fracture properties of the specimen.
The stress on the particle sample is evaluated according to Equation 2.7 (Kolsky, 1949):

$$\sigma_s(t) = E\frac{A_0}{A}\varepsilon_T(t) \qquad \text{Equation 2.7}$$

Where:

$\sigma_s(t)$: Stress applied to the particle sample (N/m^2)

E: Elastic modulus of the bar (N/m^2)

A_0: Cross-sectional area of the bar (m^2)

A: Cross sectional area of the sample (m^2)

$\varepsilon_T(t)$: Transmitted strain history (-)

At equilibrium, the strain rate of the sample can be found using Equation 2.8 (Al-Mousawi et al., 1997; Song & Chen, 2005):

$$\frac{\partial \epsilon_s(t)}{\partial \mathrm{t}} = \frac{C_0}{L}\left[\varepsilon_i(t) - \varepsilon_R(t) - \varepsilon_t(t)\right] \qquad \text{Equation 2.8}$$

Where:

$\frac{\partial \varepsilon_s(t)}{\partial \mathrm{t}}$: Sample strain rate ($s^{-1}$)

C_0: Elastic wave speed of the bar material (m/s)

L: Sample thickness prior to impact (m)

$\varepsilon_i(t)$: Incident strain history (-)

$\varepsilon_R(t)$: Reflected bar strain history (-)

$\varepsilon_t(t)$: Transmitted strain history (-)

Equation 2.8 can be integrated to determine the strain on the specimen as given by Equation 2.9:

$$\varepsilon_s(t) = \frac{C_0}{L}\int_0^t \left[\varepsilon_i(t) - \varepsilon_R(t) - \varepsilon_{t(t)}\right] dt \qquad \text{Equation 2.9}$$

The integration of force-time profiles from the incident and transmitter bars allows for the calculation of the strain energy. The lost strain energy can be subtracted from the input energy to determine the actual amount of energy used for breakage as shown in Equation 2.10 (Napier-Munn et al, 1996):

$$E_{breakage} = E_{input} - (E_{reflected} + E_{transmitted}) \qquad \text{Equation 2.10}$$

The advantages of using the SHPB are that the interactions which applied loads have on the material specimen as well as the energies associated with impact can be determined (Dai et al, 2010; Bbosa et al, 2006) .

The limitations associated with the SHPB are that conducting breakage tests is time consuming and multi-particle experiments cannot be conducted using the device. Also, tests can only be conducted on a narrow particle size range. Additionally, using the SHPB for breakage experiments leads to a large variability in the fracture behaviour observed for geological materials (Salman et al, 2007).

2.4.4. Short Impact Load Cell (SILC)

The SILC is a hybrid of the traditional drop weight tester and the Split Hopkinson Pressure Bar. The original device was developed at the University of Utah by Reiner Weichert (Bourgeois & Banini, 2002). In the SILC, a steel ball of known mass falls under gravity from a fixed height onto an ore sample. The device consists of a pneumatic drop weight mechanism which acts as a gripper to hold the ball in place before release, and a steel rod on which the particle sample rests. The steel rod is fitted with strain gauges which measure the load response (Tavares & King, 2004). A schematic showing the major components of the SILC setup is shown in Figure 2.7.

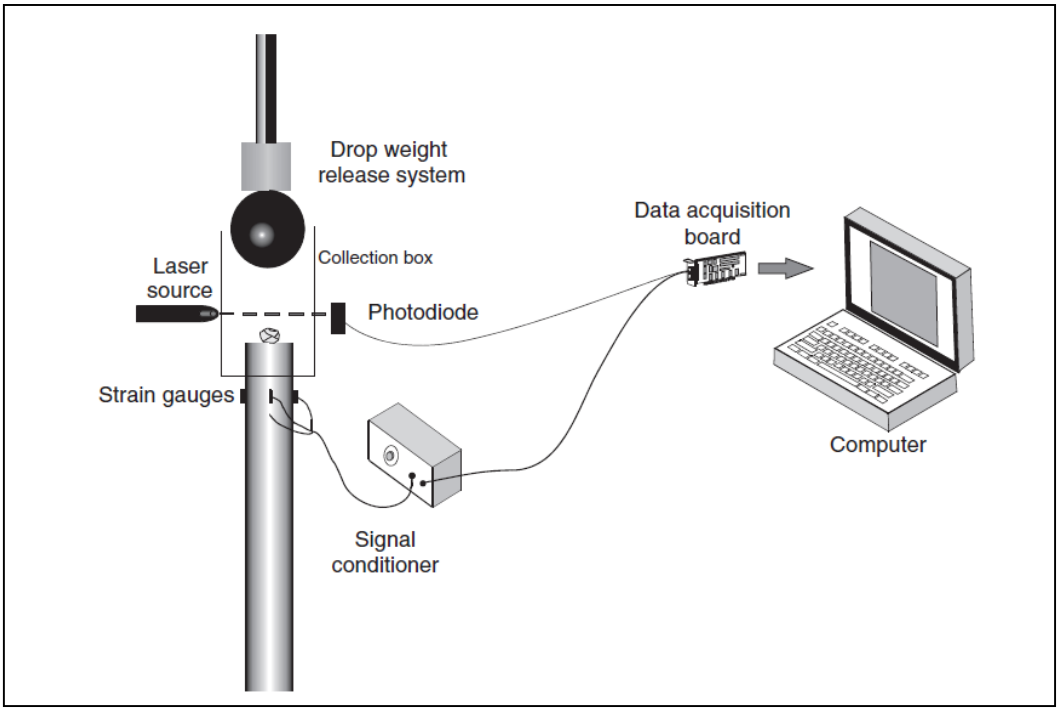

Figure 2.7: Schematic showing the main components of the SILC, namely the drop weight mechanism, steel ball, steel rod equipped with strain gauges, and the data acquisition board (Salman et al., 2007)

When a breakage test is conducted, the motion of the falling steel ball passing through a laser beam triggers a digital oscilloscope to start recording the test. When the steel ball impacts the ore sample, the resulting compressive wave travels down the rod and causes a change in resistance as it passes through the strain gauges. This results in a voltage change across the Wheatstone bridge, which is recorded as a function of time on the oscilloscope. The voltage-time data recorded on the oscilloscope can be displayed on a computer screen and used to determine the Force-time history of the breakage test (Tavares & King, 2004).

The stress applied to the steel rod is determined as:

$$\sigma = KV \qquad \text{Equation 2.11}$$

Where:

σ: Stress applied to the steel rod (N/m^2)

K: A calibration constant used to relate the measured voltage to the stress (N/Vm^2)

V: Measured voltage (V)

The force applied to the particle sample is determined using the applied stress as follows:

$$\mathrm{F} = \sigma \mathrm{A}_{\mathrm{rod}} \qquad \text{Equation 2.12}$$

Where:

F: Force applied to the particle sample (N)

σ: Stress applied to the steel rod (N/m^2)

A_{rod}: Cross sectional area of the steel rod (m^2)

To evaluate the strain energy on the rod, the work done in discrete time steps is accumulated to give the squared integral of the wave as shown in Equation 2.13. By conservation of energy, the fracture energy (strain energy absorbed by the particle up to the point of failure) is assumed to be equal to the strain energy on the rod when the breakage event occurs (Bbosa, 2007).

$$\mathrm{E}_{\mathrm{strain}} = \sum_{\mathrm{t0}}^{\mathrm{t_{final}}} \left(\frac{\left(\frac{\sigma(\mathrm{t_{n+1}}) + \sigma(\mathrm{t_n})}{2}\right)^2 (\mathrm{t_{n+1}} - \mathrm{t_n})(\mathrm{A_{rod}})}{\mathrm{C}\rho} \right) \qquad \text{Equation 2.13}$$

Where:

t_0: Initial contact time between falling ball and SILC steel rod (s)

t_{final}: Time at which particle fracture occurs (s)

σ: Stress applied to the rod (N/m^2)

t_{n+1}: Final time recorded for each time step (s)

t_n: Initial time recorded for each time step (s)

A_{rod}: Surface area of the rod (m^2)

C: Pulse speed through the rod (m/s)

ρ: Density of the rod (kg/m^3)

The main limitation associated with conventional drop weight devices is that they do not provide information which can be used to determine the fraction of input energy utilized for breakage. This limitation is overcome in the SILC and additionally, this device can be used to conduct bed breakage experiments (Tavares & King, 2004). One of the drawbacks associated with using the SILC is that it can only be used at low input energies (Bourgeois & Banini, 2002).

Because the SILC can be used for bed breakage experiments, and to evaluate the particle fracture energy, it has been selected as the most appropriate impact breakage device to use in this work. The various breakage parameters which can be determined from experimental data obtained using the SILC are discussed in the following section.

2.4.5. Rotary breakage tester

The JKMRC designed and developed the Rotary Breakage Tester (RBT) for the purposes of conducting rapid particle breakage characterization tests. Controlled kinetic energy is used to characterize particle breakage in the device. The first commercial RBT was installed at the Anglo Research labs in South Africa in 2007. Since then, more RBT devices have been installed in Australia and North America. (Shi et al, 2009).

In the RBT a rotor-anvil system is used to break particles through impact. Particles are loaded into the device through a feeder and they gain kinetic energy as they are spun around in the rotor. They are then ejected and impacted against anvils, resulting in breakage. The crushed ore particles are recovered by a vacuum system and collected in a removable bin (Wang et al., 2011). An image showing the JKRBT and its main components is given in Figure 2.8.

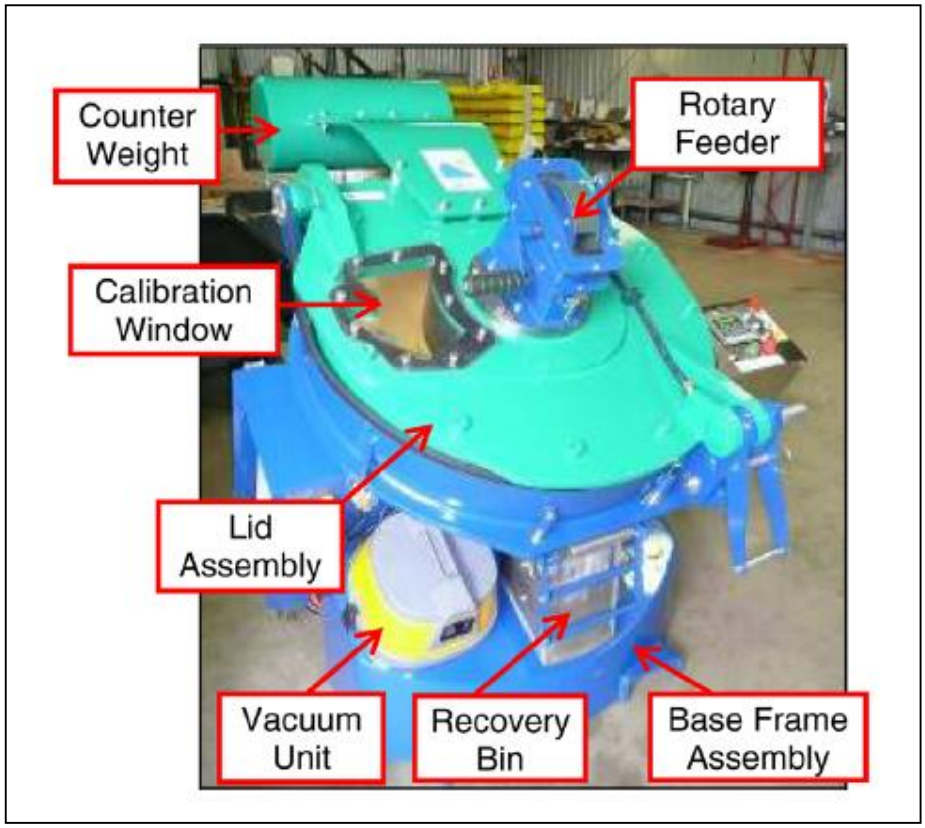

Figure 2.8: Image of the JK Rotary Breakage Tester indicating the main components of the device, namely the feeder, the vacuum unit and the particle recovery bin (Shi et al., 2009)

The specific energy of each impact in the JKRBT is computed as the kinetic energy per particle mass (Shi et al, 2009):

$$E_{cs} = \frac{E_k}{m} = \frac{0.5\ x\ m\ x\ v_i^2}{m} 0.5 v_i^2 \qquad \text{Equation 2.14}$$

Where:

E_{cs}: Specific energy - energy per unit mass (J)

E_k: Kinetic energy (J)

m: Mass (kg)

v_i: Impact velocity (m/s)

Equation 2.14 shows that the specific energy is only dependent on the impact velocity and is not affected by the particle mass, unlike in the Drop Weight Testing device.

The impact velocity is determined from the tangential and radial components, v_t and v_r, of the particle velocity as shown in Equation 2.15:

$$v_i = \sqrt{v_t^2 + v_r^2} \qquad \text{Equation 2.15}$$

If the tangential and radial components of the particle velocity are equal, the impact velocity can be expressed as:

$$v_{i(theory)=\sqrt{2}\,v_t} \qquad \text{Equation 2.16}$$

Due to frictional losses, the impact velocity of a particle is smaller than that given by Equation 2.16. Therefore, a constant is used to account for the efficiency of a given design in transferring the kinetic energy from the rotor to the particle:

$$C = \frac{V_{i(actual)}}{V_{i(theory)}} \qquad \text{Equation 2.17}$$

The specific energy is then determined as (Shi et al, 2009)::

$$E_{cs} = \frac{0.5\,x\left[C\,x\,\sqrt{2}x\left(\frac{2\,x\,\pi\,xN\,x\,r}{60}\right)\right]^2}{3600} = 3.046 \text{ x } 10^{-6}C^2N^2r^2 \qquad \text{Equation 2.18}$$

Where:

R: Rotor radius (m)

N: Rotor speed (rpm)

C: Machine design constant that governs the maximum possible velocity at a given rotor speed and operational conditions (-)

The RBT yields statistically similar breakage parameter results to the conventional drop weight testing device (Kojovic et al, 2010). However, the RBT has several advantages over the drop weight tester: it has improved precision in the input energy, better repeatability and a wider size range of particles can be tested (Shi et al, 2009). Also, conducting breakage tests on the RBT requires less time to complete in comparison to conducting tests on the drop weight tester or twin pendulum device (Larbi-Bram, 2009).

The main limitation associated with the JKRBT is that the percentage of the input energy used by particles for breakage cannot be quantified (Kojovic et al, 2010).

2.5. Parameters obtained using the SILC

The breakage related parameters that can be determined using the SILC include (Tavares & King, 1998; Bourgeois & Banini, 2002):

- *The ultimate stress of a particle*: The force at which fracture occurs in a particle
- *A measure of material stiffness*: The modulus of elasticity, which is an indication of material stiffness, relates the relative strain a material undergoes when under a

specified stress. It is not possible to directly determine the material stiffness from conducting experiments using a SILC as the state of stress is not measured. However, a parameter referred to as the 'particle stiffness' (Tavares, 1998) can be determined from the force-displacement measurement of the SILC. For spherical particles, the particle stiffness has been found to be a relatable estimate of the material stiffness. The particle stiffness is a measure that allows for qualitative comparison of the elasticity of particles with similar shape factors

- *The particle fracture energy*: The minimum energy required to fracture a particle

Details of how these parameters are determined from SILC breakage test data are given in this section.

2.5.1. Determination of parameters obtained using the SILC

A typical voltage-time curve generated from a breakage test conducted using the SILC is shown in Figure 2.9.

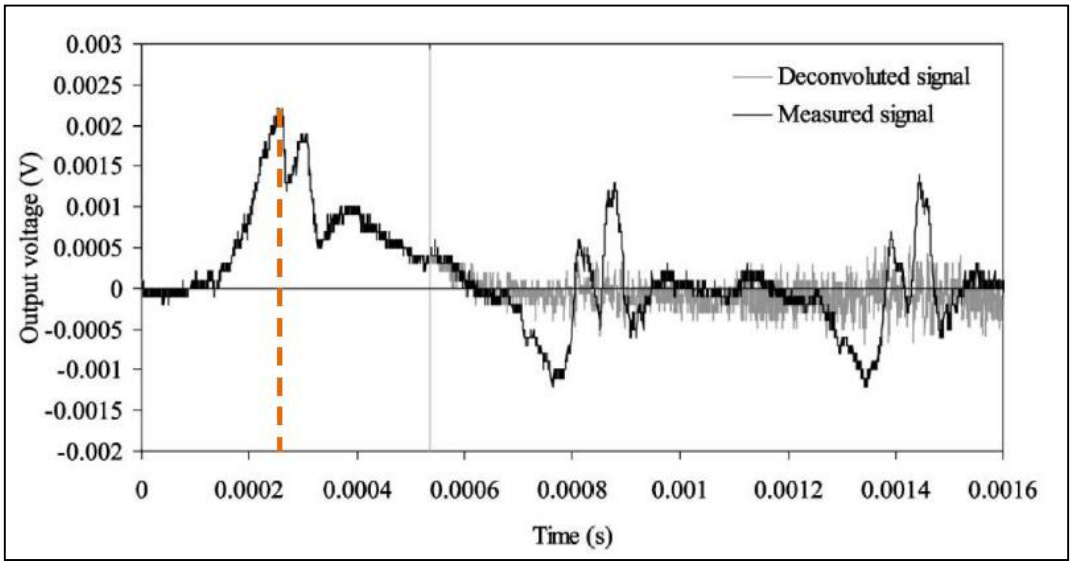

Figure 2.9: Typical voltage-time curve indicating the measured and deconvoluted signals obtained using the SILC (Bourgeois & Banini, 2002)

Figure 2.9 shows a measured signal curve in black and the deconvoluted signal in grey. The measured signal obtained from the breakage test has noise due to amplification circuitry or the SILC itself and can be corrected to give the deconvoluted signal. The maximum peak (shown by the dotted line) indicates the point of first fracture of the particles.

In order to determine particle breakage parameters, the voltage-time curve is translated into a force-time curve by making use of Equations 2.10 and 2.11. Figure 2.10 is an example of a typical force-time curve resulting from manipulation of the voltage-time signal obtained using

the SILC. The first peak indicates the point of first fracture of the particle and the second peak is due to subsequent fracture of the particle.

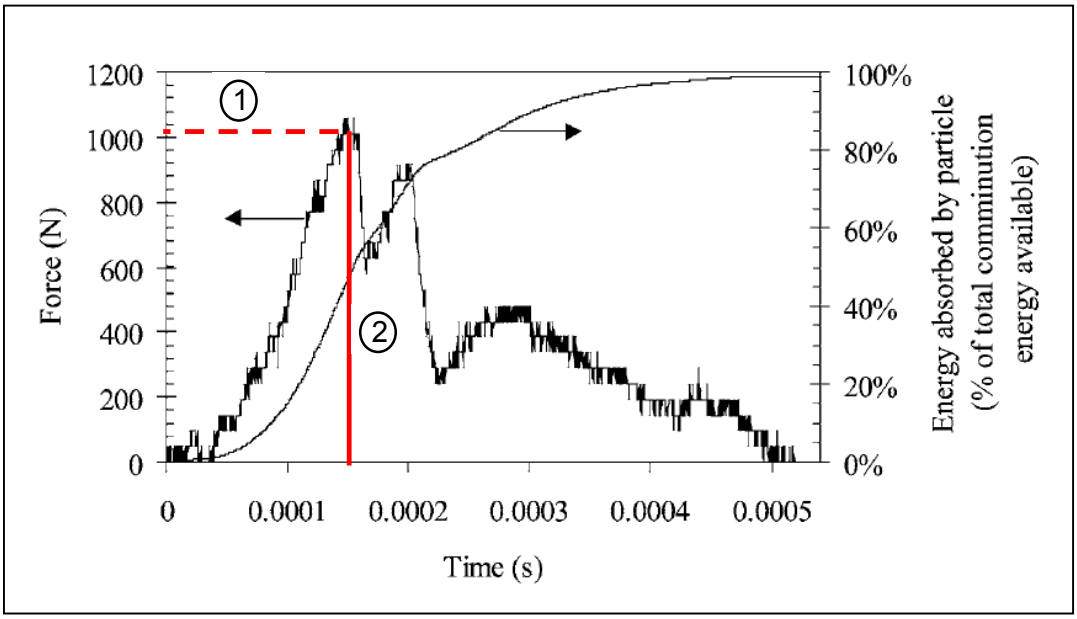

Figure 2.10: Typical force-time curve obtained from a breakage test conducted using the SILC. The figure represents parameters such as the ultimate stress and the particle fracture energy (Bourgeois & Banini, 2002)

The following parameters are represented by Figure 2.10:

1. *The ultimate stress:* This corresponds to the value of the maximum force at the point of first fracture and has been indicated by the dotted line labelled as '1' in Figure 2.10.
2. *The particle fracture energy*: The energy absorbed by the particles until the instant of fracture. This is determined from the time the breakage event is initially recorded to the point indicated by the line labelled as '2' in Figure 2.10.

2.6. Studies conducted using impact load cells

Vervoorn & Austin (1990) used an impact load cell to measure the maximum force obtained on particles subjected to impact. The results showed that there was a variation in the maximum force recorded even for a fixed striker mass and velocity. The researchers ascribed this to the different orientations of particles when tests were conducted which resulted in variances in the force-time profiles obtained.

Tavares & King (1998) used an ultra-fast load cell to investigate the fracture of single particles subject to impact with a steel ball. Quartz particles of size 1 - 1.18 mm were impacted using a 0.0283 kg steel ball at a velocity of 1.16 m/s. The Force-time results obtained for six single

particle breakage experiments are presented in Figure 2.11, where the arrows show the points of first fracture.

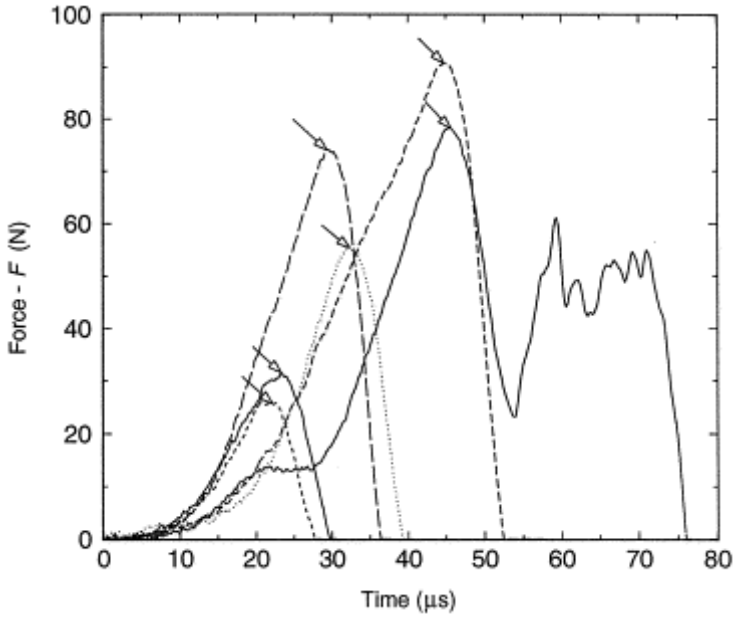

Figure 2.11: Force-time profiles for six breakage tests conducted on quartz particles using a steel ball at 1.16 m/s (Tavares & King, 1998)

The results showed that there was great variability in the mechanical response of the particles and the researchers attributed this to the individual grain and flaw structure in each particle.

In a different study, Tavares & King (2004) used a modified impact load cell to conduct experiments for the comparison of experimental data to a model that combines Hertzian contact theory and the theory of wave propagation in rods. The experiments conducted to investigate the accuracy of the device included measuring sample deformations due to impact. Individual spheres of known elastic constants and diameters were subjected to impact and the force-time history was recorded. The elastic constants of the different materials used are shown in Table 2.2.

Table 2.2: Elastic constants of spherical materials tested (Tavares & King, 2004)

Type of material	Modulus of elasticity (GPa)	Stiffness (GPa)
Tungsten	345	374
Stainless steel	206	220
Soda-lime glass	70	73

The Force-time profiles resulting from experiments conducted on the spherical particles at the same impact velocity of 0.31 m/s are shown in Figure 2.12. The results showed excellent agreement between experimental data and the theoretical model. This illustrated that the device was accurate and the experimental procedures and calculations used were reproducible. The findings also showed that tungsten, which had the highest modulus of elasticity and stiffness had the highest force to fracture and shortest contact time. The lowest force to fracture and longest contact time were obtained for soda-lime glass which had the lowest elastic constants.

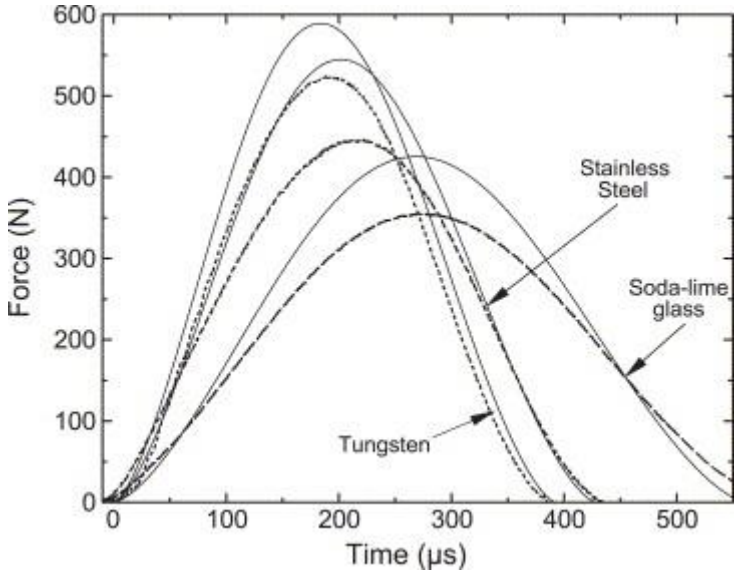

Figure 2.12: Force-time profiles from impact of 3.2 mm spherical particles of different materials at a velocity of 0.31 m/s. Solid lines represent the theoretical model and dotted lines represent experimental data (Tavares & King, 2004)

2.7. Factors affecting the breakage behaviour of particles

The factors which affect particle breakage include the energy available to cause breakage, particle size and shape, the hardness of the ore, and the conditions (single particle or bed breakage and confined or unconfined conditions) in which particles are broken (Sikong et al.,1990; Schonert, 1991; Tavares & King, 1998; Stamboliadis, 2002; Nguyen et al., 2002). The factors relevant to this work are discussed in the sections that follow.

2.7.1. The effect of varying the input energy on the breakage of particles

From the conservation of energy, the input energy onto a particle sample when a breakage test is conducted is assumed to be equal to the potential energy of the steel ball before it is

released. The input energy is dependent on the mass of the ball and the drop height used and is given by (Salman et al, 2007):

$$E_{input} = m_{sb} g h_0 \qquad \text{Equation 2.19}$$

Where:

E_{input}: Energy input onto the bed of particles (J)

m_{sb}: Mass of the steel ball (kg)

g: Acceleration due to gravity (m/s^2)

h_0: Initial height of the steel ball before it is released (m)

In order to determine the effect of input energy on the breakage behaviour of an ore, Morrison & Cleary (2004) investigated the relationship between the specific input energy (energy available to cause fracture per mass present, E_{cs}) and the degree of breakage obtained.

The degree of breakage is used to measure the breakage obtained when a test is conducted. Breakage indicators are used to quantify the degree of breakage and are defined as:

t_n: Percentage of the material passing through a screen whose aperture size is $\frac{1}{n}$ of the original geometric mean particle size, where n can be any integer value (Napier-Munn et al, 1996).

Typical breakage indicators include t_{75}, t_{50}, t_{10}, t_4 and t_2; where t_2 is the percentage of the material passing through a screen whose aperture size is $\frac{1}{2}$ of the original geometric mean particle size and t_4 is the percentage of the material passing through a screen whose aperture size is $\frac{1}{4}$ of the original geometric mean particle size, etc. The t_{10} breakage indicator is the most commonly used to characterize the degree of breakage in comminution studies (Napier-Munn et al, 1996).

An example of the relationship between the specific input energy (E_{cs}) and the degree of breakage obtained by Morrison & Cleary (2004) is shown in Figure 2.13.

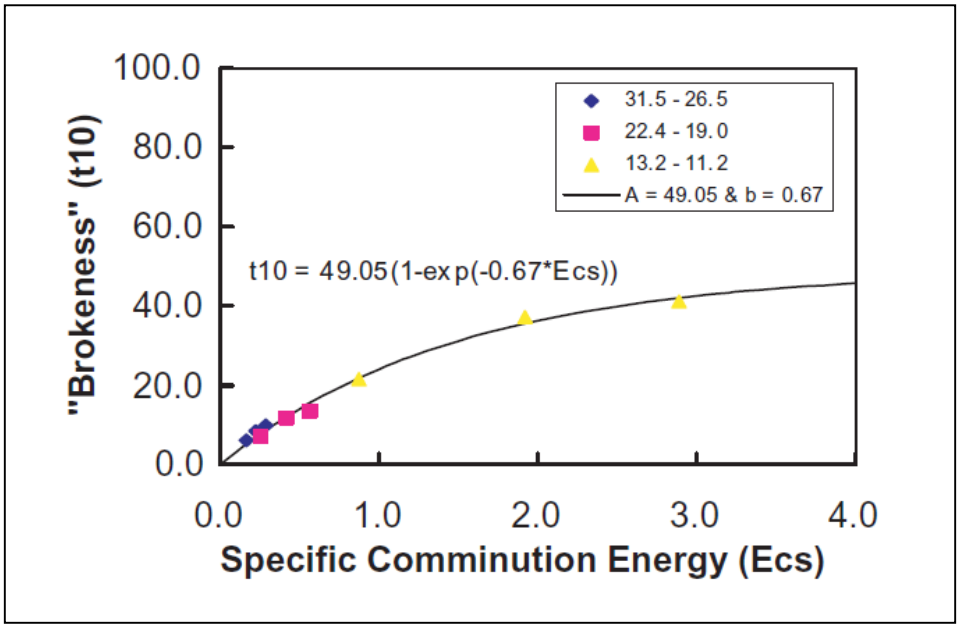

Figure 2.13: The t_{10} breakage indicator as a function of the specific comminution energy (Morrison & Cleary, 2004)

Figure 2.13 shows that the degree of breakage obtained (t_{10}) for a particle sample increases with an increase in the specific input energy (E_{cs}) at low E_{cs} values. However, as the E_{cs} values continue to increase, the degree of breakage of the particles reaches a constant value. This illustrates that there is a maximum degree of breakage that can be obtained regardless of the subsequent increase in input energy.

Research done by Stamboliadis (2002) and Shi & Kojovic (2007) also showed synonymous findings to those made by Morrison & Cleary (2004).

2.7.2. The effect of particle size on the breakage behaviour of particles

Sikong et al. (1990) conducted an investigation in which the relationship between the particle strength, defined as the maximum stress that a particle can undergo before permanent deformation, and size was studied for brittle particles. In a similar study, Schonert (1991) compared the particle strength with increasing particle size for nine different materials. From the results obtained by Sikong et al. (1990) and Schonert (1991), it was observed that the particle strength increases with a decrease in the particle size. This means that there is a greater resistance for particles to break with a decrease in size. This trend is observed because smaller particles contain fewer flaws than larger ones; hence, a higher stress is required to meet the fracture criterion of finer particles in comparison to coarse particles Schonert (1991).

Tavares & King (1998) investigated the deformation and fracture of single particles when subjected to impact. The effects of particle size, shape and material composition on the fracture characteristics of brittle materials were studied. The researchers used an Ultra-Fast Load Cell (UFLC) to carry out their experiments. The UFLC is a larger type of Impact Load Cell which is used to investigate the deformation and fracture of particles under impact loading and is operated similarly to the SILC.

The procedure followed by Tavares & King (1998) allowed them to determine the particle fracture energy, particle strength and particle stiffness (a measure of how much the particle deforms due to the stress applied by a load). The results obtained in the study confirmed that the particle stiffness is a material property is independent of the size of the particle. The investigation also showed that the particle strength and fracture energy increase with a decrease in particle size, making it more difficult to break finer particles in comparison to coarse ones. This result is the same as that obtained by Sikong et al. (1990) and Schonert (1991) who noted that the resistance for particles to fracture becomes greater as the particles become smaller in size.

2.7.3. Breakage behaviour of particles contained in beds

Fundamental research done in comminution studies is mainly based on three cases: the breakage of single particles, one-layer particles and particles contained in beds. In crushers, which are mostly used for the comminution of coarse materials, the particles are mainly stressed as single or one-layer particles (Nikolov, 2004). The interaction between particles stressed in such conditions is negligible. In mills used to grind finer particles, materials are mainly stressed as particle beds between grinding media and inter-particle interference cannot be ignored. In the application of stress to beds of particles it is useful to consider the particle arrangement and confinement on the breakage behaviour of particles (Nguyen et al., 2002).

There are significant differences between the stressing of single particles and that of particles contained in a bed. Schonert (1996) and Gutsche & Fuerstenau (1999) state that better size reduction is obtained when stress is applied to a single particle in comparison to that obtained in the stressing of a particle bed. The researchers explain that when stress is applied to a bed, a fraction of the input energy is used to rearrange the particles within the bed, which reduces the amount of energy available for particle breakage. This illustrates that breaking a single particle leads to greater energy utilization in comparison to breaking particles contained in a bed.

Another notable difference is with regards to the amount of energy received by the particles. In single particle stressing the amount of input energy is known. However, when stress is applied to a particle bed it is difficult to accurately determine the fraction of the stressing energy that is received by particles in different parts of the bed Barrios et al. (2011).

According to Khanal et al. (2007), an increase in the depth of the bed leads to a reduction in the energy utilized for breakage. This is because a higher fraction of the input energy is used for particle repositioning with an increase in the bed depth; therefore less energy is available to be absorbed by the bed for breakage. The researchers also state that an increase in the bed depth increases the stiffness of the bed. This leads to a reduction in the degree of brokenness obtained when the particle bed is subjected to a compressive force.

Work done by Barrios et al. (2011) on bed breakage behaviour under impact has shown that particles undergo the greatest amount of breakage when they are contained in a single layer at the bottom of the bed. It has been suggested that this occurs because the stress on the particles in the upper layers of the bed are too low or are applied for a short time, resulting in little or no breakage. Particles only experience adequate stress to cause significant breakage when they reach the bottom layer of the bed.

2.7.4. Breakage behaviour of particles in confined and unconfined conditions

A bed of particles can be stressed in confined or unconfined conditions. Confinement refers to any surfaces which affect the lateral movement of particles when stress is applied to the bed. Wall friction affects the stress distribution in the bed; particles in contact with the confining surface are stressed differently to internal ones. The non-uniform stress distribution leads to a complex stress field in the bed (Schönert, 1996).

In confined conditions, typically those found in devices such as high pressure grinding rolls, the movement of particles contained in the bed is restricted. Therefore, most of the particles undergo stressing when an impact force is applied as very few particles escape from the bed. Fully confined particle beds, defined as ideal particle beds, have been widely used to investigate inter-particle breakage within the bed (Tang et al., 2001). An ideal particle bed is characterized as possessing: a homogeneous structure, homogeneous compaction, a known volume or mass of the stressed particles and negligible wall effects in respect to the overall size reduction effect (Nguyen et al., 2002).

In fine grinding devices such as roller, tumbling and vibration mills, some of the particles stressed between the grinding media can escape and be re-positioned within the bed. In these devices particles are stressed in unconfined conditions, in which no lateral restriction of

particles occurs. Unconfined conditions are useful for investigating the breakage behaviour of particles stressed in a similar manner to that occurring in industrial grinding machines.

In work done by Barrios et al. (2013) very thin sheets of paper were used to prevent the particles from falling off the bed. It was assumed that the thin paper did not offer significant resistance to the movement of particles when impacted; hence the bed could be classified as unconfined. Because material is not constrained within unconfined beds, a part of it gets ejected when stresses are applied to the bed (Schonert, 1991).

2.8. Summary

Comminution operations are energy intensive, accounting for approximately 3-4 % of global electricity demand (Pokrajcic, 2008) and are only 1-2 % efficient (Sadrai et al., 2006). In industrial comminution devices particle breakage is known to occur through various mechanisms but impact breakage has been found to be the most elementary form of particle size reduction (Schönert, 1991). As a result, comminution research has been dedicated to understanding the fundamentals of particle fracture under impact loading in an effort to develop energy efficient particle size reduction techniques.

Laboratory characterization tests such as single particle impact breakage testing are a useful tool for determining the breakage behaviour of materials in comminution machines. Ore characterization tests such as the twin pendulum and drop weight tests are used to measure ore-specific energy/size reduction behaviour and determine comminution parameters that are applied in breakage modelling and simulation. Other techniques and devices which have been developed to characterize particle breakage include the Split Hopkinson Pressure Bar, Rotary Breakage Tester and the Short Impact Load Cell (SILC) which is used in this work. The SILC, which is a combination of the drop weight device and the Split Hopkinson Pressure Bar can be used to determine parameters such as the ultimate stress of particles and the particle fracture energy (Bourgeois & Banini, 2002; Tavares & King, 2004). Additionally, this device can be used to conduct bed breakage experiments.

Factors responsible for particle breakage include the input energy, particle size, ore hardness, and the confinement conditions in which stressing occurs. Stamboliadis (2002), Morrison & Cleary (2004), and Shi & Kojovic (2007) found that at low values of the specific comminution energy the degree of breakage increases with increasing specific comminution energy. However as the specific comminution energy continues to increase, the degree of breakage approaches a constant value. This indicates that the degree of breakage obtained reaches a maximum beyond which it will not increase regardless of an increase in input energy.

The work done by Sikong et al. (1990), Schonert (1991) and Tavares & King (1998) illustrated that smaller, fine particles have a greater resistance to break in comparison to larger, coarser particles. In research done by Khanal et al. (2007) and Barrios et al. (2011) pertaining to the breakage behaviour of particles contained in beds it was found that increasing the number of particle layers contained in the bed results in a reduction in the degree of breakage obtained when the particle bed is subjected to a compressive force.

Although particles stressed in fully confined conditions are useful for investigation of inter-particle breakage within the bed, the fully confined particle bed arrangement does not occur in comminution practice (Nguyen et al., 2002). Consequently, researchers such as Oettel & Husemann (2004) and Barrios et al (2011) have investigated the stressing of particles in unconfined conditions. In work done by Barrios et al. (2013) paper was used to hold the particles in the bed as it was said that it offered negligible resistance and the bed could be classified as unconfined.

The findings made in the literature will be relevant in addressing the key issues in this research work. The SILC will be used to conduct bed breakage experiments to determine the ultimate stress of particles, the particle fracture energy and the degree of breakage obtained. The trend observed by Stamboliadis (2002), Morrison & Cleary (2004), and Shi & Kojovic (2007) pertaining to the relationship between the degree of breakage obtained with increasing specific comminution energy will be compared to the findings made in this work. This work also involves extending coarse particle breakage characterization to the breakage characterization of finer particles. Therefore understanding the effect of particle size as described by Sikong et al. (1990), Schonert (1991), Tavares & King (1998) and Tavares & King (2004) on breakage behaviour is of importance. The findings made by Khanal et al. (2007) and Barrios et al. (2011) relating the degree of breakage obtained to the bed depth will be compared to the findings made in this work. Additionally, in this work the breakage behaviour of particles under partial confinement is investigated. The bed is contained in a material that offers more resistance than the paper used by Barrios et al. (2013), but also allows for movement and repositioning of the particles within the bed unlike in fully confined conditions.

2.9. Hypotheses and research questions

The following hypotheses have been formulated:

1. The fraction of input energy used for particle fracture is reliant on the three variables investigated in this work: steel ball mass, drop height and bed depth. Although the fracture energy changes with the three variables, the greatest variation occurs with bed depth. The thickness and arrangement of particles within the bed greatly influence

the amount of energy utilized for breakage, where an increase in bed depth results in a decrease in the energy used for particle fracture.

2. For an increase in input energy resulting from increasing either steel ball mass or drop height, a larger relative increase in the degree of particle breakage obtained is caused by increasing ball mass rather than drop height. Of the two variables, an increase in ball mass leads to an increase in contact surface area for balls of the same material density. This leads to an increase in contact surface area, exposing more particles to impact and resulting in higher breakage.

On the basis of the postulated hypotheses and the objectives of the study, breakage experiments will be conducted to answer the following key questions:

- What is the effect of altering the three variables: steel ball mass, drop height and bed depth on the peak force obtained?
- What is the effect of changing the three variables on the fraction of input energy used for particle fracture?
- What effect does changing the three variables have on the degree of particle breakage obtained?
- What is the relationship between the fracture energy and the degree of breakage obtained?

3. EXPERIMENTAL

Overview

This chapter provides details of the experimental work done for the purposes of addressing the research questions. A description of the apparatus used for experiments is given, followed by the procedure followed for SILC calibration. The sample preparation and experimental methods used to conduct breakage experiments are then given. The design of the experiments used to obtain breakage data is included at the end of this section.

3.1. Description of the apparatus

As mentioned in Section 2.4.5, the SILC consists of a steel rod on which the bed of particles sits, and a pneumatic drop weight mechanism used to release the steel ball when a breakage test is conducted. The rod is fitted with strain gauges to measure the load response due to the steel ball dropped from a known height. The voltage-time data saved from the test can be displayed on a computer screen and used to determine the Force-time history of the breakage test.

A schematic indicating the main components of the SILC is shown in Figure 3.1.

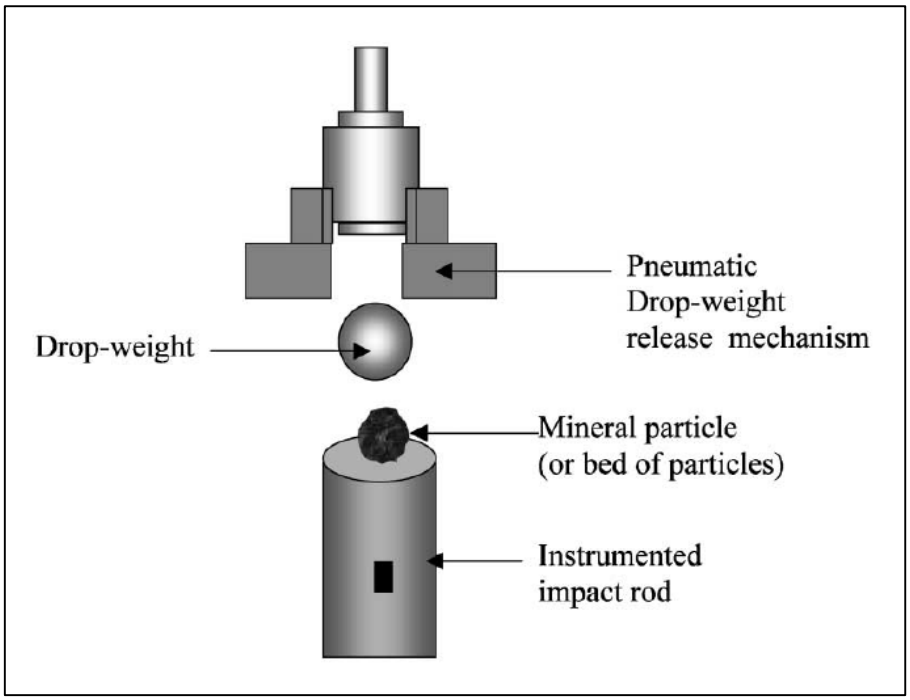

Figure 3.1: The drop weight mechanism and rod fitted with strain gauges which comprise the main components of the SILC. The particle sample rests on the steel rod and the ball is released from the drop weight mechanism at various heights (Bourgeois & Banini, 2002).

The SILC and computer experimental set-up used for this work are shown in the image in Figure 3.2. The experimental work was conducted at the Centre for Minerals Research (CMR) laboratories at the University of Cape Town.

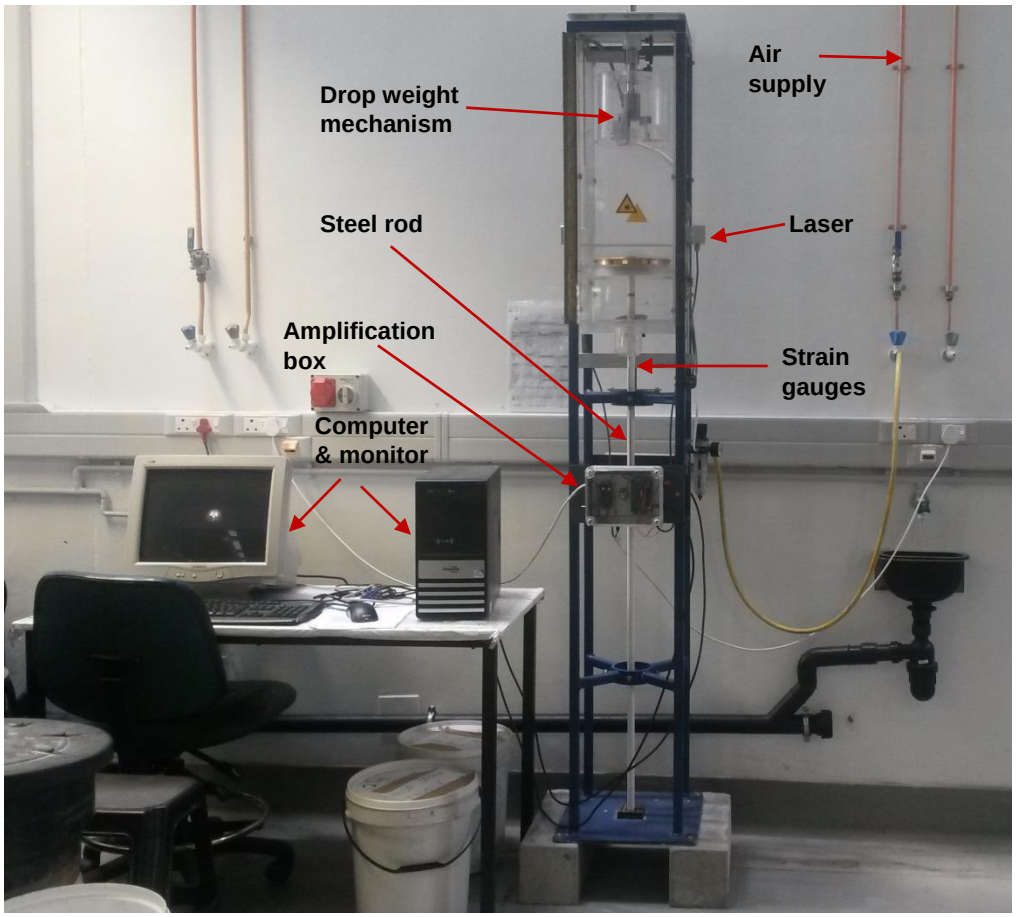

Figure 3.2: Experimental set-up showing the SILC used to conduct breakage tests and the computer used to view the test results

Kyowa strain gages of type KFG-5-120-C1-11L1M2R and resistance 120.4 ± 0.4 Ω (manufacturer's specifications) are fitted onto the steel rod used in the SILC. A proprietary amplifier circuit was designed and built by the Chemical Engineering electronics workshop, which passed the signal from the strain gauges through a low pass filter to reduce the noise and amplify the signal with an adjustable gain. A capture card was used to capture the signal onto a computer. The computer's data acquisition software was a GUI built in National Instruments DAQ for which one could adjust the capture frequency. The properties of the SILC steel rod are given in Table 3.1.

Table 3.1: Properties of the SILC steel rod

Length (m)	1.50
Diameter (mm)	20
Density (kg/m^3)	7815
Young's modulus (N/m^2)	2.11E+11

Five steel balls of varying mass and size were used. Their respective masses and diameters are shown in Figure 3.3.

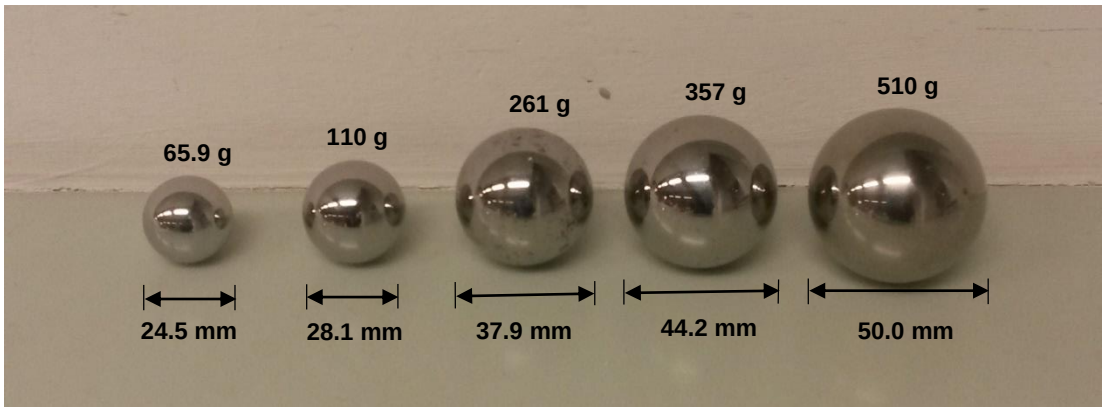

Figure 3.3: The five steel balls used to conduct breakage tests arranged in increasing size, from the smallest to the largest diameter

3.2. Calibration of the SILC

The largest steel ball weighing 510 g was used for SILC calibration, where it was dropped directly onto the rod to obtain steel-on-steel velocity-time profiles. Four drop heights were used for calibration tests: 120, 180, 240 and 300 mm and three tests were conducted at each drop height for repeatability. Data generated from the steel-on-steel tests was used to calculate a calibration factor (See Section 3.2.3.)

3.2.1. Calibration procedure

The calibration procedure used in this work is as follows:

1. Adjust the pneumatic drop-weight mechanism so that it can accommodate the 510 g steel ball which will be used for steel-on-steel impact tests
2. Use the height adjustment system on the SILC to obtain a drop height of 300 mm

3. Run a calibration test, releasing the steel ball directly onto the rod and saving the steel-on-steel impact results generated from the test
4. Repeat steps 1-3 three times, ensuring to save the generated breakage test data each time
5. Repeat steps 3-4, using drop heights of 240, 180 and 120 mm
6. Calculate a calibration constant (See Section 3.2.3)

3.2.2. Calibration results

The output obtained when a calibration test is conducted is in the form of a voltage vs time curve. The voltage is shown as Amplitude and the time is shown as Sample number. A typical voltage vs time signal obtained for steel-on-steel impact is shown in Figure 3.4. The voltage scale is in Volts x 10^4. The sample number can be converted to units of time by using the sample rate as follows:

$$Time = \frac{Sample\ number}{Sample\ rate} \qquad \text{Equation 3.1}$$

In work done by Bourgeois & Banini (2002) a 2.5 MHz sample rate was used and Tavares & King (2004) used a sample rate of 2 MHz for experiments. Before experiments were conducted, new strain gauges were fitted onto the SILC used in this work to improve the sample rate from the low value of 4000 Hz. The sample rate of 3 MHz was selected as the most suitable as it is in line with that used by other researchers.

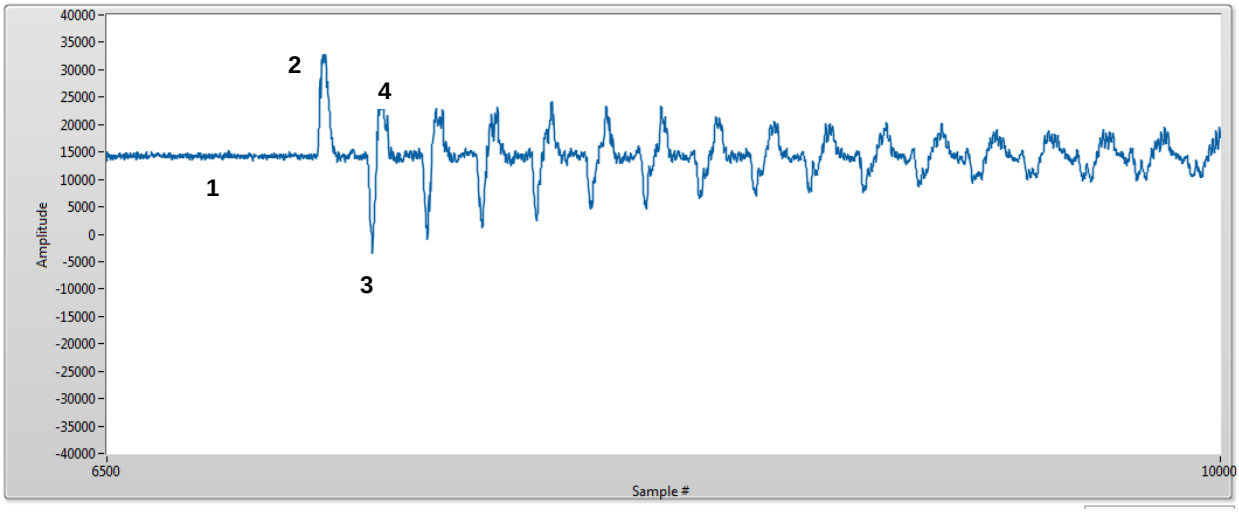

Figure 3.4: Voltage vs time signal generated from a test conducted using the 510 g steel ball dropped from a height of 300 mm

Figure 3.4 shows that there is a time delay, labelled as '1', before impact occurs. This is because test data is recorded from the instant the falling ball passes the laser beam, and impact only occurs after several microseconds have elapsed. The impact event is shown by the pulse labelled as '2'. The signal wave decays with time because it naturally disperses due to radial inertia as it travels through the rod. Because the strain gauges are situated closer to the anvil, the initial pulse '2' travels through the rod where it is partially absorbed at the base of the rod. The remainder of the pulse is reflected back up the rod as the pulse labelled as '3'. Thereafter, there is a shorter duration between pulse '3' and '4' because pulse '3' travels through a shorter distance up the rod before returning down as pulse '4'. This contributes to the attenuation in the oscillations which is observed.

Figure 3.5 shows the voltage vs time signals of the three steel-on-steel tests done for calibration using the largest ball weighing 510 g released from the 300 mm drop height. The calibration voltage-time signals obtained at the 120, 180 and 240 mm drop heights are shown in Appendix B.

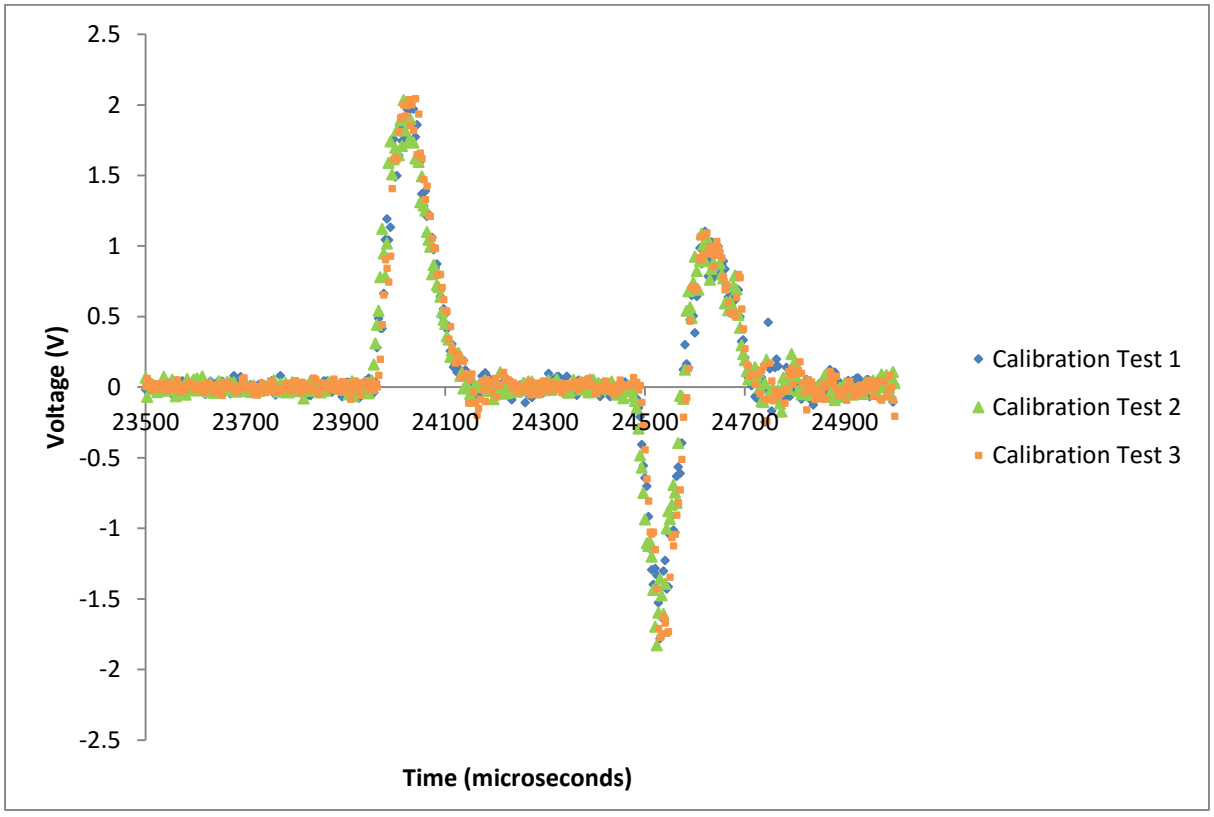

Figure 3.5: Plot of three steel-on-steel calibration tests conducted for the 510 g ball dropped at a height of 300 mm

Figure 3.5 shows that the voltage-time signals were consistent which indicates that the calibration tests were repeatable.

3.2.3. Determination of the calibration factor

In this section the steps followed to determine the calibration factor used to relate the voltage-time data to the stress transmitted through the SILC steel rod are given.

To determine the ball velocity, v_b, the falling ball is assumed to be in free fall and the collision of the ball with the particle sample is assumed to be perfectly elastic. Therefore, the potential energy of the ball before release is assumed to be equal to its kinetic energy just before impact as shown in Equation 3.2:

$$mgh_0 = \frac{1}{2}mv_{ball}^2 \qquad \text{Equation 3.2}$$

Where:

m: Mass of the steel ball (kg)

g: Acceleration due to gravity (m/s^2)

h_0: Initial height of the steel ball before it released (m)

v_{ball}: Velocity of the steel ball just before impact (m/s)

The velocity of the rod upon impact is found by elastic contact theory and is given as (Bbosa, 2007):

$$v_{rod} = v_{ball}\left(\frac{A_{ball}}{A_{ball} + A_{rod}}\right) \qquad \text{Equation 3.3}$$

Where:

v_{rod}: Rod velocity (m/s)

v_{ball}: Ball velocity (m/s)

A_{ball}: Effective area of the ball (m^2)

A_{rod}: Cross-sectional area of the rod (m^2)

Note: The effective area of impact of a steel ball with a steel surface is approximated as 10 % of the ball's cross sectional area.

One dimensional stress wave theory is used to evaluate the stress applied to the steel rod. This is given by Wang (2011) as:

$$\sigma = Cv_{rod}\rho \qquad \text{Equation 3.4}$$

Where:

σ: Stress applied to the steel rod (N/m^2)

C: Pulse speed (m/s)

v_{rod}: Rod velocity (m/s)

ρ: Steel rod density (kg/m^3)

The pulse speed through the rod, C, is determined from the relationship shown in Equation 3.5:

$$C = \frac{2L}{pulse\ time} \qquad \text{Equation 3.5}$$

Where:

L: Length of the rod (m)

From the calibration test, the average maximum voltage can be determined by finding the mean value when the voltage signal is at its peak.

The calibration factor is given as a ratio of the stress per unit voltage and is determined using Equation 3.6:

$$K = \frac{\sigma}{V_{avg}} \qquad \text{Equation 3.6}$$

Where:

K: Calibration factor (Pa/V)

σ: Stress applied to the steel rod (Pa)

V_{avg}: Maximum average velocity obtained for a breakage test (V)

For each calibration involving a different height it was assumed that all the energy evolved from the falling ball was transferred to the rod upon impact. To verify the constistency of the calibration constants calculated at each of the four heights, Equation 3.6 was manipulated into the linear function $\sigma = KV_{avg}$ which was plotted using the experimental values as shown in Figure 3.6.

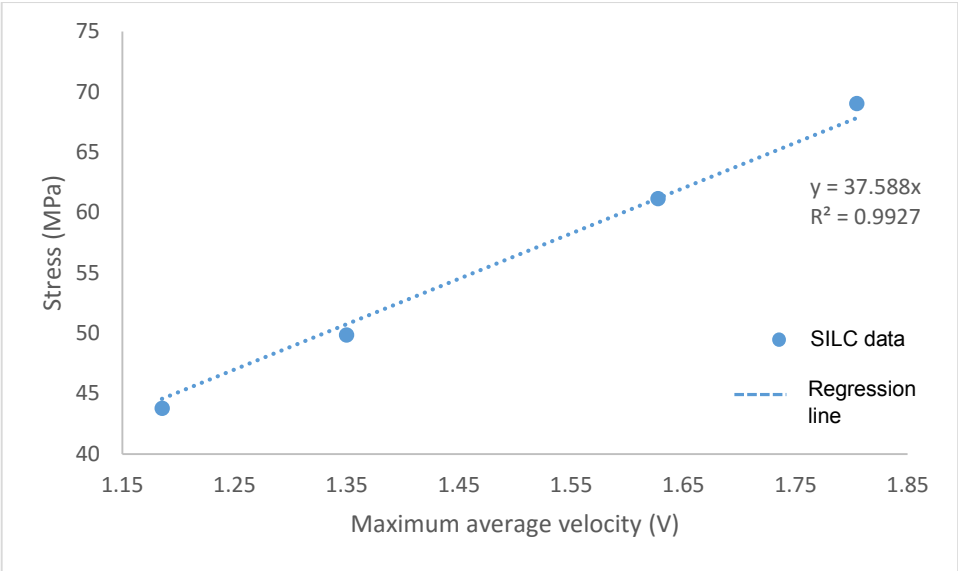

Figure 3.6: The stress as a function of maximum average velocity at the four drop heights used for calibration

The experimental calibration constant, which was found to have a value of 37.6 MPa/V, was determined as the gradient of the linear equation shown in Figure 3.6. The R-squared value of 0.993 obtained was close to unity indicating that the SILC data was a very close fit to the linear regression line.

The calculated calibration constant was compared to a theoretical one given by Equation 3.7 (Bbosa, 2007):

$$K_{theoretical} = \frac{4E}{ABvF} \qquad \text{Equation 3.7}$$

Where:

E: Young's modulus of the rod

A: Amplifier gain

B: Bridge factor

V: Bridge excitation voltage

F: Gauge factor

The theoretical calibration constant was found to be 40.4 MPa/V, signifying a 6.9 % deviation between the theoretical and experimentally determined values. The calculations done to evaluate both calibration constants are given in Appendix A.

3.3. Sample preparation

3.3.1 Ore used for breakage tests

The breakage tests conducted in the proposed study are done on two different ore types: Blue stone and UG2 ore. These two ore types have been discussed further in the sections that follow.

Blue stone

Blue stone is igneous, dark bluish-grey coloured rock which has a consistent grain structure (Bbosa, 2007). This material is easy to process due to its homogeneity which makes it suitable for use as an aggregate in construction. Crushed blue stone can be used as a road base, concrete and asphalt pavement aggregate, and as filter stone in drain fields.

Upper Group 2 (UG2) chromitite ore

South African reserves of platinum group metals (PGMs) are found in the Bushveld Complex which consists of three layers, namely the Merensky Reef, Platreef and the UG2 chromitite layer (Schouwstra et al., 2000). These three layers each have their own distinctive associated mineralogy (McLaren & De Villiers, 1982). UG2 ore consists mainly of chromitite (60-90%), orthopyroxene, and plagioclase. It also consists of small amounts of talc, chlorite, and phlogopite, as well as smaller amounts of base-metal and other sulphides and platinum-group minerals. The base metals contained in the ore are predominantly pentlandite, chalcopyrite, pyrrhotite and pyrite. UG2 grades vary from 3-8 g/t PGM but the Cr_2O_3 content of the ore presents major challenges in processing (Cramer, 2001).

The elastic properties of the two ores differ as blue stone has a modulus of elasticity of 78 GPa at ambient temperature and pressure and that of UG2 is approximately 50 GPa (Schultz, 1995; Singh et al., 2005).

Figure 3.7 shows the ore hardness of different commodities. The parameter used as an indicator of the ore's resistance to break is the Drop Weight Index (DWi) which is expressed as in kWh/t. Lower DWi values indicate softer ores and higher values are an indication of hard ores.

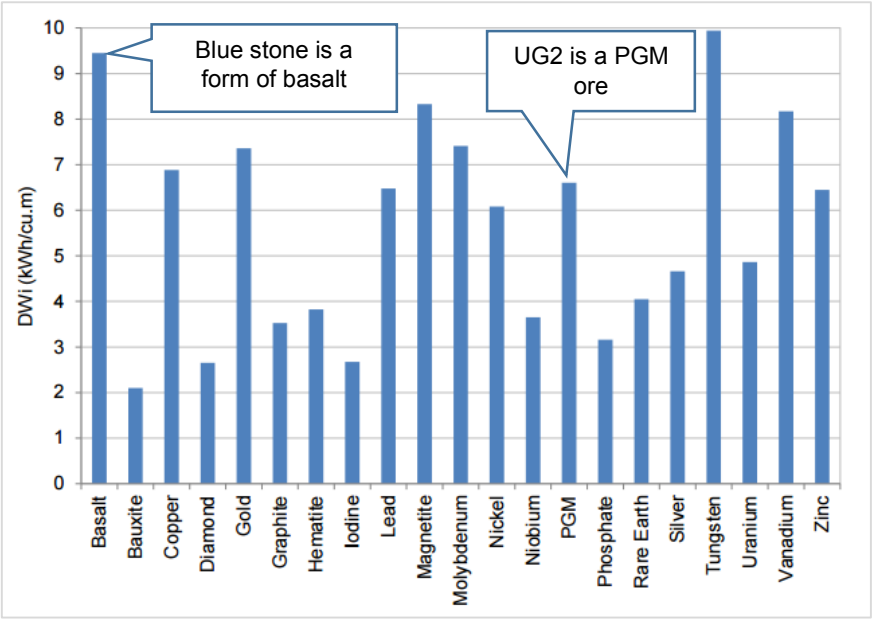

Figure 3.7: Mean DWi values for different ores (Morrell, 2015)

From Figure 3.7 it is seen that basalt has a DWi value of approximately 9.5 kWh and PGMs have a lower DWi of approximately 6.7 kWh. From this it can be inferred that, although both ores can be classified as hard ores, blue stone is harder than UG2.

For both ores used to conduct experimental work, particles of similar mean geometric size were used. A summary of the particle sizes used for each ore is given in Table 3.2.

Table 3.2: Mean particle sizes used for experimental test work conducted on the SILC

Ore	Particle size range (mm)	Mean geometric size (mm)
Blue stone	-5.6 + 4	4.73
UG2	-6.7 + 3.35	4.74

These particle sizes were considered adequate based on the size of the SILC, where large sizes were not suitable for the attainment of a bed of particles as the steel rod only has a diameter of 20 mm. Using these particle sizes, a bed could be obtained as between five and six particles could sit on the rod surface.

3.3.2. Sample preparation for blue stone

Agitated sieves in series were used to obtain three size classes of the ore which had already been crushed to sizes < 10 mm. The size classes were identified as - 4mm, - 5.6 + 4 mm and +6.5 mm. For this work, blue stone particles of size - 5.6 + 4 mm were used to conduct

breakage tests because it was presumed that particles smaller than this size would result in little or no breakage due to the hardness of the ore. The particles used were irregularly shaped and angular as shown in Figure 3.8. The South African one rand coin was used as an indication of the size of the particles.

Figure 3.8: Blue stone ore particles used to conduct bed breakage tests

3.3.3. Sample preparation for UG2

The 250 kg ore sample, received from the Bathopele mine in Rustenburg South Africa, was initially screened to remove the particles smaller than 3.35 mm as these were smaller than the size range required in this work. Particles in the size range -32 + 13.2 mm were reduced in size using the cone crusher in the UCT Centre for Minerals Research labs. Rocks larger than 32 mm were reduced in size using the jaw crusher in the UCT Geological Sciences department. The crushed particles were all blended and then screened to remove particles of sizes + 6.7 and -3.35 mm as they were not in the particle size range that would allow for a similar geometric mean size as that of the blue stone particles used. The size range of UG2 particles used for experiments was – 6.7 + 3.35 mm. The particles which were in the desired size range were proportioned into 10 kg batches using a riffle splitter. The samples were then further proportioned into 1 kg amounts using a rotary splitter, where each 1 kg batch was considered to be representative of the ore received from Bathopele mine. The UG2 particles used for experiments are shown in Figure 3.9. Similarly to Figure 3.8, the one rand coin was used as an indication of the size of the particles.

Figure 3.9: UG2 particles used for bed breakage tests on the SILC

3.3.4. Obtaining the desired bed thickness

The effect of altering the particle bed thickness was investigated by varying the number of particle layers contained in each bed, ranging from one to nine layers. Each bed of particles was contained in a cylindrical ring designed to accommodate the desired number of particle layers. In order to test for the most suitable material to use for construction of the cylindrical rings, breakage tests were conducted in which paper, stiff paper and duct tape were used to make the rings. Using each ring, three breakage tests at identical conditions (510 g steel ball, 300 mm drop height and 3 layers contained in the bed) were conducted. The force-time profiles obtained for the different materials are shown in Figure 3.10 to Figure 3.12. These were compared to determine the best material to use for test work.

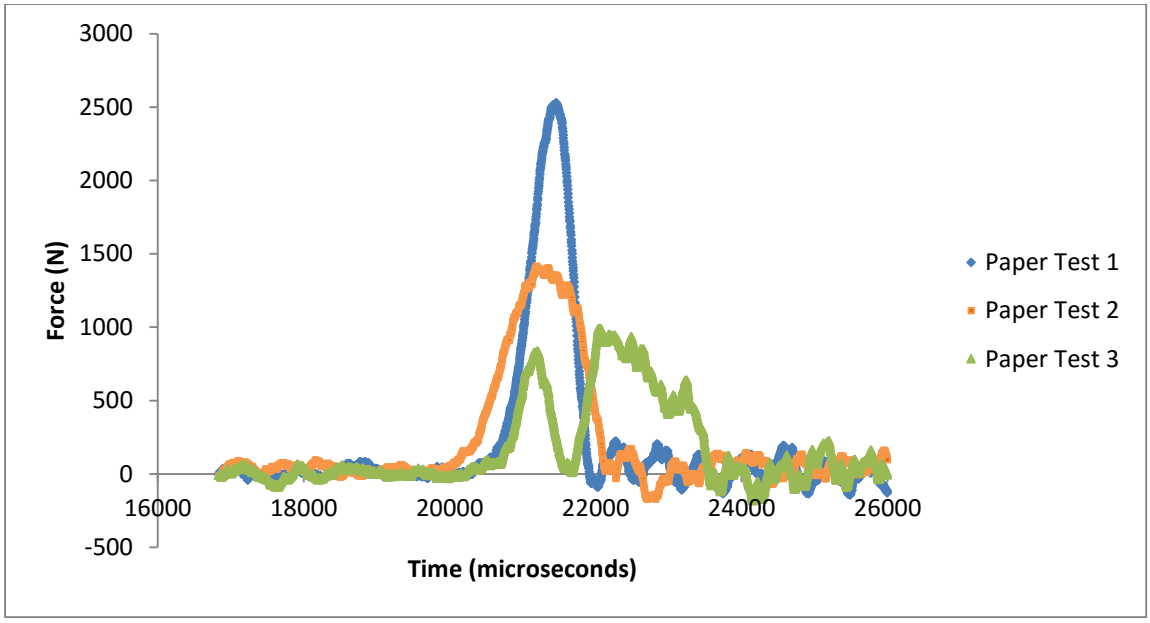

Figure 3.10: Force-time profiles obtained using paper to construct cylindrical rings used to hold particles contained in the bed

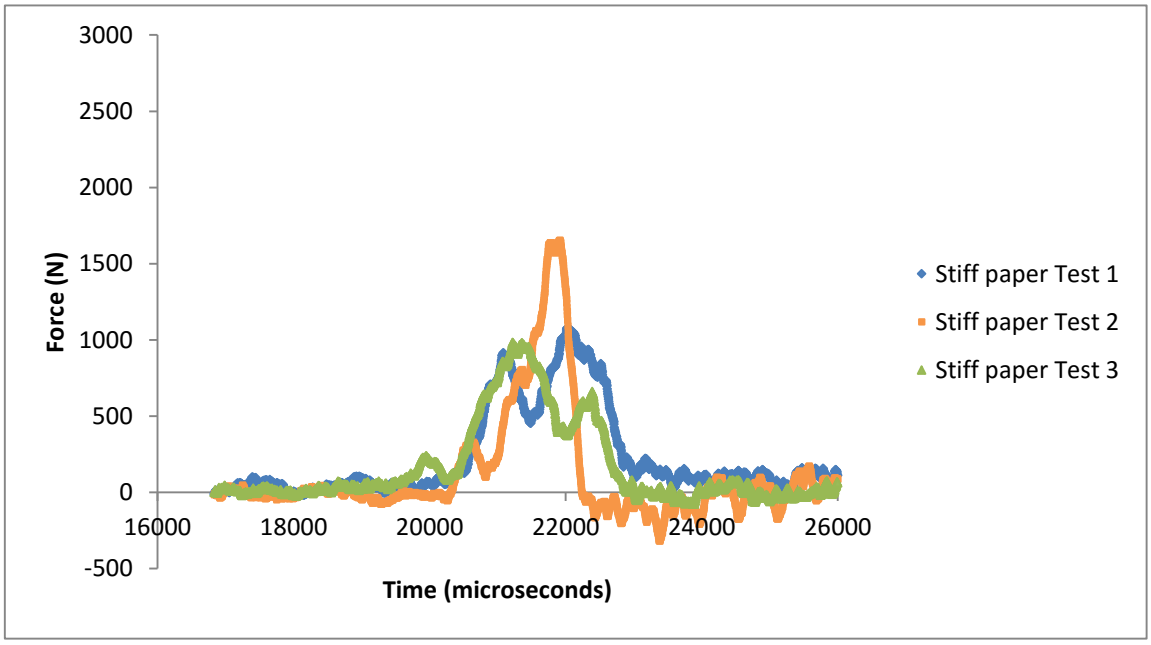

Figure 3.11: Force-time profiles obtained using stiff paper to construct cylindrical rings used to hold particles contained in the bed

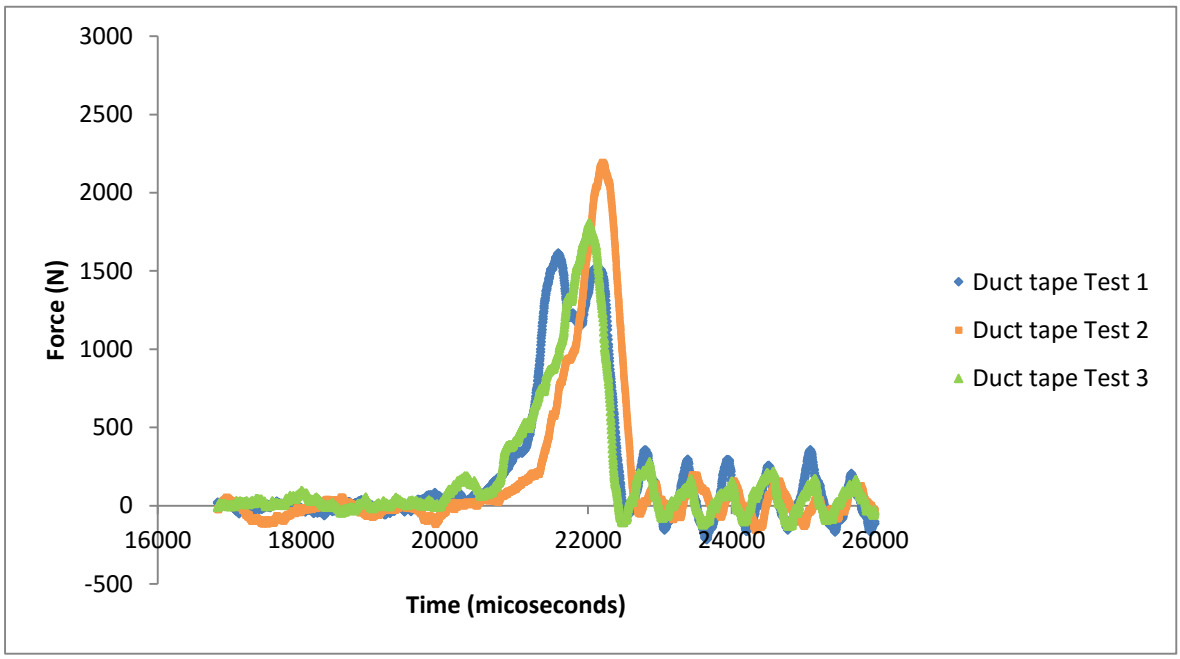

Figure 3.12: Force-time profiles obtained using duct tape paper to construct cylindrical rings used to hold particles contained in the bed

From comparison of Figure 3.10 to Figure 3.12, duct tape was selected to be the most suitable material to use for the construction of the cylindrical rings used to hold particles contained in the bed. This is because it yielded the most consistent Force-time results in comparison to paper and stiff paper.

The five cylindrical rings of varying height that were constructed using duct tape to hold 1, 3, 5, 7 and 9 layers of particles for test work are shown in Figure 3.13.

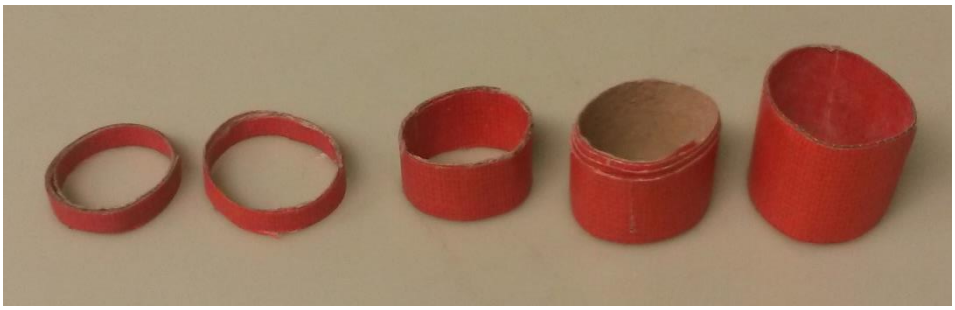

Figure 3.13: The cylindrical rings used to contain particles in a bed for breakage tests, arranged in increasing number of layers contained in the bed

For blue stone, tests were conducted using 1, 3, 5, 7 and 9 layers contained in the bed and tests conducted on UG2 only contained 1 to 7 layers. The cylindrical rings remained intact upon impact when breakage tests were conducted.

3.4. Experimental procedure used to conduct bed breakage tests using the SILC

The standard procedure outlined in the SILC Data Acquisition Module-Operation and Design (De Beers, 2002) was adapted to conduct breakage tests:

1. Adjust the pneumatic drop-weight mechanism so that it can accommodate the steel ball which will be used for the breakage test.
2. Obtain the desired drop height by using the height adjustment system on the SILC.
3. Place particles of the desired bed depth in a hollow cylindrical ring, constructed of duct tape, on the SILC steel rod. The ring is used to ensure that the particles are a partially confined.
4. Release the steel ball onto the bed of particles to break the ore sample upon impact. The impact breakage event is recorded and can be viewed on a computer in the form of a voltage-time signal.
5. After the test has been conducted, collect and weigh the broken sample. The broken sample is used to determine the particle size distributions resulting from the breakage test.

Figure 3.14 (a) is indicates a typical setup used to conduct a breakage test. The partially confined particles sit on the SILC steel rod. The ruler on the height adjustment system is used to achieve the desired drop height and the steel ball is kept in place using the pneumatic drop weight mechanism. Figure 3.14 (b) is a close up image of the particles resting on the steel rod.

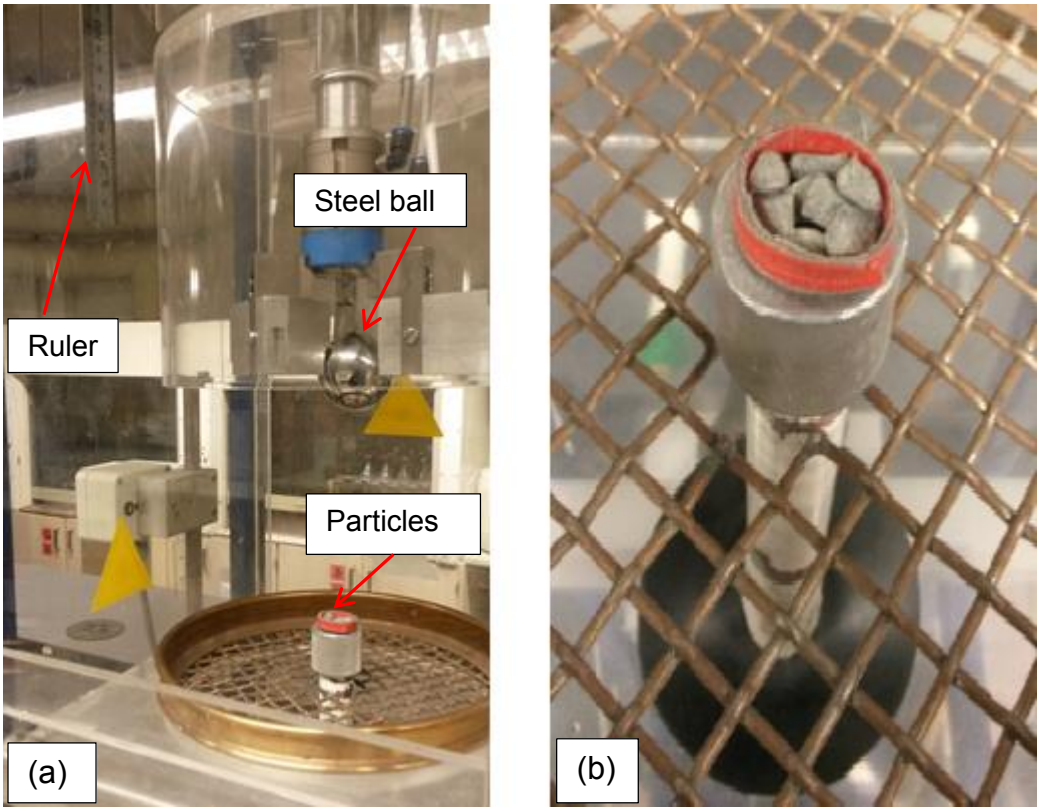

Figure 3.14: Typical setup of the bed of particles, steel ball and drop height for a breakage test on the SILC

Figure 3.15 shows the outcome of a typical breakage test conducted using the SILC, where the pulse indicates when the breakage event occurred. Note: The sample number on the x-axis can be converted to units of time by using Equation 3.1 (Section 3.2.2). The Amplitude on the y-axis represents Voltage (in Volts x 10^{-4}).

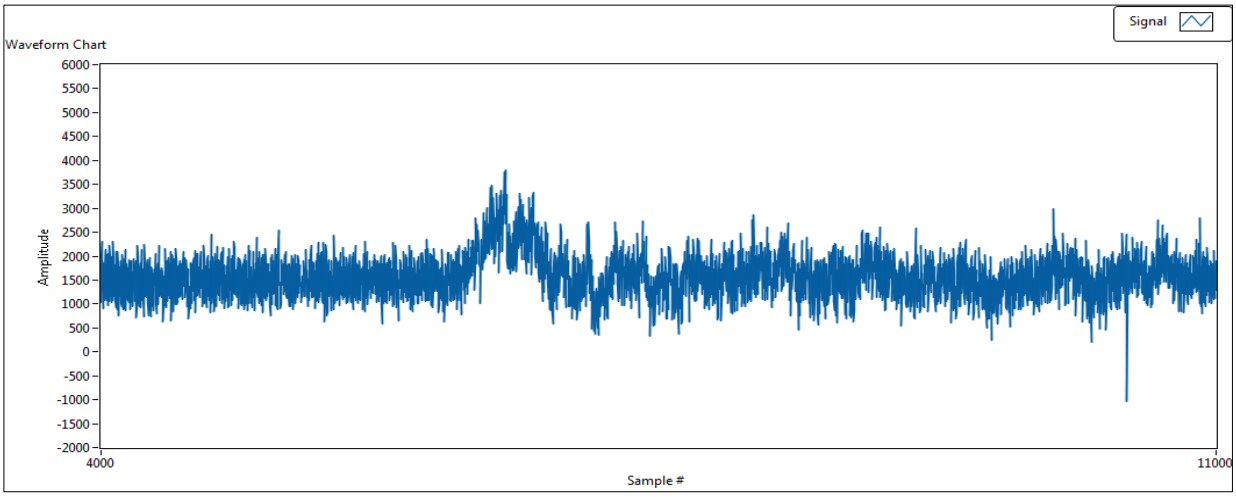

Figure 3.15: Typical breakage test outcome obtained on the SILC at a drop height of 300 mm using the 510 g steel ball

From Figure 3.15 it is seen that there was a large amount of noise in the raw signals obtained from tests. For calculations, the raw Voltage-time data was converted to Force-time signals and a moving average of 100 data points was used on Microsoft Excel to clean up the signals. It was found that this methodology deconvoluted the electrical noise from the strain gauges while maintaining the integrity of the signal.

3.5. Determination of the Particle Size Distributions (PSDs)

Particle size distributions were used to evaluate the extent to which the particle sample was broken when breakage tests were conducted. Sieves of different aperture sizes were used in series and the mass of ore retained on each sieve was recorded and used to determine the PSD.

For blue stone, sieves of aperture sizes 8, 5.6, 4, 2.8 and 2 mm were used on an agitated shaker to screen the samples after breakage tests were conducted. For UG2, sieves of aperture sizes of 8, 5.6, 4, 2.8, 2 and 1.4 mm were used.

3.6. Design of experiments

In the experiments, the effect of varying the steel ball mass, drop height and bed depth on the degree of breakage was investigated. Each of the three variables was considered at different values: a range of low, intermediate and high values. This was done for each of the two ores on which breakage tests were conducted.

3.6.1. Experiments conducted on blue stone

The steel ball mass, drop height and number of layers contained in the bed were each varied between five values which are shown in Table 3.3.

Table 3.3: Values of the variables which were altered in the experiments conducted on blue stone

Number of particle layers	Drop height (mm)	Steel ball mass (g)
1	60	66
3	120	110
5	180	261
7	240	357
9	300	510

The number of different possible variable configurations was determined using Equation 3.8:

$$N = N_{PL} \times N_{DP} \times N_{SBM} \qquad \text{Equation 3.8}$$

Where

N: Number of possible variable configurations

N_{PL}: Number of particle layers

N_{DP}: Number of drop heights

N_{SBM}: Number of steel ball masses

From using Equation 3.8, it was found that 125 different variable configurations were required to test the three variables at five different levels. Reproducibility of the experiments was tested by conducting three tests at each variable configuration.

3.6.2. Experiments conducted on UG2

For UG2, no breakage tests were conducted using the 66 g ball and 60 mm drop height. Also, no tests containing 9 layers of particles in the bed were conducted (See Section 5.1). The steel ball mass, drop height and number of layers contained in the bed were each varied between four values which are shown in Table 3.4.

Table 3.4: Values of the variables used for experiments done on UG2

Number of particle layers	Drop height (mm)	Steel ball mass (g)
1	120	110
3	180	261
5	240	357
7	300	510

From using Equation 3.8, it was found that 64 different variable configurations were required to test the three variables at four different levels. Similarly to the tests conducted on blue stone, reproducibility of the experiments done on UG2 was tested by conducting three tests at each variable configuration.

4. BLUE STONE RESULTS

Overview

This chapter presents the experimental results for breakage tests conducted on blue stone. Screening of the progeny particles resulting from breakage tests showed that at all input energies, negligible breakage was obtained as all the particles remained in the same starting size range of -5.6 + 4 mm. Therefore, only peak force results are reported and no fracture energy or breakage results are presented for this ore.

4.1. Peak force results

Breakage tests were conducted at twenty-five input energies, by varying the steel ball mass and drop height on the Short Impact Load Cell between the values shown in Table 3.3 (Section 3.6.1). Tests were conducted on one, three, five, seven and nine layers. All tests were conducted in triplicate so the standard error was representative.

The peak force results are presented for each steel ball mass, with increasing drop height and bed depth. Sample calculations showing the method used to determine the peak forces are given in Appendix A.

4.1.1. Peak force results obtained using the 510 g steel ball

The input energy values used for breakage tests are shown in Table 4.1. The input energies were calculated using Equation 2.14 from the assumption that energy is conserved, therefore the input energy onto the particles is equal to the potential energy of the steel ball before it is released (Section 2.6.1).

Table 4.1: Input energy values for the 510 g steel ball released from various heights

Drop height (mm)	Input energy (J)
60	0.30
120	0.60
180	0.90
240	1.20
300	1.50

The peak force results for the steel ball dropped from the five different heights are shown in Figure 4.1. For the 60, 180, 240 and 300 mm heights the maximum peak forces were obtained

at one layer of particles. At one, three, five and seven layers the highest peak forces were obtained at the greatest drop height; however at the largest bed depth the peak force at 240 mm was 11 % greater than that at 300 mm.

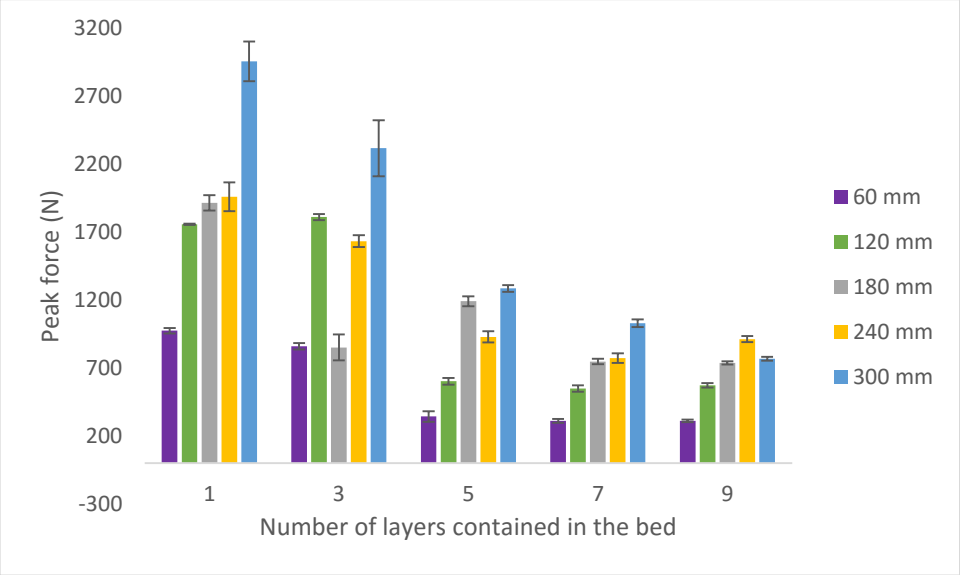

Figure 4.1: Peak forces obtained at various drop heights, represented as a function of the number of layers contained in the bed for tests conducted using the 510 g ball

At the lowest height of 60 mm, the peak force decreased by 8 % when the bed depth was increased from one to three layers. There was a greater reduction, of 60 %, in the peak force with an increment in the bed depth from three to five layers. Increasing the bed depth from five to seven and nine layers resulted in statistically similar peak forces being obtained.

For tests conducted at the 120 mm drop height, statistically similar peak force results were obtained at bed depths of one and three layers. Similar findings to those observed at 60 mm were made when the bed depth was increased from three to nine layers. The peak force decreased by 67 % when the number of layers was increased from three to five and statistically identical peak forces were obtained with an increment in the bed depth from five to seven and nine layers.

For the 180 mm drop height the greatest peak force was obtained at one layer and it decreased by 56 % with an increase in bed depth to three layers. This result differed from that obtained for the 120 mm drop height, where statistically similar peak forces were attained at the two lowest bed depths. Also, in different findings to those made at the two lowest drop heights, at 180 mm the peak force obtained at five layers was 20 % greater than that obtained at three layers. Statistically equal peak forces were obtained at seven and nine layers, which were the lowest for all bed depths at this input energy.

At a drop height of 240 mm the peak force followed a continuous decreasing trend with an increase in layers from one to seven. In different findings to those made at the lower drop heights, there was an increment of 17 % in the peak force when the bed depth was increased from seven to nine layers.

For tests conducted at the 300 mm drop height the largest peak force was obtained at one layer and it continuously decreased for all layers. This result differed from that obtained at the lower drop heights, as none of the other results showed a continuously decreasing trend with increasing bed depth.

For the tests conducted, the greatest peak forces were generally attained at the 300 mm drop height and the lowest were found at 60 mm. Statistically identical peak forces were obtained at the adjacent drop heights of 180 and 240 mm for one and seven layers. Several tests showed a result in which the peak forces found at lower drop heights were greater than those at larger heights for the same bed depth. At three layers, the peak force at 120 mm was greater than both those at 180 and 240 mm. At five layers the peak force at 180 mm was greater than that at 240 mm and was statistically similar to that at 300 mm.

4.1.2. Peak force results obtained using the 357 g steel ball

The input energy values for the ball released from each drop height are given in Table 4.2.

Table 4.2: Input energy values for the 357 g steel ball released from various heights

Drop height (mm)	Input energy (J)
60	0.21
120	0.42
180	0.63
240	0.84
300	1.05

Figure 4.2 shows the peak force results obtained. Similar to the findings made for the 510 g ball, the highest peak forces were found at one layer for all the input energies. At all bed depths the greatest peak forces were attained at the two largest input energies. Comparison of the results shown in Figure 4.2 and Figure 4.1 shows that the peak forces at all bed depths were greater for the 510 g ball than they were for the 357 g ball.

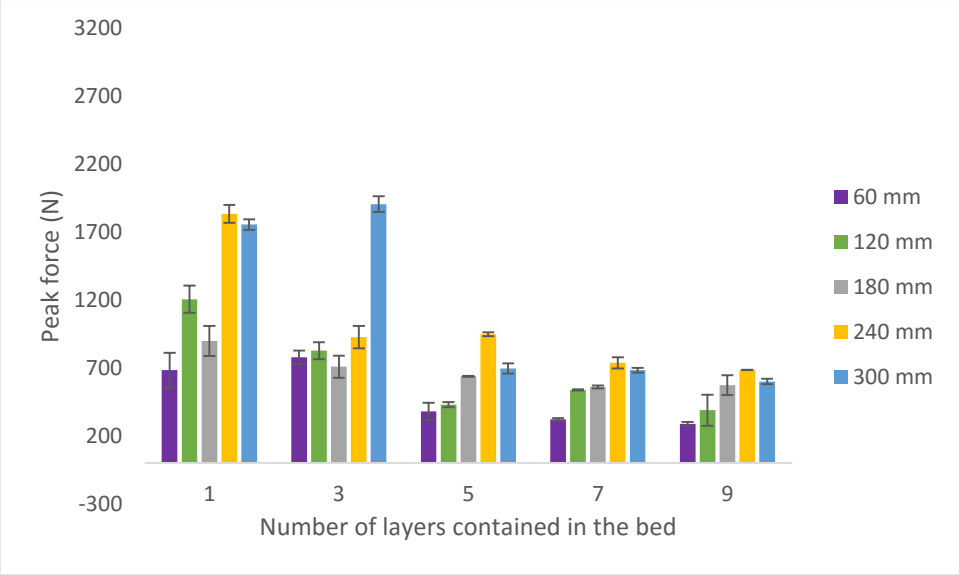

Figure 4.2: Peak forces obtained at various drop heights, represented as a function of the number of layers contained in the bed for tests conducted using the 357 g ball

At a drop height of 60 mm, statistically equal peak forces were obtained at one and three layers. This finding is similar to that made for the 510 g ball at this drop height. When the number of layers was increased from three to five the peak force decreased by 51 %. The peak forces obtained at five, seven and nine layers were statistically similar, and were also the lowest which is synonymous with the trends observed from tests conducted using the 510 g ball.

For breakage tests conducted at the 120 mm drop height, the peak force decreased continuously with an increase in layers from one to five. The peak force obtained at seven layers was 20 % greater than that at five layers. Statistically, the peak force obtained at a bed depth of nine layers was identical to that at seven layers.

At the 180 mm drop height statistically similar peak forces were found at one and three layers. A 10 % reduction in peak force was obtained when the bed depth was increased from three to five layers. Statistically, the peak forces at five, seven and nine layers were the same. This result is similar with that obtained at the 60 mm drop height, where statistically equal results were also found at the three largest bed depths.

For the 240 mm drop height the greatest peak force was obtained at one layer and it decreased by 49 % when the number of layers was increased from one to three. The peak forces obtained at three and five layers were statistically identical and there was a 12 % reduction in peak force when the bed depth was increased from five to seven layers. The results obtained at seven and nine layers were statistically equal, which is a similar finding to that made at the 60 and 180 mm drop heights.

At a drop height of 300 mm the peak force at three layers was slightly greater than that obtained at one layer. There was a decrease of 60 % in the peak force when the bed depth was increased from three to five layers. Statistically, the results obtained at five and seven layers were equal and the peak force at nine layers was slightly lower (by 12 %) than these.

For the tests conducted, the lowest peak forces were generally found at the 60 mm drop height at all bed depths. Statistically similar peak forces were obtained at the adjacent drop heights of 240 and 300 mm at one, seven and nine layers. Some tests showed a result in which the peak force found at a lower drop height was greater than at a larger height for the same bed depth. At 120 mm the peak force was larger than at 180 mm for one layer, and at 240 mm it was greater than at 300 mm for five layers.

4.1.3. Peak force results obtained using the 261 g steel ball

Table 4.3 shows the input energy values used to conduct tests.

Table 4.3: Input energy values for the 261 g ball released from various heights

Drop height (mm)	Input energy (J)
60	0.15
120	0.31
180	0.46
240	0.61
300	0.77

The peak force results are shown in Figure 4.3. At the four lowest bed depths the highest peak forces were obtained at the largest drop height which is a similar finding to that made for the 510 and 357 g balls. At a bed depth of nine layers the greatest peak force was attained at 180 mm, where this value was slightly larger than that at 300 mm. The peak forces obtained at 180 and 240 mm were statistically similar at the four lowest bed depths; however at a bed depth of nine layers the peak force at 180 mm was 27 % greater than that at 240 mm. Comparison of the results shown in Figure 4.3 and Figure 4.2 shows that the peak forces obtained using the 261 g and 357 g balls were similar.

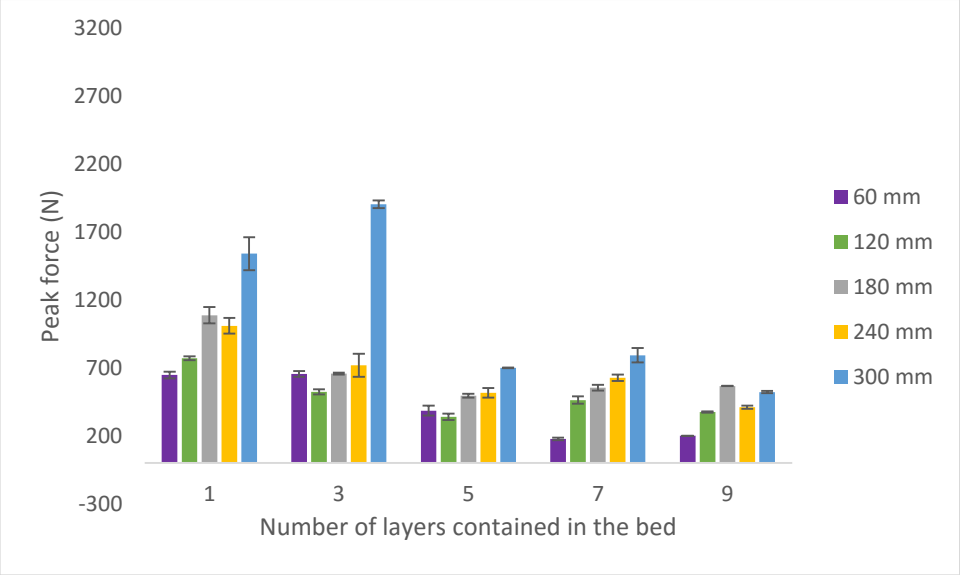

Figure 4.3: Peak forces obtained at various drop heights, represented as a function of the number of layers contained in the bed for tests conducted using the 261 g ball

At the 60 mm drop height the peak forces at one and three layers were almost identical. This result is similar to the findings made for the 510 g and 357 g balls at this drop height. Increasing the bed depth from three to five layers resulted in a 41 % decrease in the peak force. When the bed depth was increased from five to seven layers the peak force decreased by 54 %, and it remained approximately the same when the depth of the bed was increased to nine layers. The findings made, where similar peak forces were obtained at bed depths of seven and nine layers, are similar to those made for the 510 g and 357 g balls at the 60 mm drop height.

At the 120 mm drop height a continuous decreasing trend in peak force was observed when the bed depth was increased from one to five layers. The peak force obtained at nine layers was similar to that at five layers; however at seven layers it was found to be 21 % greater than that at five layers.

For breakage tests conducted at the 180 mm drop height it was found that the peak force continuously decreased with increasing bed depth from one to five layers. The 39 % decrease in peak force observed when the number of layers was increased from one to three was larger than the 25 % reduction obtained when the bed depth was increased from three to five layers. At seven and nine layers statistically similar peak forces were obtained, which is a synonymous result to that found at the 60 mm drop height.

At the 240 mm drop height a similar trend to that observed at 120 mm was found. The peak force decreased continuously when the number of particle layers was increased from one to five. However, increasing the number of layers from five to seven resulted in an 18 % increase in peak force. The lowest peak force, 35 % lower than that at seven layers, was obtained at a bed depth of nine layers.

The results obtained at the 300 mm drop height were unlike any of the findings made at the lower drop heights, as the peak force at three layers was found to be greater than at one layer. When the bed depth was increased from three to five layers a 63 % reduction in peak force was obtained. The peak force at seven layers was slightly greater than that at five layers and there was a reduction of 34 % when the number of layers was increased from seven to nine.

For all the tests conducted, the greatest peak forces were generally obtained at the 300 mm drop height. Statistically equal peak forces were obtained at the adjacent drop heights of 180 and 240 mm at the four lowest bed depths. For some tests the peak force at a lower drop height was greater than at a larger height for the same bed depth. The peak force at 60 mm was greater than at 120 mm for a bed depth of three layers, and at nine layers the peak force at 180 mm was larger than at 240 mm and was statistically similar to that at 300 mm.

4.1.4. Peak force results obtained using the 110 g steel ball

Table 4.4 shows the input energy values used for breakage tests.

Table 4.4: Input energy values for the 110 g ball released from different heights

Drop height (mm)	Input energy (J)
60	0.07
120	0.13
180	0.19
240	0.26
300	0.32

The peak force results are shown in Figure 4.4. For the four largest drop heights, the greatest peak forces were obtained at one layer of particles; however at the lowest drop height the peak force at three layers was slightly greater than that at one layer. The peak forces at the largest input energy were not consistently greater than those at lower input energies for all the bed depths, which is seen in the results obtained at one, three and nine layers. At one layer the peak force at 180 mm was greater than that at 300 mm. At a bed depth of three layers the peak forces at the 120 and 300 mm drop heights were statistically equal, and nine layers the results obtained for the 240 and 300 mm drop heights were statistically similar. Comparison of these results with those obtained for the larger steel balls showed that the peak forces obtained using the 110 g ball were the lowest.

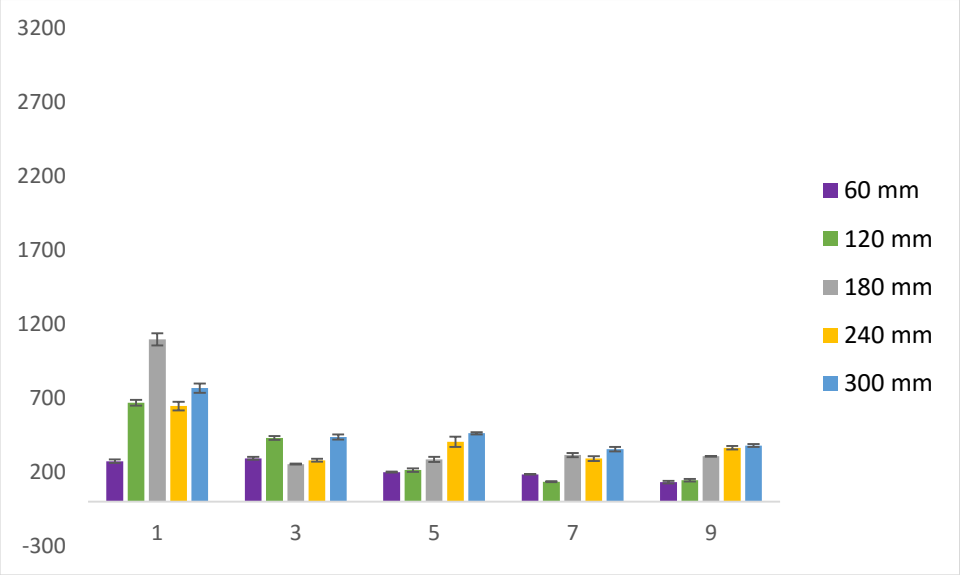

Figure 4.4: Peak forces obtained at various drop heights, represented as a function of the number of layers contained in the bed for tests conducted using the 110 g ball

At the 60 mm drop height a similar trend to that observed for the larger steel balls was found with increasing layers from one to five, where statistically identical peak forces were obtained at one and three layers and the peak force decreased, by 32 %, when the bed depth was increased from three to five layers. The peak force obtained at a bed depth of seven layers was statistically similar to that at five layers; however it decreased by 29 % when the number of layers was increased to nine.

At the 120 mm drop height the peak force decreased continuously with increasing number of layers from one to seven. Statistically, equal peak forces were obtained at seven and nine layers, where these were the lowest attained for this input energy. The similar peak force results obtained at the two largest bed depths were synonymous with the findings made at this drop height using the 510 and 357 g balls.

For breakage tests conducted at the 180 mm drop height the highest peak force was obtained at one layer and it decreased by 77 % when the number of layers was increased to three. The peak force increased slightly with increasing bed depth from three to five layers. Statistically similar peak forces were obtained at bed depths of five, seven and nine layers.

Similar to the 120 and 180 drop heights, the highest peak force at 240 mm was also obtained at one layer. It decreased by 57 % when the number of layers was increased to three; however it increased by 31 % when the layers were increased from three to five. Increasing the bed depth from five to seven layers resulted in a 28 % reduction in peak force; however the peak force increased by 20 % when the number of layers was increased from seven to nine.

For the 300 mm drop height the maximum peak force was obtained at one layer and it decreased by 43 % when the number of layers was increased to three. Statistically similar results were obtained at bed depths of three and five layers. The peak force decreased by 23 % when the number of layers was increased to seven and the result at nine layers was statistically the same as that at seven layers.

For the tests conducted, statistically similar peak forces were obtained at five and seven layers for the 240 and 300 mm drop heights. For some tests the peak forces at smaller drop heights were greater than at larger heights. For one layer, the peak force at 180 mm was larger than at 300 mm. For three layers the peak force at 120 mm was greater than both those obtained at 180 and 240 mm and was statistically similar to that at 300 mm.

4.1.5. Peak force results obtained using the 66 g steel ball

The input energy values used for tests are shown in Table 4.5.

Table 4.5: Input energy values for the 66 g ball released from various heights

Drop height (mm)	Input energy (J)
60	0.04
120	0.08
180	0.12
240	0.16
300	0.20

The input energy values obtained using this ball were very low. As a result, the voltage-time signals, which are used to determine the Force-time results, were indistinguishable from the noise generated by the SILC. The peak force results for tests conducted at 66 g could therefore not be determined and all data generated using this steel ball could not be used for results analysis.

5. UG2 RESULTS

Overview

The experimental results obtained for breakage tests conducted at the different input energies used are presented in this chapter. The results are given in three sections: Section 5.1 presents the peak force results, the fracture energy results are given in Section 5.2 and Section 5.3 presents the breakage results obtained.

The experimental matrix for tests was determined based on the observations made for tests conducted on blue stone. The drop heights and steel ball masses used are given in Table 3.4 (Section 3.6.2). The number of layers contained in the bed was varied from one to seven because the blue stone results revealed that the peak force was not significantly affected by the presence of a ninth layer. Additionally, no breakage tests were conducted at the 60 mm drop height because this input energy had resulted in very low peak forces for blue stone, and it was expected that the same results would be obtained for UG2. Furthermore, breakage tests were not conducted using the 66 g steel ball because it had not yielded any useful results for blue stone. Similar to the blue stone experiments, tests were done in triplicate in order to determine the experimental error associated with each test.

5.1. Peak force results

The peak force results are shown for each steel ball mass, with increasing drop height and bed depth.

5.1.1. Peak force results obtained using the 510 g ball

The input energy values used for breakage tests are given in Table 4.1 (Section 4.1.1).

The peak force results are shown in Figure 5.1. For all input energies, the maximum peak force was obtained at one layer of particles. At one layer the greatest peak force was found at the largest input energy; however at bed depths of three, five and seven layers the peak forces obtained at the two largest input energies were statistically identical. For the two lowest input energies, statistically similar peak force results were obtained at bed depths of one, three and seven layers. Comparison of the results shown in Figure 5.1 with those for blue stone presented in Figure 4.1 shows that the peak forces obtained for blue stone were higher than those obtained for UG2 at the same input energies.

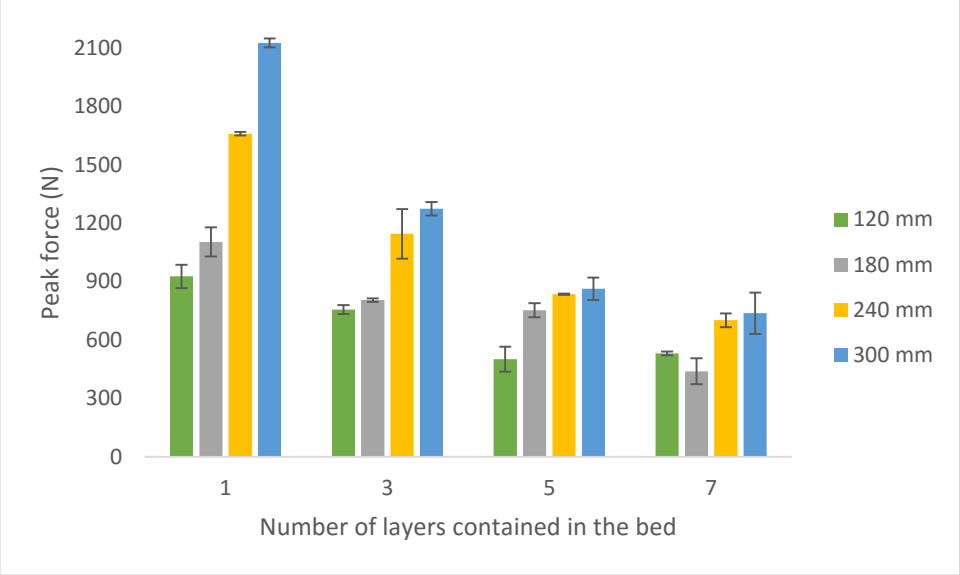

Figure 5.1: Peak forces obtained at various drop heights, represented as a function of the layers contained in the bed for tests conducted using the 510 g ball

At the 120 mm drop height the peak force decreased, by 46 %, with increasing bed depth from one to five layers. Statistically equal peak force results were obtained at five and seven layers, which were the lowest obtained at this drop height.

For tests conducted at 180 mm the peak force decreased by 27 % when the number of layers was increased from one to three. Statistically, the peak force obtained at five layers was similar to that at three layers; however it decreased by 35 % when the bed depth was increased to seven layers.

At the 240 mm drop height, the peak force decreased continuously with an increase in the number of layers from one to seven. The decrease in peak force was greater at lower bed depths of one and three layers than it was with increasing number of layers at the largest bed depths.

A similar trend to that observed at the 120 mm drop height was found at 300 mm, where the peak force decreased continuously with an increase in the number of layers from one to five. For this drop height it was also observed that increasing the number of layers at the lowest bed depths of one and three layers led to a larger reduction, of 40 %, in the peak force than that obtained (31 %) when the number of layers was increased from three to five. Statistically similar peak force results were obtained at bed depths of five and seven layers.

From all the tests conducted it was found that the peak force increased continuously with increasing drop height at one layer. Discrepancies from this observation were made at larger bed depths. Results where statistically similar peak forces were obtained at adjacent drop

heights were found for tests conducted at 120 and 180 mm at three layers, and at 240 and 300 mm for the three largest bed depths.

5.1.2. Peak force results obtained using the 357 g ball

The input energies used to conduct breakage tests are shown in Table 4.2 (Section 4.1.2).

The peak force results are shown in Figure 5.2. Comparison of these results with those obtained for the largest ball showed that the peak forces found using the 357 g ball were lower. In similar findings to those made for the 510 g ball, the maximum peak forces were obtained at one layer of particles for all input energies. At each bed depth, the greatest peak forces were found at the largest drop height. Comparison of the results shown in Figure 5.2 with the blue stone results presented in Figure 4.2 showed that the blue stone peak forces were higher than those obtained for UG2 at the same input energies. This observation is synonymous with the findings made for the largest steel ball.

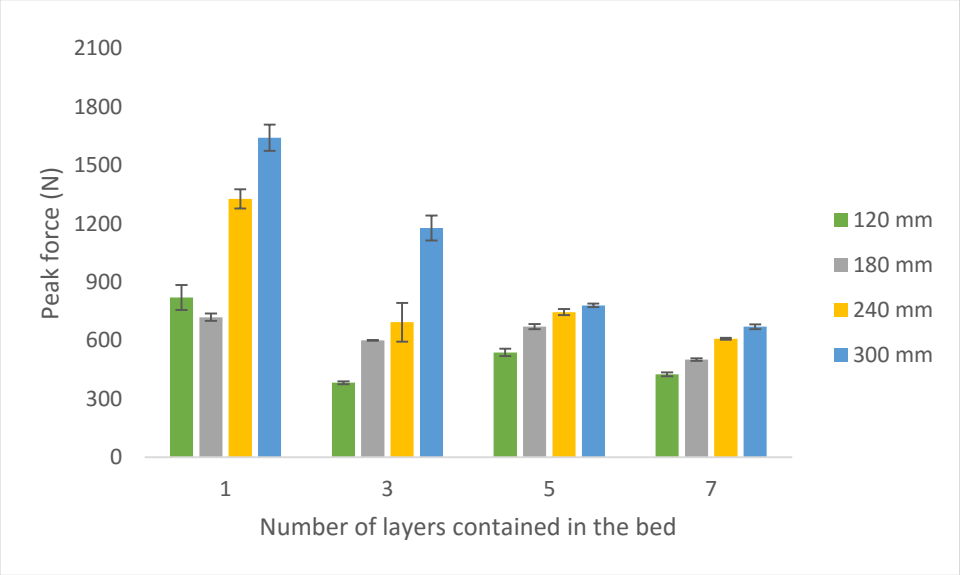

Figure 5.2: Peak forces obtained at various drop heights, represented as a function of the number of layers contained in the bed for tests conducted using the 357 g ball

At the 120 mm drop height the results obtained across the bed depths did not follow a specific trend. The largest peak force was obtained at one layer and it decreased by 53 % when the number of layers was increased to three. There was a 29 % increase in peak force when the bed depth was increased from three to five layers and a 20 % reduction when the number of layers was increased from five to seven.

Similar observations to those made for the 120 mm drop height were found at 180 mm. The peak force decreased by 16 % when the number of layers was increased from one to three.

Increasing the bed depth from three to five layers resulted in a 10 % increase in peak force; however it decreased by 25 % when the bed depth was increased from five to seven layers.

For the 240 mm drop height the peak force decreased by 48 % with an increment in number of layers from one to three. The peak forces at five and seven layers were statistically similar to that at three layers.

At 300 mm the peak force decreased continuously with increasing number of layers from one to seven. The reduction in peak force was greater at lower bed depths than it was at larger bed depths: there was a 28 % decrease in peak force when the number of layers was increased from one to three and a 14 % reduction when the bed depth was increased from five to seven layers. This finding is synonymous with that made at 240 and 300 mm using the largest steel ball.

From the tests conducted, it was found that the peak force increased continuously with increasing drop height at bed depths of five and seven layers. Statistically identical peak forces were obtained at the adjacent drop heights of 180 and 240 mm at three layers.

5.1.3. Peak force results obtained using the 261 g ball

The input energies used for breakage tests are shown in Table 4.3 (Section 4.1.3).

Figure 5.3 shows the peak force results obtained. Comparison of these results with those obtained for the 357 g ball showed that the peak forces found using the 261 g ball were slightly lower. In different findings to those made for tests conducted using the 510 and 357 g balls, it was found that for the input energies used, the peak forces obtained at one layer were not consistently greater than those at the larger bed depths.

At one layer the highest peak force was found at the largest input energy; however at bed depths of three, five and seven layers the peak forces obtained at the two largest input energies were statistically equal. This result is similar to that obtained for tests conducted using the 510 g ball.

Comparison of the results in Figure 5.3 to those obtained for blue stone presented in Figure 4.3 showed that the peak forces obtained for blue stone were greater than those for UG2. This result is similar to that found for the 510 g and 357 g balls.

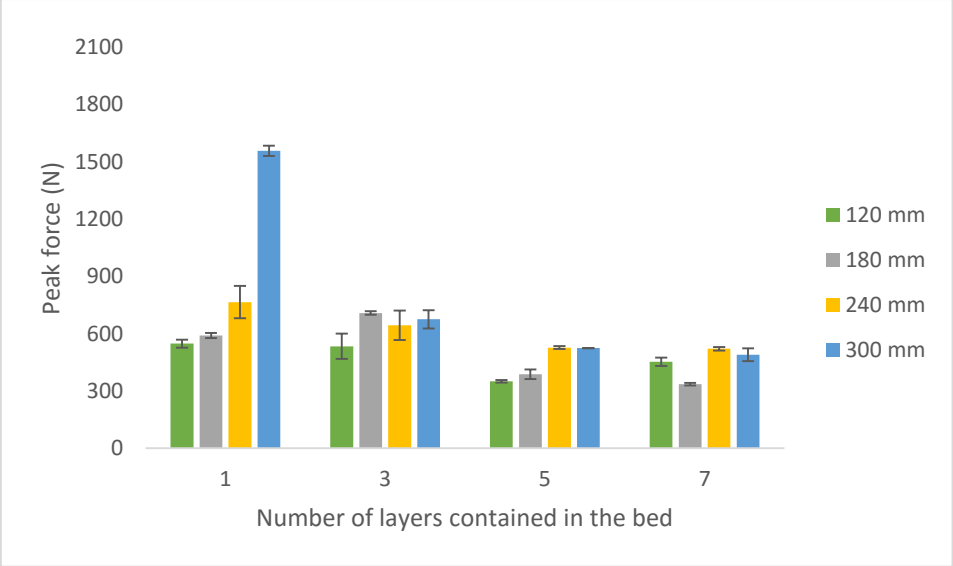

Figure 5.3: Peak forces obtained at various drop heights, represented as a function of the number of layers contained in the bed for tests conducted using the 261 g ball

At the 120 mm drop height the peak forces obtained at one and three layers were statistically similar. When the bed depth was increased from three to five layers there was a 34 % reduction in peak force; however the peak force at seven layers was 23 % greater than that at five layers.

At the 180 mm drop height the peak force at three layers was 17 % greater than that at one layer. It decreased by 49 % with increasing number of layers from three to seven.

For breakage test conducted at the 240 mm drop height the peak forces obtained at one and three layers were statistically identical. This result is the same as that obtained at 120 mm. The peak force decreased slightly when the bed depth was increased from three to five layers and identical peak forces were obtained at bed depths of five and seven layers.

At 300 mm the peak force decreased continuously with increasing number of layers from one to five. Increasing the number of layers from one to three layers led to a larger reduction, of 57 %, in the peak force than that obtained (20 %) when the number of layers was increased from three to five. This finding is the same as that made for tests conducted at this drop height using the largest steel ball. Statistically, the peak forces obtained at bed depths of five and seven layers at this drop height were equal.

For all the tests conducted, statistically identical results were obtained for the adjacent heights of 120 and 180 mm at one layer, and 240 and 300 mm at the three largest bed depths. One test showed a result where the peak force obtained at a smaller drop height was greater than that at a larger height for the same bed depth. This finding was made at a bed depth of seven layers where the peak force at 120 mm was greater than at 180 mm.

5.1.4. Peak force results obtained using the 110 g ball

The input energies used for breakage tests are shown in Table 4.4 (Section 4.1.4).

The peak force results are shown in Figure 5.4. Comparison of these results with those obtained for the larger balls showed that the peak forces found using the 110 g ball were the lowest. At all bed depths, the greatest peak forces were obtained at the two largest input energies. Similar findings to those made for tests conducted using the 510 and 261 g balls were made where at one layer the highest peak force was found at the largest input energy; however statistically similar results were obtained at the two largest input energies at bed depths of three, five and seven layers.

Comparison of the results shown in Figure 5.4 to those for blue stone presented in Figure 4.4 showed that the peak forces obtained for blue stone were higher than those for UG2 for all input energies. This result is synonymous with that obtained for tests conducted using the larger steel balls.

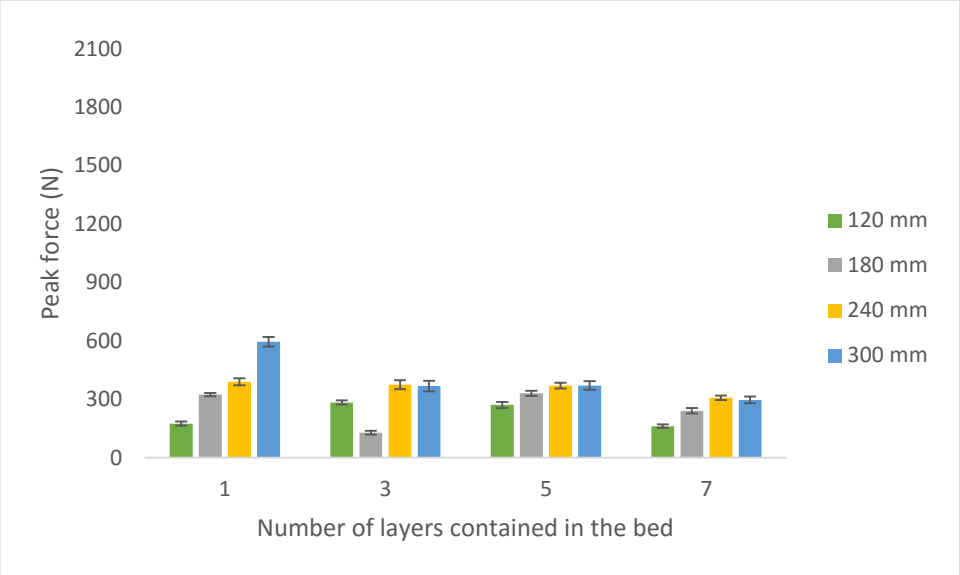

Figure 5.4: Peak forces obtained at various drop heights, represented as a function of the number of layers contained in the bed for tests conducted using the 110 g ball

At the 120 mm drop height, different findings to those made for tests conducted using the larger steel balls were made as the peak forces at three and five layers were both greater than at one layer. The results obtained at these two bed depths were statistically equal and the peak force decreased when the bed depth was increased from five to seven layers.

For the 180 mm drop height the peak force decreased by 60 % when the number of layers was increased from one to three. However, the peak force obtained at five layers was 61 % greater than that at three layers. There was a 27 % reduction in peak force when the depth of the bed was increased from five to seven layers.

At the 240 mm drop height the results at one, three and five layers were statistically similar. The peak force decreased by 17 % when the bed depth was increased from five to seven layers.

At 300 mm the peak force decreased by 38 % when the number of layers was increased from one to three. Statistically similar peak force results were obtained at bed depths of three and five layers. The lowest peak force at this input energy, which was 20 % lower than that at five layers, was obtained at seven layers.

For all the tests conducted, a result in which the peak force increased continuously with increasing drop height was found at one layer. This result was not obtained at the larger bed depths. Statistically similar peak forces were found at the adjacent drop heights of 240 and 300 mm for the three largest bed depths. A result in which the peak force at a smaller drop height was greater than at a larger height for the same bed depth was found for one test: at a bed depth of three layers where the peak force at 120 mm was larger than that at 180 mm.

5.2. Fracture energy results

The fracture energy results are presented in this section. These results are shown as a percentage of the input energy used to cause failure in the specimen for increasing ball mass, drop height and bed depth.

5.2.1. Fracture results obtained using the 510 g steel ball

The fracture energy results are shown in Figure 5.5. Relative to the input energy, the energy utilized for particle fracture was low, with the maximum values ranging between 1.8 and 2.5 %. For all bed depths the maximum fracture energy was obtained at the two largest drop heights. The fracture energy values for these drop heights at one, three and seven layers were statistically identical.

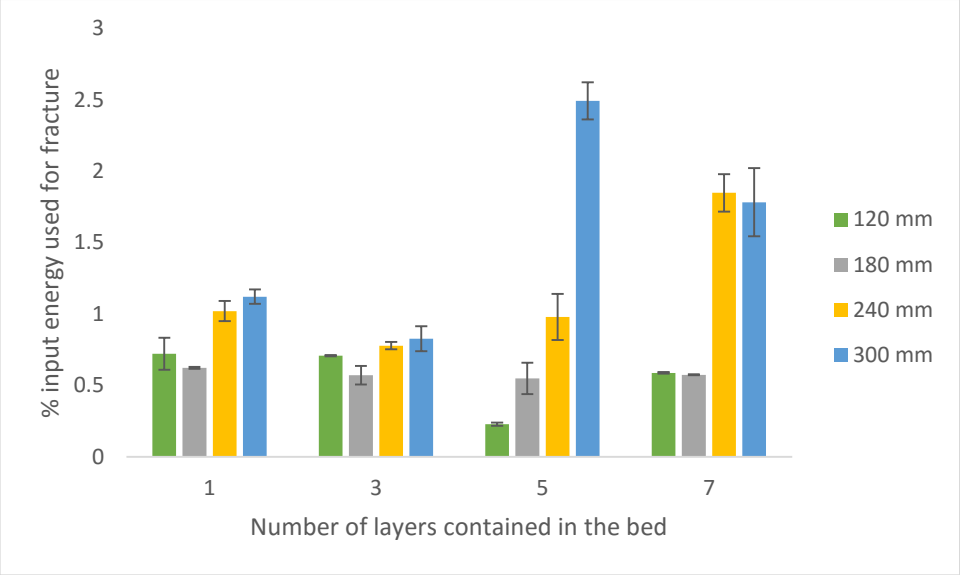

Figure 5.5: The fracture energy at various drop heights, represented as a function of the number of layers contained in the bed for tests conducted using the 510 g ball

At the 120 mm drop height the fraction of input energy used for particle fracture was low and below 1 % at all bed depths. Statistically similar values were obtained at one and three layers. Increasing the number of layers from three to five resulted in a decrease from 0.7 to 0.2 % in the amount of energy used for fracture, where this value was the lowest obtained at this drop height. The fracture energy increased slightly to 0.6 % of the input energy when the bed depth was increased from five to seven layers.

At the 180 mm drop height a low fracture energy value of 0.6 % of the input energy was obtained at one layer. Statistically identical fracture energy results were obtained at all the other bed depths.

For tests conducted at the 240 mm drop height it was found that the energy used for fracture decreased slightly from 1.0 to 0.8 % when the number of layers was increased from one to three. The small difference of 0.2 % in the results obtained at these bed depths is negligible and suggests that these values were the same. The result at five layers was statistically similar to that at one layer and there was an increase to 1.8 % energy used for fracture when the bed depth was increased from five to seven layers.

At 300 mm no specific trend in the results was observed. The energy used for fracture decreased from 1.1 to 0.8 % with an increase in the number of layers from one to three; however it increased to 2.5 % with increasing bed depth from three to five layers. The fraction of energy utilized for fracture decreased to 1.8 % when the bed depth was increased from five to seven layers.

For all the tests conducted, a result in which statistically similar % input energy used for fracture values were obtained at adjacent drop heights was found for tests conducted at 120 and 180 mm for one and seven layers, and 240 and 300 mm for one, three and seven layers.

Comparison of the peak forces shown in Figure 5.1 and the % energy used for particle fracture presented in Figure 5.5 showed that the maximum peak forces were obtained at one layer when a low fraction of the input energy was utilized for particle fracture. Likewise, the highest amount of energy was used for fracture at the largest bed depths of five and seven layers when the peak forces were low.

5.2.2. Fracture energy results obtained using the 357 g ball

Figure 5.6 shows the fracture energy results. Similar to the results obtained for the 510 g ball, the fraction of input energy used for particle fracture was low, with the maximum values ranging between 2.0 and 2.7 %.

The highest % energy used for fracture was obtained at the largest input energy for all bed depths, with the maximum value obtained at a bed depth of seven layers. At the lowest bed depths, one and three layers, there was only a marginal difference in the amount of energy used for fracture at 240 and 300 mm. The difference in the results obtained at these two drop heights became more distinct at the largest bed depths of five and seven layers, where higher fracture energy values were obtained at 300 mm.

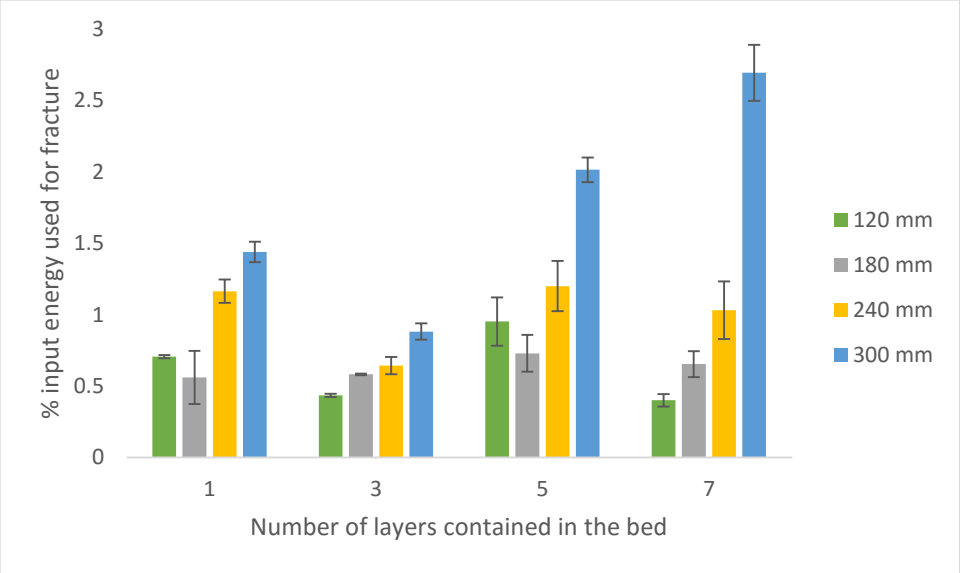

Figure 5.6: The fracture energy at various drop heights, represented as a function of the number of layers contained in the bed for tests conducted using the 357 g ball

For the 120 mm drop height the fracture energy values were low and were all below 1.5 %. The fracture energy decreased slightly from 0.7 to 0.4 % with an increment in number of layers from one to three, where the small difference of 0.3 % in the results obtained at these bed depths suggests that these values were inherently the same. The amount of energy used for fracture increased to 0.95 % when the bed depth was increased from three to five layers. Increasing the number of layers from five to seven led to a reduction to 0.4 % in the energy utilized for fracture.

At 180 mm statistically similar fracture energy values were obtained at one and three layers. There was a marginal increase from 0.6 to 0.7 % energy used for fracture with increasing bed depth from three to five layers. The slight difference of 0.1 % in these results is negligible and it can be said that these values were the same. The fracture energy results obtained at five and seven layers were statistically equal.

At 240 mm the % fracture energy decreased slightly from 1.1 to 0.6 % when the bed depth was increased from one to three and increased to 1.2 % when the number of layers was increased from three to five. Statistically identical fracture energy results were obtained at five and seven layers.

For tests conducted at 300 mm the % energy used for fracture decreased slightly from 1.4 to 0.9 % when the number of layers was increased from one to three. Increasing the bed depth from three to seven layers led to an increase to 2.7 % energy used for fracture, where this was the maximum value attained at this drop height.

Comparison of the peak forces shown in Figure 5.2 and the fracture energy results in Figure 5.6 showed that the maximum peak forces were obtained at one layer when low energies were used for particle fracture. The greatest fraction of energy was used for breakage at five and seven layers when the peak forces were low.

5.2.3. Fracture energy results obtained using the 261 g ball

The fracture energy results are shown in Figure 5.7. Similar to the results obtained for the 510 g and 357 g steel balls, the fracture energy values for this ball were also low, with the maximum values ranging between 1.4 and 1.7 %.

At the largest bed depths of five and seven layers, the highest fracture energy values were obtained at the two largest drop heights. However, this result was not observed at one and three layers. At these bed depths the difference in the % energy used for fracture at the four drop heights was marginal.

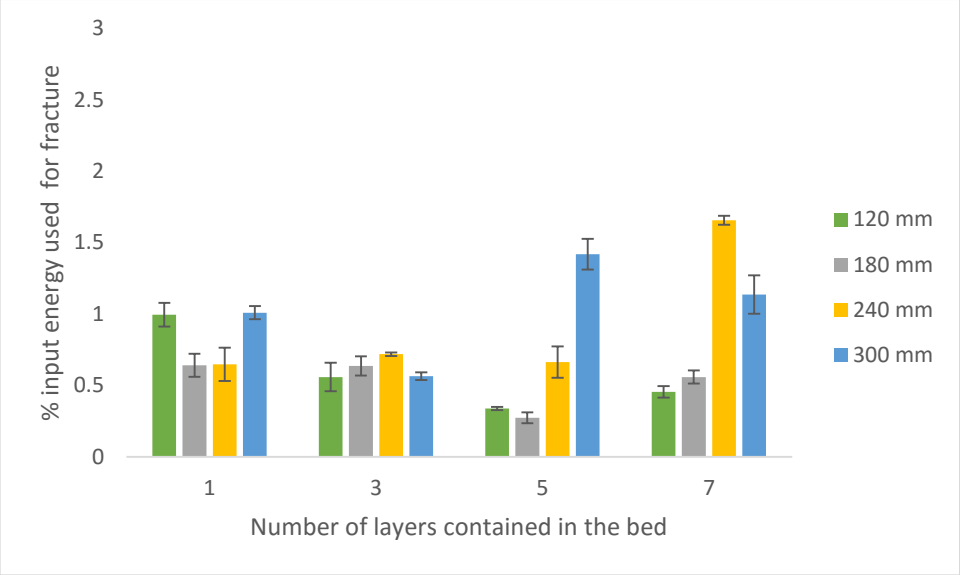

Figure 5.7: The fracture energy at various drop heights, represented as a function of the number of layers contained in the bed for tests conducted using the 261 g ball

At the 120 mm drop height the maximum energy used for fracture of 1 % was obtained at one layer. This value decreased to 0.3 % with increasing bed depth from one to five layers. When the number of layers was increased from five to seven, the fracture energy increased marginally to 0.5 %. The negligible increase in the results at the two largest bed depths suggests that these values were the same.

For the 180 mm drop height the fracture energy results obtained at one and three layers were statistically equal. A reduction from 0.6 to 0.3 % energy used for fracture was obtained when the number of layers was increased from three to five. The fracture energy increased slightly to 0.6 % when the bed depth was increased from five to seven layers. From the small difference of 0.3 % energy used for fracture at the two largest bed depths it can be said that these values were in essence the same.

At 240 mm, statistically identical fracture energy values were obtained at one, three and five layers. The % energy used for fracture increased from 0.7 to 1.7 % when the bed depth was increased from five to seven layers, where the highest % energy used for fracture at this drop height was obtained at the largest bed depth.

At the 300 mm drop height the % fracture energy decreased from 1.0 to 0.6 % when the bed depth was increased from one to three layers. An increase to 1.4 % energy used for fracture was obtained when the number of layers was increased from three to five. Increasing the bed depth from five to seven layers resulted in a minor decrease to 1.1 % energy used for fracture. The small difference of 0.3 % in the results obtained at five and seven layers suggests that these values were inherently the same.

Statistically similar fracture energy values were generally obtained at the adjacent drop heights of 120 and 180 mm. A finding in which the result obtained at a smaller drop height was greater than at a larger height was obtained at seven layers, where the fracture energy at 240 mm was greater than at 300 mm.

In comparison of the peak forces shown in Figure 5.3 and % energy used for fracture in Figure 5.7, observations similar to those found for the 510 g and 357 g balls were made. The maximum values of energy used for fracture were obtained at five and seven layers when the peak forces were low.

5.2.4. Fracture energy results obtained using the 110 g ball

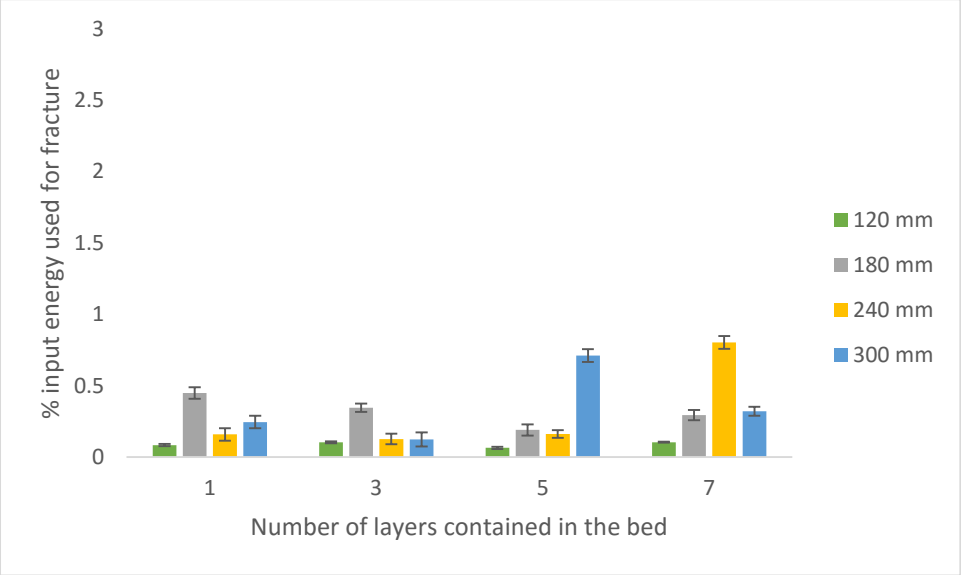

Figure *5.8* shows the fracture energy results. Comparison of these results to those obtained using the larger steel balls showed that these values were the lowest, with the highest values ranging between 0.7 and 0.8 %.

The two highest values of % energy used for fracture, which were found at 240 and 300 mm, were obtained at the largest bed depths of five and seven layers. This result is similar to that obtained for the same drop heights using the 510 g and 261 g balls. In different findings to the results obtained at five and seven layers, at one and three layers the maximum energy used for fracture was obtained at the 180 mm drop height.

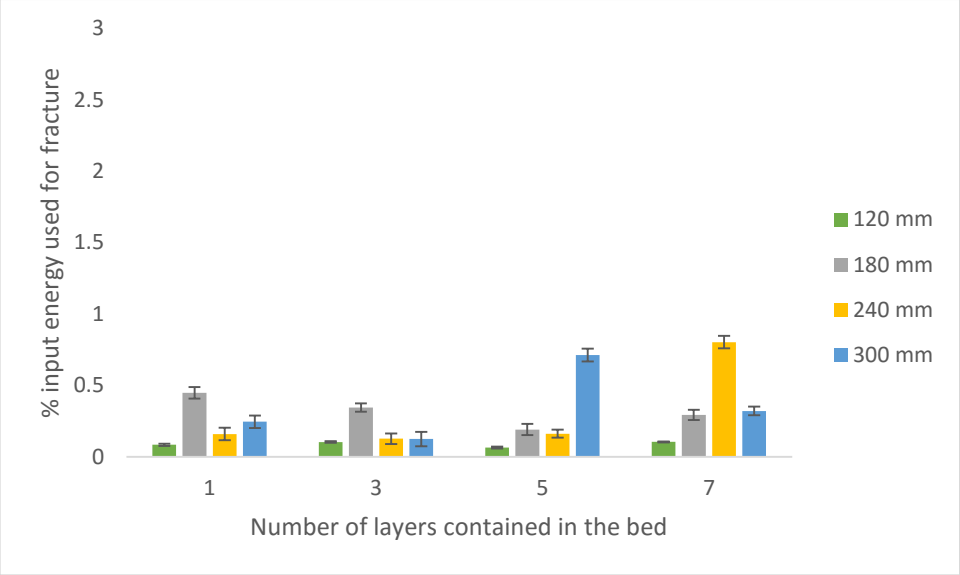

Figure 5.8: The fracture energy at various drop heights, represented as a function of the number of layers contained in the bed for tests conducted using the 110 g ball

At the 120 mm drop height, statistically equal results were obtained at all bed depths and the % energy used for fracture was the lowest, with the maximum being 0.15 %.

At the 180 mm drop height, a similar trend to that observed for some tests conducted using the 510 g and 357 g balls was found. The % energy used for fracture decreased from 0.45 to 0.2 % when the bed depth was increased from one to five layers. Increasing the number of layers from five to seven resulted in a slight increase to 0.3 % energy used for fracture. The marginal difference of 0.1 % in the fracture energy results obtained at five and seven layers suggests that these values were the same.

For the 240 mm drop height, statistically identical fracture energy results were obtained at one, three and five layers. When the bed depth was increased from five to seven layers, the % energy used for fracture increased from 0.2 to 0.8 %, resulting in the highest value obtained at this drop height.

At 300 mm the fracture energy values were the lowest at one and three layers, and there was an increase from 0.15 to 0.7 % energy used for particle fracture with increasing bed depth from three to five layers. This value decreased to 0.3 % when the bed depth was increased from five to seven layers. This result is consistent with that found for the 510 g and 261 g balls at this drop height, where the maximum energy utilized for breakage was also obtained at five layers.

For all the tests conducted, statistically equal fracture energy values were obtained at the adjacent drop heights of 240 and 300 mm at one and three layers. A finding in which the % energy used for fracture at smaller drop heights was greater than at larger heights was made

for some tests. At one and three layers the 5 energy used for fracture at 180 mm was greater than at 240 and 300 mm, and at a bed depth of seven layers the fracture energy at 240 mm was larger than at 300 mm.

In comparison of the peak forces shown in Figure 5.4 and the fracture energy values presented in

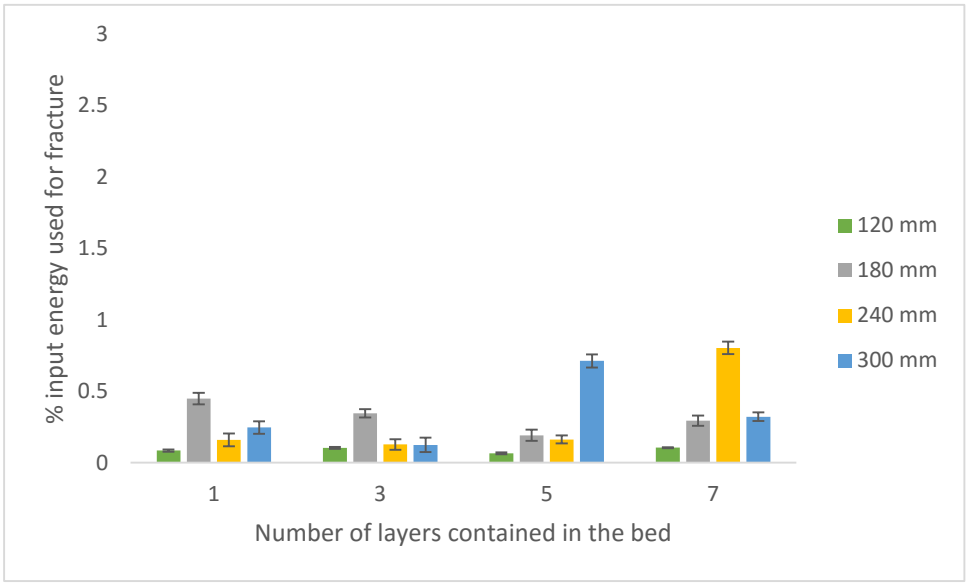

Figure *5.8*, it was found that the highest fracture energy values were not obtained at the greatest peak forces. This finding is synonymous with that found for the larger balls.

5.3. Breakage results

The breakage results obtained using the different input energies are presented in this section. These results are shown as t_2 (percentage passing defined in Section 2.6.1) for increasing input energy and bed depth. Sample calculations showing the method used to determine the degree of breakage are given in Appendix A.

The relationship between the amount of energy used for particle fracture and the degree of breakage obtained is also presented in this chapter.

5.3.1. Justification for using the t_2 breakage indicator

As mentioned in Section 2.6.1, the degree of breakage obtained when breakage tests are conducted can be quantified using various breakage indicators such as t_2, t_4, t_{10}, t_{50} and t_{75}.

To select the most suitable breakage indicator, the particle sizes corresponding to the different t_n parameters were calculated using UG2 particle size of -6.7 + 3.35 mm (Section 2.6.1). These

values were then compared with the particle size distributions resulting from breakage tests in order to determine which indicator was the most appropriate to use. The different particle sizes calculated for the various indicators are shown in Table 5.1.

Table 5.1: Particle sizes for the various t_n parameters

Breakage indicator t_n	**Particle size (mm)**
t_2	2.37
t_4	1.18
t_{10}	0.47
t_{50}	0.09
t_{75}	0.06

Due to the low input energies used, it was not possible to obtain the particle sizes for the t_{75}, t_{50} and t_{10} indicators. Therefore, these indicators were not considered. The particle size corresponding to the t_4 indicator was found to be smaller than the screen with the smallest aperture (1.4 mm) used to determine the resultant particle size distributions. As a result, this indicator could not be used and the t_2 indicator was found to be the most suitable to quantify breakage.

5.3.2. Breakage results obtained using the 510 g ball

The breakage results, given as t_2 (% passing) are shown in Figure 5.9. For all input energies the greatest degree of breakage was obtained at one layer of particles, and the maximum breakage (27 % passing) was found at the highest input energy. Figure 5.5 in Section 5.2.1 showed that the highest fraction of input energy was used to cause particle fracture at the largest bed depths of five and seven layers; however Figure 5.9 shows that the lowest breakage was attained at these bed depths.

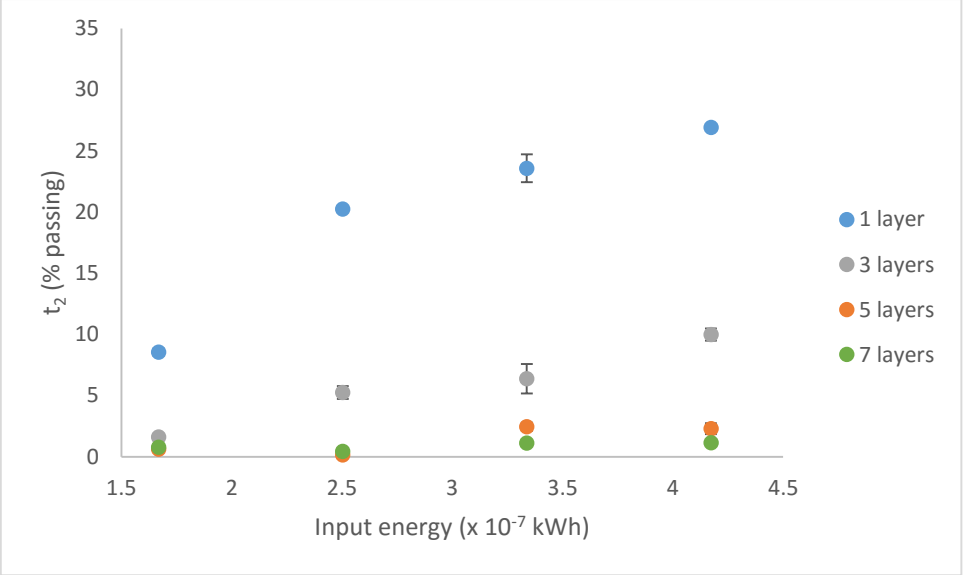

Figure 5.9: Degree of breakage obtained with increasing input energy and bed depth for tests conducted using the 510 g ball

For tests conducted on one layer of particles, the least breakage of 8.6 % passing was obtained at the smallest input energy. Increasing the input energy from 1.7 x 10^{-7} to 2.5 x 10^{-7} kWh resulted in the largest increment, to 20 % passing, in the breakage attained at this bed depth. A smaller increase to 24 % passing was obtained with increasing input energy from 2.5 x 10^{-7} to 3.3 x 10^{-7} kWh, and increasing the input energy to the largest value of 4.2 x 10^{-7} kWh resulted in a slight increase to 27 % passing in the breakage obtained.

Similar findings to those at one layer were made at a bed depth of three layers, where the greatest increase in the breakage (1.6 to 5.3 % passing) was obtained when the input energy was increased from 1.7 x 10^{-7} to 2.5 x 10^{-7} kWh. The breakage obtained at an input energy of 3.3 x 10^{-7} kWh was statistically identical to that at 2.5 x 10^{-7} kWh. For this bed depth the greatest breakage of 10 % passing was obtained at the largest input energy.

At bed depths of five and seven layers minimal breakage was obtained for all input energies, as the breakage results obtained were low and below 2.5 % passing.

For all input energies, the largest decrease in breakage was obtained when the number of layers was increased from one to three. At the lowest input energy of 1.7 x 10^{-7} kWh a negligible amount of breakage occurred at three, five and seven layers as the breakage results were all below 1 %. At the three largest input energies, increasing the number of layers from three to five led to a smaller reduction in the breakage obtained than that observed with increasing bed depth from one to three layers. There was a marginal difference in the breakage attained when the number of layers was increased from five to seven.

Figure 5.10 shows the relationship between the breakage obtained and the fracture energy. The relationship between the two parameters is only shown for one and three layers because the t_2 (% passing) values for bed depths of five and seven layers were too low.

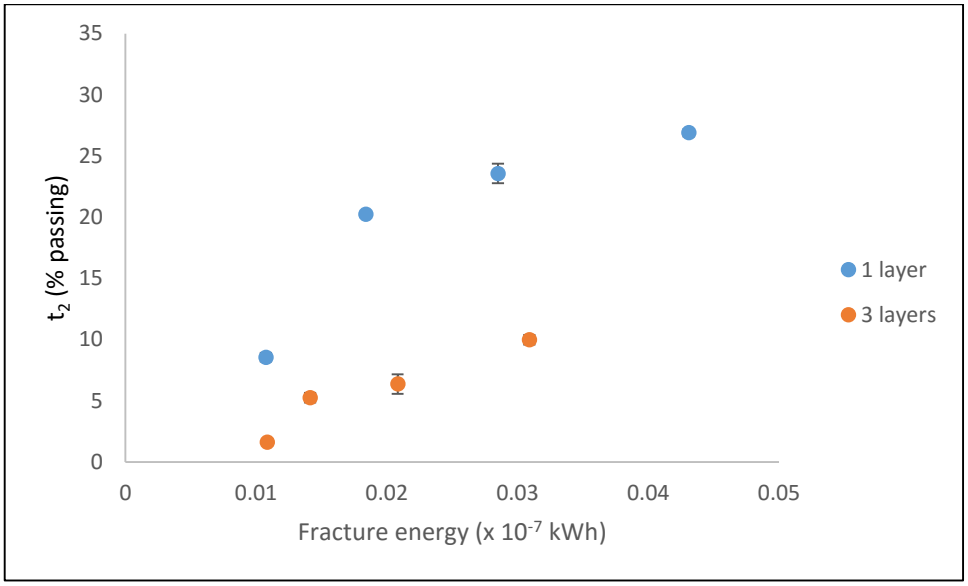

Figure 5.10: The degree of breakage obtained with increasing fracture energy for one and three layers for tests conducted using the 510 g ball

For one layer the lowest breakage of 8.6 % passing was obtained at the lowest fracture energy of 0.01 x 10^{-7} kWh. A slight increase to 0.018 x 10^{-7} kWh fracture energy resulted in a larger increase in the breakage from 8.6 to 20.2 % passing. A further increase in the fracture energy to the highest value of 0.043 x 10^{-7} kWh resulted in a slight increase from 20.2 to 26.9 % passing in the breakage obtained. For three layers the lowest breakage of 1.6 % passing was also obtained at the lowest fracture energy of 0.01 x 10^{-7} kWh. A small increase in the fracture energy to 0.014 x 10^{-7} kWh resulted in a slight increase from 1.6 to 5.3 % passing in the breakage obtained. A further increase in the fracture energy to the highest value of 0.03 x 10^{-7} kWh led to a slight increase from 5.3 to 9.9 % passing in the breakage attained.

5.3.3. Breakage results obtained using the 357 g ball

The breakage results are shown in Figure 5.11. For all input energies, the highest breakage was obtained at one layer it showed a decreasing trend with increasing number of layers. The maximum breakage of 31.7 % passing occurred at the second largest input energy of 2.3 x 10^{-7} kWh. This result is different from that obtained for the 510 g ball, where the maximum breakage was obtained at the largest input energy. Comparison of the results in Figure 5.11 to the fracture energy results presented in Figure 5.6 showed that the lowest breakage, found at bed depths of five and seven layers, was obtained at the highest fracture energies. This result is synonymous to that obtained for the 510 g ball.

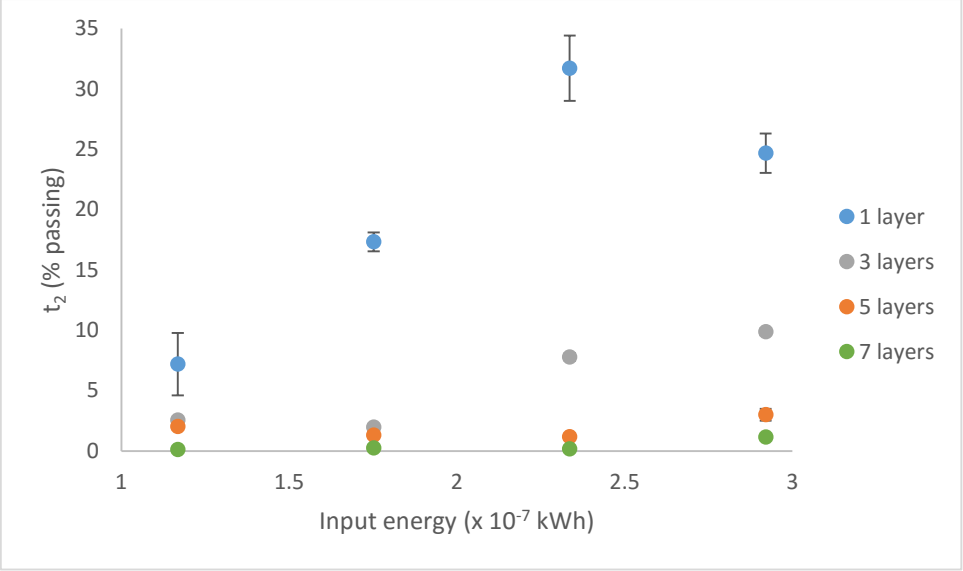

Figure 5.11: Degree of breakage obtained with increasing input energy and bed depth for tests conducted using the 357 g ball

For one layer of particles the breakage was lowest (7.2 % passing) at the smallest input energy of 1.2 x 10^{-7} kWh. Increasing the input energy to 1.8 x 10^{-7} kWh resulted in an increase to 17.3 % passing in the breakage obtained. The largest increase in breakage, from 17.3 to 31.7 % passing, was obtained with increasing input energy from 1.8 x 10^{-7} to 2.3 x 10^{-7} kWh. At the largest input energy the degree of breakage decreased to 25 % passing.

At a bed depth of three layers there was a marginal difference in the results obtained at the two lowest input energies, where the breakage values were low and below 2.6 % passing. Increasing the input energy from 1.8 x 10^{-7} kWh to 2.3 x 10^{-7} kWh resulted in an increase, from 2.0 to 7.8 % passing, in the breakage obtained. The breakage increased slightly, to 9.9 % passing, when the input energy was increased to 2.9 x 10^{-7} kWh.

Similar to the results obtained for the 510 g ball, minimal breakage occurred at five and seven layers for all input energies, where the t_2 values obtained were below 3 % passing.

For all input energies the largest reduction in the breakage was obtained with an increase in number of layers from one to three. At the two lowest input energies, increasing the bed depth from three to seven layers resulted in negligible changes to the results obtained, where the breakage was low and below 2 % passing. At the two largest input energies, increasing the bed depth from three to five layers resulted in a smaller reduction in the breakage compared to that obtained with an increase in layers from one to three. For both input energies, increasing the bed depth from five to seven layers resulted in a marginal difference in the breakage obtained.

Figure 5.12 shows the relationship between the particle fracture energy and the breakage obtained for bed depths of one and three layers. Similar to the results obtained using the 510 g ball, the t_2 (% passing) values attained at five and seven layers were too low and have therefore not been shown in the figure.

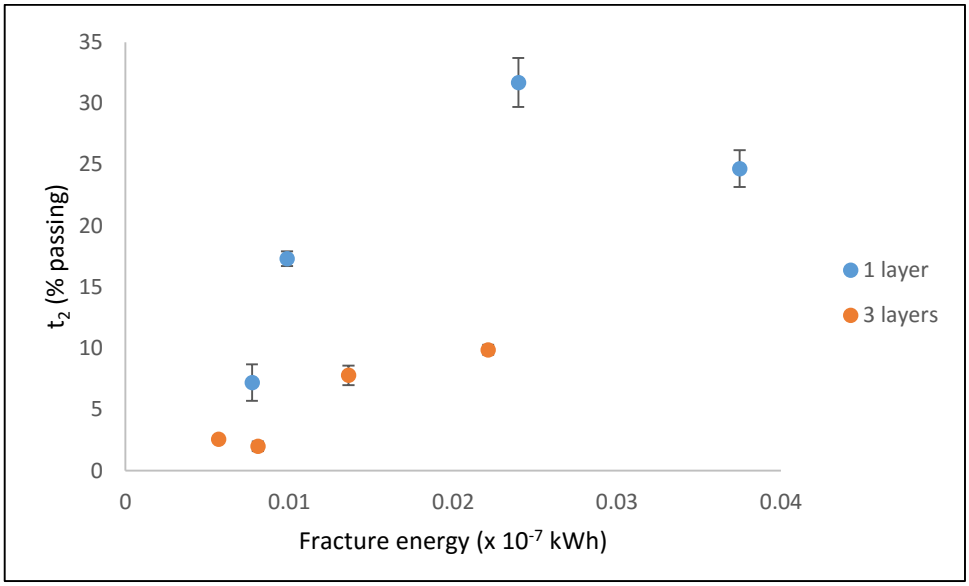

Figure 5.12: The degree of breakage obtained with increasing fracture energy for one and three layers for tests conducted using the 357 g ball

For one layer the lowest breakage of 7.2 % passing was obtained at the lowest fracture energy of 0.008 x 10^{-7} kWh. An increase in the fracture energy to 0.024 x 10^{-7} kWh resulted in a large increase in the breakage from 7.2 to 32 % passing, where this was the highest breakage obtained. An increase in the fracture energy to 0.037 x 10^{-7} kWh led to a reduction from 32 to 25 % passing in the breakage obtained. For a bed depth of three layers the lowest breakage was obtained at the two lowest fracture energy values of 0.006 and 0.008 x 10^{-7} kWh. A slight increase in the fracture energy from 0.008 to 0.014 x 10^{-7} kWh resulted in a more significant increase in the breakage obtained from 1.9 to 7.8 % passing. A further increase in the fracture energy from 0.014 to 0.022 x 10^{-7} kWh did not significantly change the breakage as only a small increase from 7.8 to 9.9 % passing was obtained.

5.3.4. Breakage results obtained using the 261 g ball

The breakage results are shown in Figure 5.13. Although the results for one layer had the greatest variability, it is clear that the breakage obtained was the highest for all the input energies used. In similar findings to those made for the 510 g and 357 g balls, it was observed that the breakage decreased with increasing number of layers from one to seven.

Comparison of the results in Figure 5.13 with the fracture energy results in Figure 5.7 showed that the least breakage was obtained at bed depths of five and seven layers when the fracture

energy was the greatest. This finding is synonymous with that made for tests conducted using the larger balls.

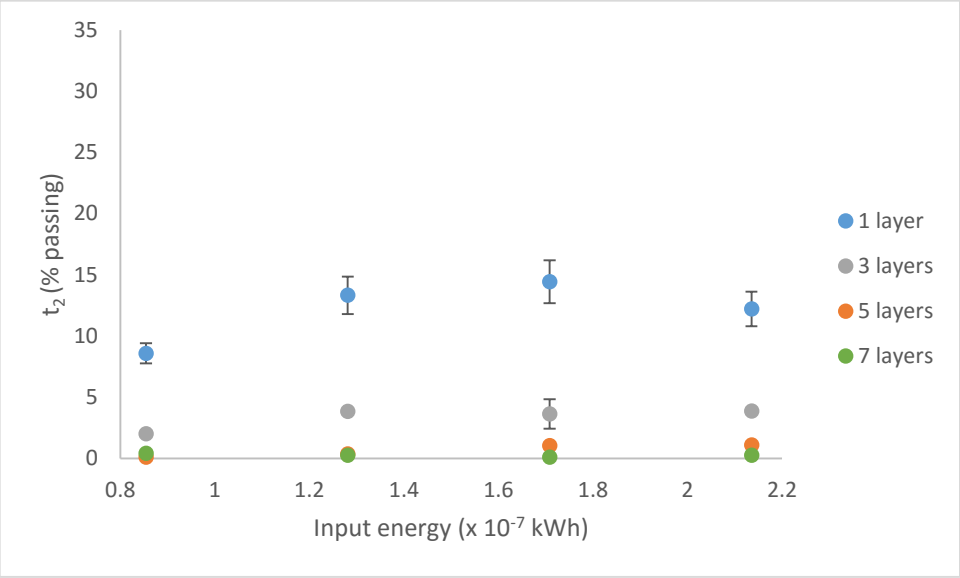

Figure 5.13: Degree of breakage obtained with increasing input energy and bed depth for tests conducted using the 261 g ball

For one layer of particles the least breakage, 8.6 % passing, was obtained at the lowest input energy of 0.85 x 10^{-7} kWh. Increasing the input energy to 1.3 x 10^{-7} kWh resulted in a breakage increase to 13.3 % passing. The results attained at the three largest input energies were statistically similar.

Compared to the results at one layer, for the bed depth of three layers the breakage obtained at all input energies was low, below 5 % passing. The least breakage of 2 % passing was found at the lowest input energy and it increased slightly to 3.8 % passing with an increase in input energy to 1.3 x 10^{-7} kWh. Statistically equal breakage results were obtained at the three largest input energies.

Increasing the bed depth from three to five layers resulted in low (maximum 1% passing) breakage being obtained for all the input energies. A negligible amount of breakage occurred with increasing number of layers from five to seven. This result is synonymous with that found for both the 510 g and 357 g balls.

The same trend observed for the 510 and 357 g balls, where the largest reduction in breakage was obtained with an increase in bed depth from one to three for all input energies, was found. An increase in bed depth from three to five layers resulted in a smaller reduction in the breakage obtained. At the two lowest input energies no breakage occurred at both five and seven layers. At the two largest input energies, there was a marginal difference in the

breakage obtained at five and seven layers, therefore these values were considered to be the same.

The relationship between the breakage obtained and the fracture energy is shown in Figure 5.14. This relationship is only shown for one and three layers as the breakage values obtained at five and seven layers were too low.

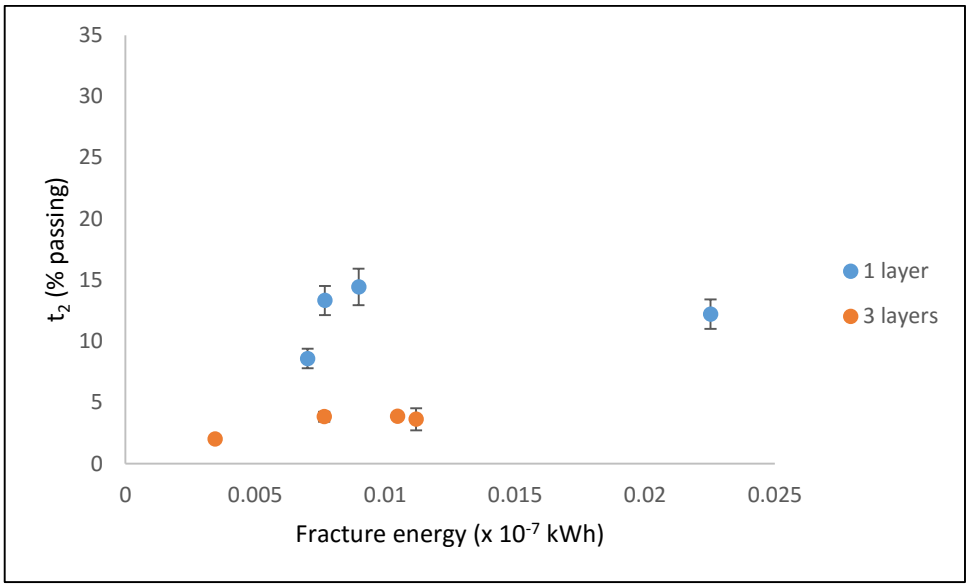

Figure 5.14: The degree of breakage obtained with increasing fracture energy for one and three layers for tests conducted using the 261 g ball

For both one and three layers the lowest breakage was obtained at the lowest fracture energies. This result is synonymous with that found for tests conducted using the larger steel balls. For one layer, a very small increase in the fracture energy from the lowest value of 0.007 to 0.008 x 10^{-7} kWh resulted in a larger increase from 8.6 to 13.3 % passing in the breakage obtained. A further increase in the fracture energy from 0.008 x 10^{-7} kWh to the highest value of 0.023 x 10^{-7} kWh did not change the breakage as statistically identical t_2 (% passing) values were attained. For three layers a similar trend to that observed for tests conducted on one layer of particles was found. The largest increase in breakage from 2.0 to 3.8 % passing was obtained with an increase in fracture energy from the lowest value of 0.003 x 10^{-7} kWh to the second lowest value of 0.008 x 10^{-7} kWh. A further increase, to the highest value of 0.011 x 10^{-7} kWh, in the fracture energy did not result in changes to the breakage as statistically equal t_2 (% passing) values were obtained.

5.3.5. Breakage results obtained using the 110 g ball

The breakage results are shown in Figure 5.15. For all input energies the maximum breakage was obtained at one layer, which is the same result found for the larger balls. Also in similar findings to those made for the larger balls, it was observed that the breakage obtained

decreased with increasing number of layers contained in the bed. Comparison of the results shown in Figure 5.15 to the fracture energy results in

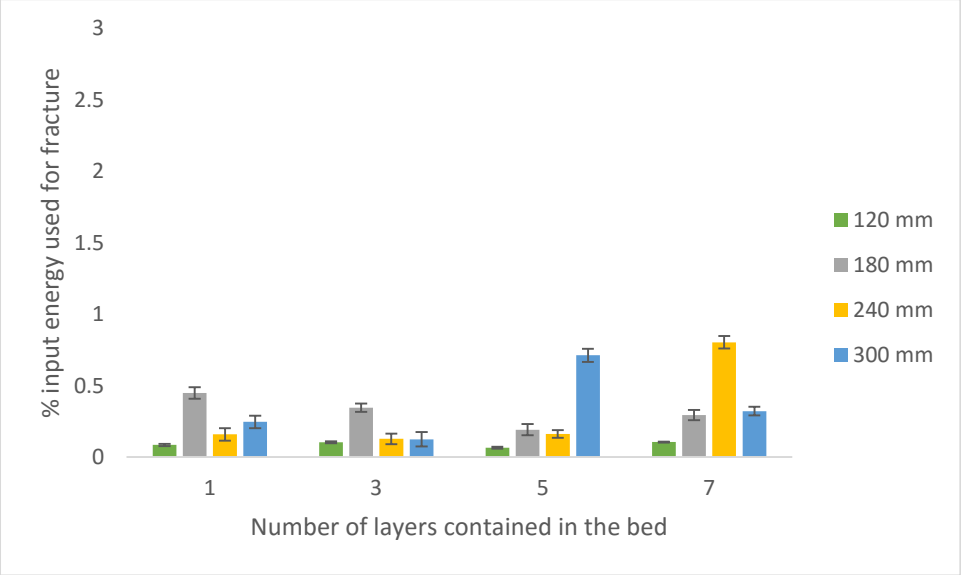

Figure *5.8* showed that the lowest breakage was obtained at the largest bed depths when the fracture energy was the highest. This is the same finding made for all the larger balls.

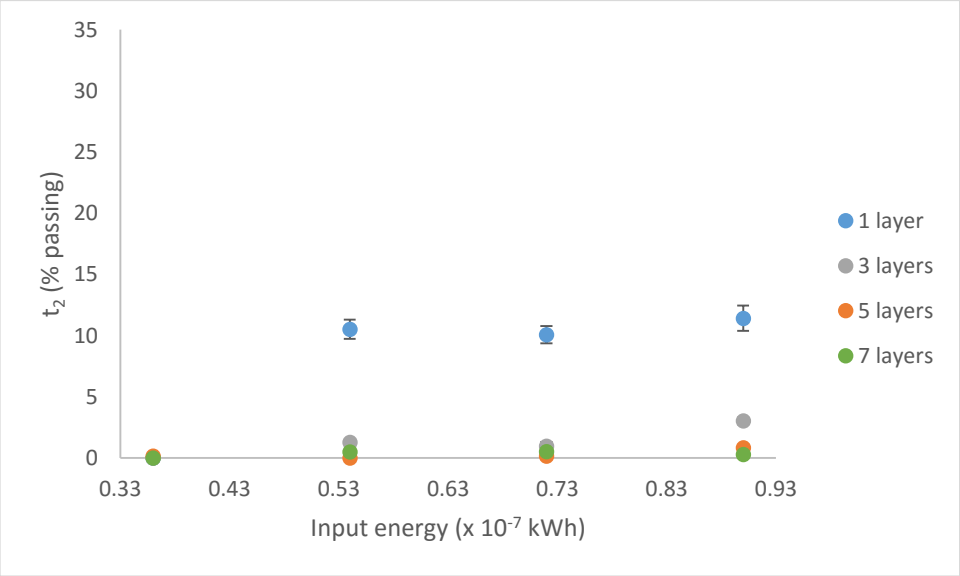

Figure 5.15: Degree of breakage obtained with increasing input energy and bed depth for tests conducted using the 110 g ball

Note: At the lowest input energy of 0.36 x 10^{-7} kWh no breakage was obtained for all the bed depths.

For tests conducted on one layer of particles, breakage of 10.5 % passing was obtained at 0.53 x 10^{-7} kWh. Breakage results which were statistically identical to this value were attained at the two largest input energies.

At three layers the breakage results were low, and were all below 3.5 % passing. A breakage result of 1.3 % passing was obtained at 0.53 x 10^{-7} kWh which was statistically equal to that found at 0.72 x 10^{-7} kWh. The maximum breakage of 3 % passing was obtained at the highest input energy of 0.9 x 10^{-7} kWh.

At bed depths of five and seven layers a negligible amount of breakage was obtained for all input energies. This result is synonymous with that found for the 510 g, 357 g and 261 g balls.

In similar findings to those made for the larger steel balls, it was found that the greatest reduction in breakage was obtained with increasing number of layers from one to three. Increasing the bed depth from three to five layers led to a smaller decrease in breakage. There was a minimal difference in the breakage obtained at five and seven layers, therefore these values were considered to be the same.

Figure 5.16 shows the relationship between the fracture energy and the breakage obtained for one and three layers. Similar to tests conducted using the larger steel balls, the breakage values attained at bed depths of five and seen layers were too low; hence they have not been shown in the figure.

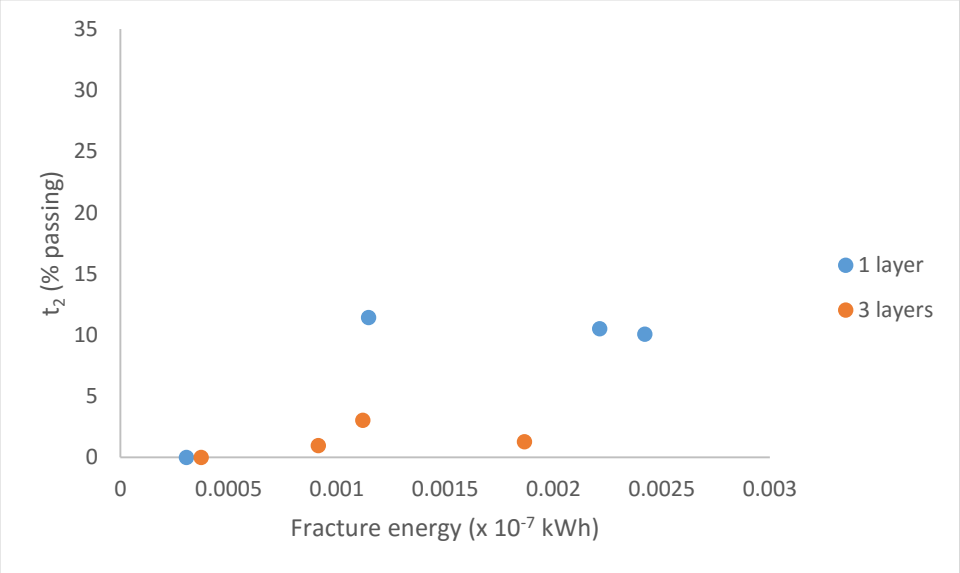

Figure 5.16: The degree of breakage obtained with increasing fracture energy for one and three layers for tests conducted using the 110 g ball

For both one and three layers no breakage was obtained at the lowest fracture energy values. For one layer, an increase in the fracture energy from the lowest value of 0.0004 to 0.0011 x 10^{-7} kWh resulted in the largest increase from 0 to 10.5 % passing in the breakage obtained. An increase in the fracture energy from 0.0011 x 10^{-7} kWh to the highest value of 0.0024 x 10^{-7} kWh did not result in changes to the breakage, as statistically similar t_2 (% passing) values were obtained. For a bed depth of three layers an increase in the fracture energy from the

lowest value of 0.0004 x 10^{-7} kWh to a value of 0.0011 x 10^{-7} kWh led to an increase in breakage from 0 to 3.1 % passing, where this value was the highest breakage obtained. A further increase in the fracture energy from 0.0011 to 0.0020 x 10^{-7} kWh resulted in a slight decrease in breakage from 3.1 to 1.3 % passing.

6. DISCUSSION OF THE RESULTS OBTAINED

Overview

The blue stone results presented in Chapter 4 and those for UG2 presented in Chapter 5 are discussed in this chapter. The discussion of the results is divided into three sections: The peak force results are discussed in Section 6.1, the fracture energy results are discussed in Section 6.2 and the discussion of the breakage results is done in Section 6.3.

6.1. Discussion of the peak force results

In this section the effect of varying the three variables: steel ball mass, drop height and bed depth of particles on the peak forces obtained is discussed. The linear and exponential fits shown in this section were plotted between the steel ball mass, drop height and bed depth data points used for experiments. No extrapolation was done for values outside of this range as these would have to be determined through experimental work for an accurate reflection.

6.1.1. Effect of increasing the steel ball mass

From theory, the impact force on a particle sample increases with increasing input energy as a result of an increase in the impact velocity (Salman et al., 1995; Thornton et al., 1999; Mishra & Thornton, 2001). In Section 2.7.1 it was shown that the input energy is directly related to the steel ball mass, therefore it was expected that the peak force would increase with increasing steel ball mass from 110 to 510 g.

In order to determine the most suitable trend line for the data relating the peak force to the steel ball mass, two trend lines (linear and exponential) were fit to the data and their goodness of fit was compared. The R-squared (R^2) parameter, whose values range from 0 to 1, was used as an indicator of the goodness of fit, where values closer to 1 were an indication of a better fit to the data than those further from 1.

The linear trend line is in the form $y = mx + c$; where:

y: Peak force (N)

m: Slope of the trend line (N/g)

x: Steel ball mass (g)

The exponential trend line is in the form $y = me^{kx}$; where:

y: Peak force (N)

x: Steel ball mass (g)

m: Model parameter (constant)

k: Growth/decay rate (g^{-1})

The two trend lines which were compared were fit to the data obtained for tests conducted on one layer of particles at the largest drop height of 300 mm for both blue stone and UG2. For each ore, the two trend lines, their respective R^2 values and equations are shown in Figure 6.1 and Figure 6.2.

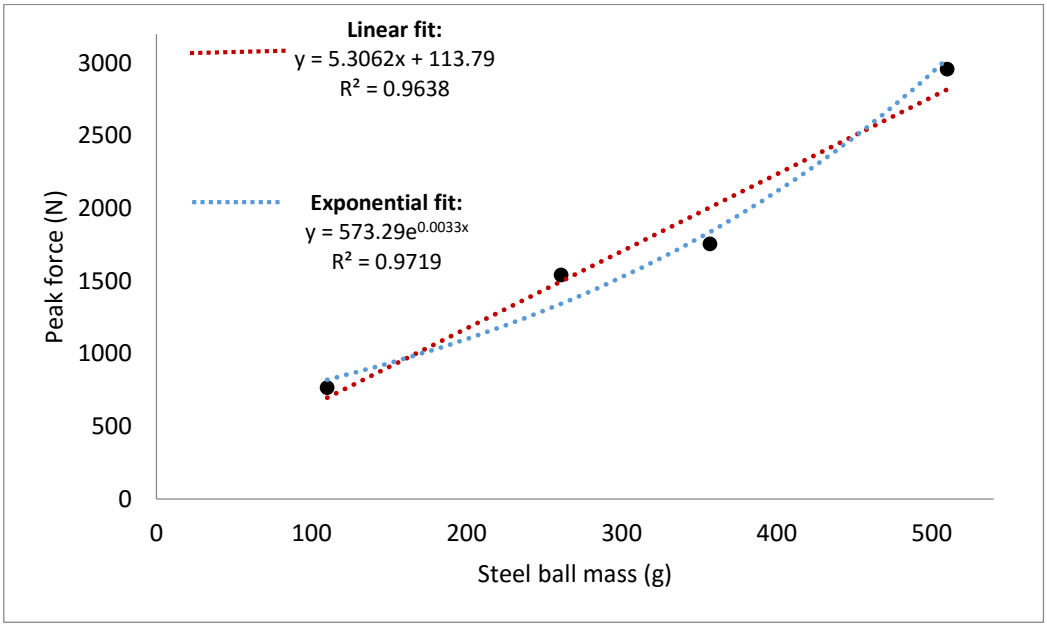

Figure 6.1: Peak force vs steel ball mass data fitted to linear and exponential trend lines for blue stone

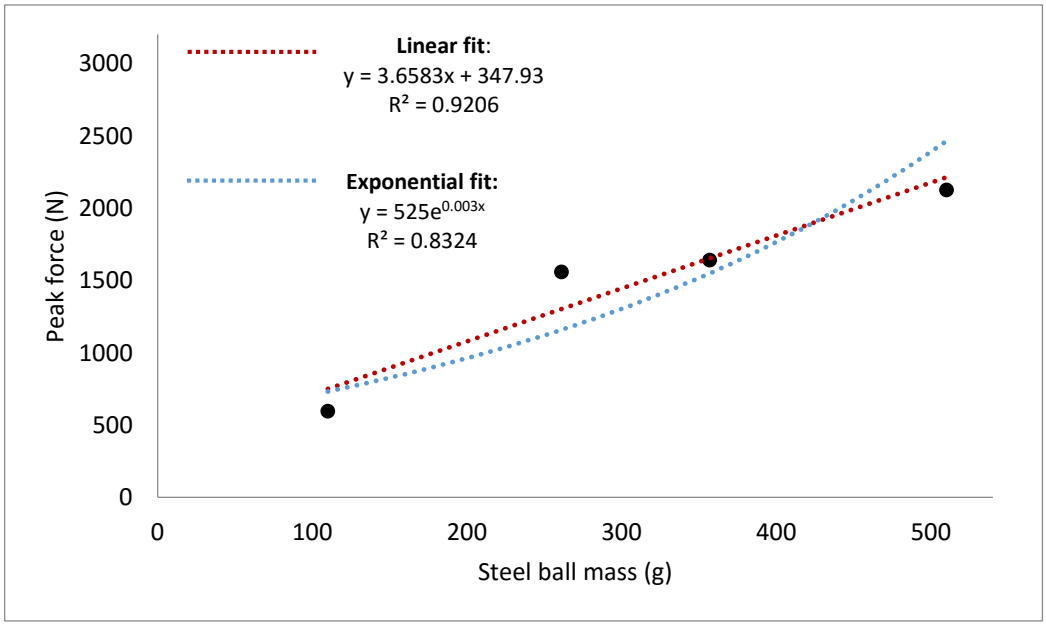

Figure 6.2: Peak force vs steel ball mass data fitted to linear and exponential trend lines for UG2

The R^2 values of 0.964 and 0.972 obtained for the linear and exponential trend lines shown in Figure 6.1 are both close to unity indicating that both trend lines were a good fit to the blue stone data. Similarly, the R^2 values of 0.921 and 0.832 obtained for the linear and exponential trend lines shown in Figure 6.2 are also both close to one. However, since the difference in R^2 values is more pronounced that that shown in Figure 6.1 it can be said that the linear trend line was a better fit to the UG2 data compared to the exponential trend line.

The residuals of the data presented in Figure 6.1 and Figure 6.2 were plotted against increasing steel ball mass in order to assess the linearity of the relationship presented by the data. For each ore, the residuals obtained for tests conducted on one layer of particles were plotted against the steel ball mass and are shown in Figure 6.3.

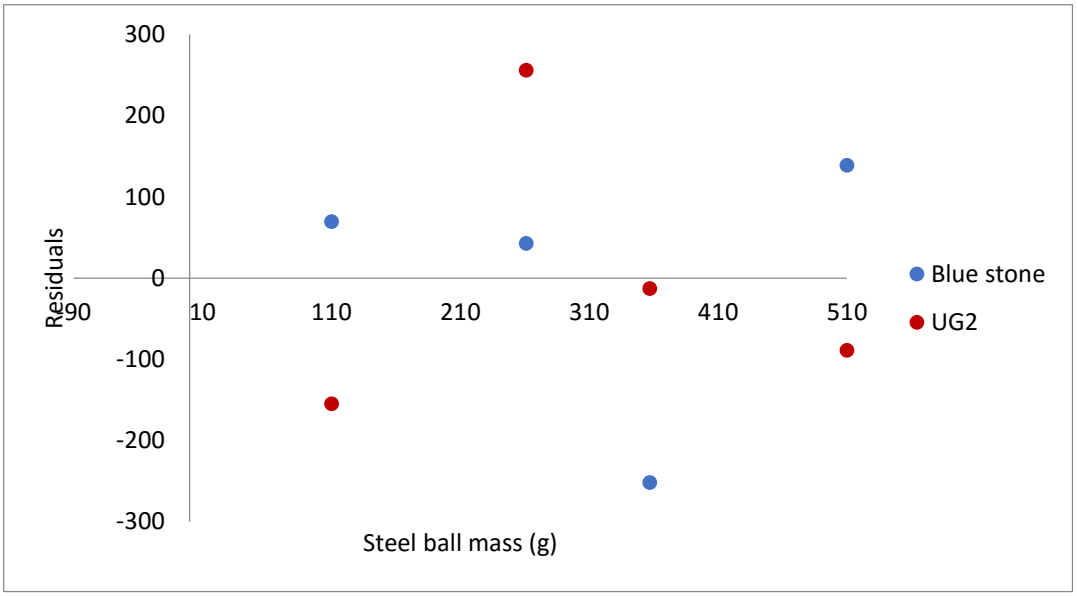

Figure 6.3: Residuals obtained for increasing steel ball mass for both blue stone and UG2

The data plotted in Figure 6.3 shows a random pattern of residuals around the x-axis for both ores which indicates that the data is a good fit for a linear model. Therefore, the peak force was said to increase linearly with increasing steel ball mass for both blue stone and UG2.

Figure 6.4 shows the effect of increasing steel ball mass on the peak forces obtained at a constant drop height of 300 mm for tests conducted on blue stone. The data is presented with increasing bed depth for one, five and nine layers. Figure 6.5 shows the effect of increasing steel ball mass on the peak forces obtained at a constant drop height of 300 mm for tests conducted on UG2. The data is presented for increasing bed depth for one, three and seven layers.

From the results presented in Section 4.1, Section 5.1, Figure 6.4 and Figure 6.5 it is seen that the peak force showed an increasing trend with increasing ball mass for both ores.

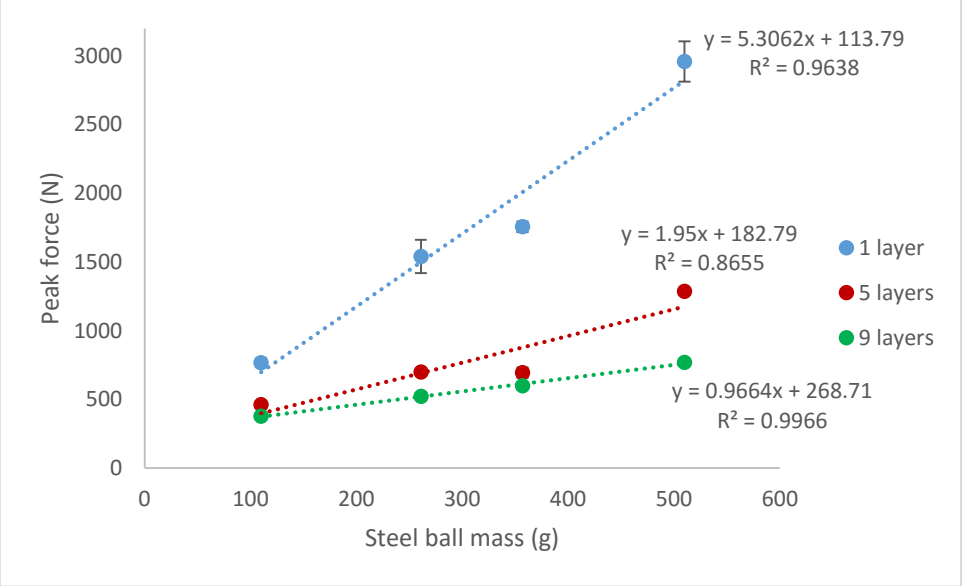

Figure 6.4: Peak force as a function of the steel ball mass with increasing bed depth for tests conducted on blue stone

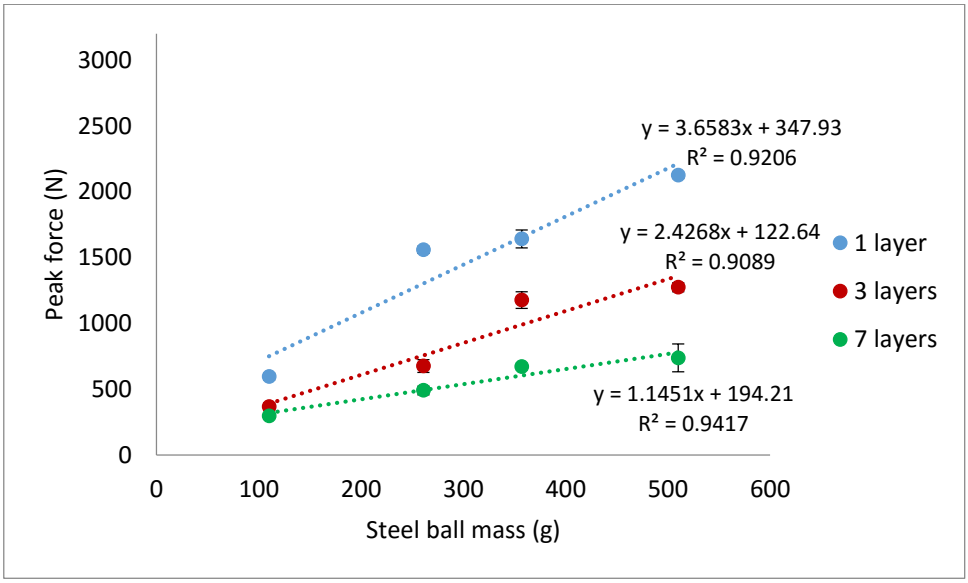

Figure 6.5: Peak force as a function of steel ball mass with increasing bed depth for tests conducted on UG2

The R^2 values shown in Figure 6.4 and Figure 6.5 for each bed depth were close to unity, indicating that the experimental data was a close fit to the linear regression lines. The R^2 value of 0.964 obtained for tests conducted on one layer of blue stone particles (Figure 6.4) indicates that 96.4 % of the variation in peak force is predicted by the steel ball mass. Likewise, the R^2 values of 0.866 and 0.997 obtained for five and nine layers indicate that, respectively, 86.6 % and 99.7 % of the variation in peak force is dependent on the steel ball mass.

Similarly, the R^2 values of 0.921, 0.909 and 0.942 obtained for tests conducted at one, three and seven layers of UG2 particles (Figure 6.5) indicate that, respectively, 92.1, 90.9 and 94.2 % of the variation in peak force is predicted by the steel ball mass.

From the regression line equations given in Figure 6.4 and Figure 6.5 it is seen that the regression line for one layer of particles had the largest slope and the steepness of the regression lines decreased with increasing bed depth. This indicates that for each steel ball, a bed depth of one layer had the greatest impact on the peak force and increasing the bed depth resulted in a reduced effect on the peak force obtained.

Comparison of the peak forces obtained for blue stone (Section 4.1) with those for UG2 (Section 5.1) showed that the peak force results for blue stone were generally higher than those for UG2 for tests conducted using the same steel ball mass. The dissimilarity in peak forces obtained for the two ores is due to the differences in elastic constants and hardness of each ore (Section 2.6 and Section 3.3.1).

6.1.2. Effect of increasing the drop height

In Section 6.1.1 it was mentioned that the impact force increases with increasing input energy as a result of an increase in the impact velocity (Salman et al., 1995; Thornton et al., 1999; Mishra & Thornton, 2001). In Section 2.7.1 it was shown that the input energy is directly related to the drop height, therefore the expected outcome was an increase in peak force with increasing drop height from 60 to 300 mm.

A similar procedure to that followed to determine the most suitable trend line relating the peak force and steel ball mass (Section 6.1.1) was followed to determine the most suitable trend line for the data relating the peak force to the drop height. Linear and exponential trend lines were fit to the data and their respective goodness of fit was compared.

The linear and exponential trend lines which were compared were fit to the data obtained for tests conducted on one layer of particles using the largest steel ball mass of 510 g for both blue stone and UG2. Figure 6.6 and Figure 6.7 show the two different trend lines, their respective R^2 values and equations for each ore.

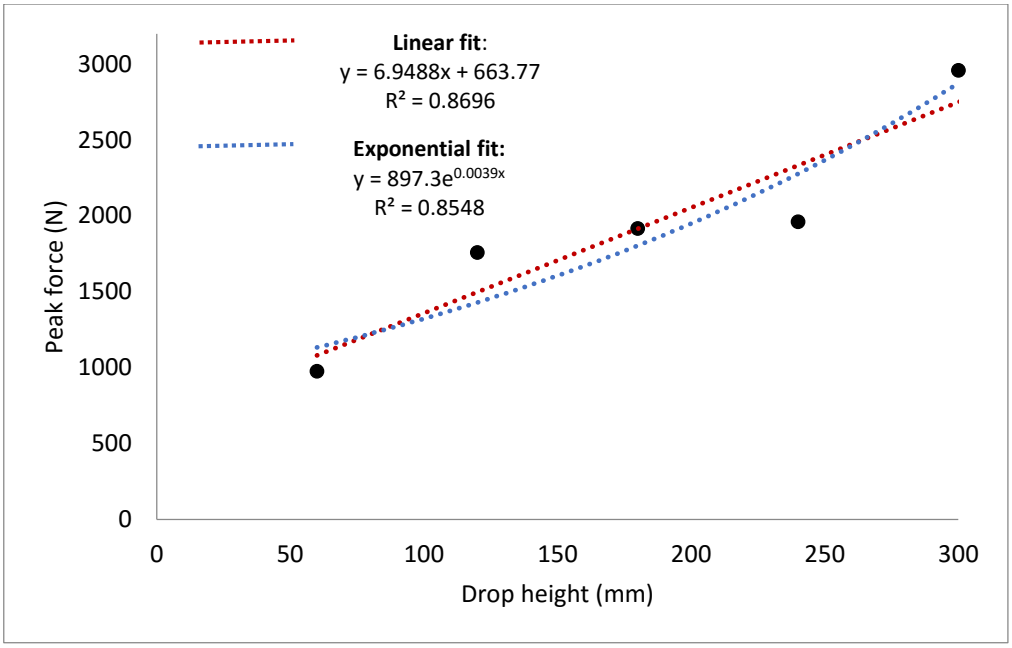

Figure 6.6: Peak force vs drop height data fitted to linear and exponential trend lines for blue stone

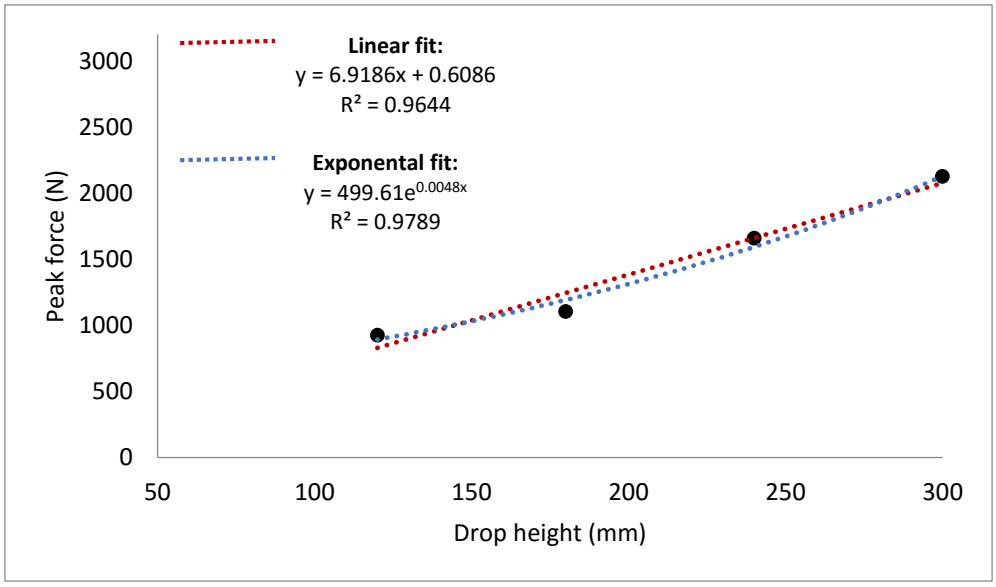

Figure 6.7: Peak force vs drop height data fitted to linear and exponential trend lines for UG2

The R^2 values of 0.869 and 0.855 shown in Figure 6.6 and 0.964 and 0.979 shown in Figure 6.7 are all close to 1 which indicates that both the linear and exponential trend lines were a good fit to the peak force vs drop height data obtained for both blue stone and UG2.

The residuals of the data presented in Figure 6.6 and Figure 6.7 were plotted against increasing drop height in order to evaluate the linearity of the relationship presented by the data. For each ore, the residuals obtained for tests conducted on one layer of particles were plotted against the drop height and are shown in Figure 6.8.

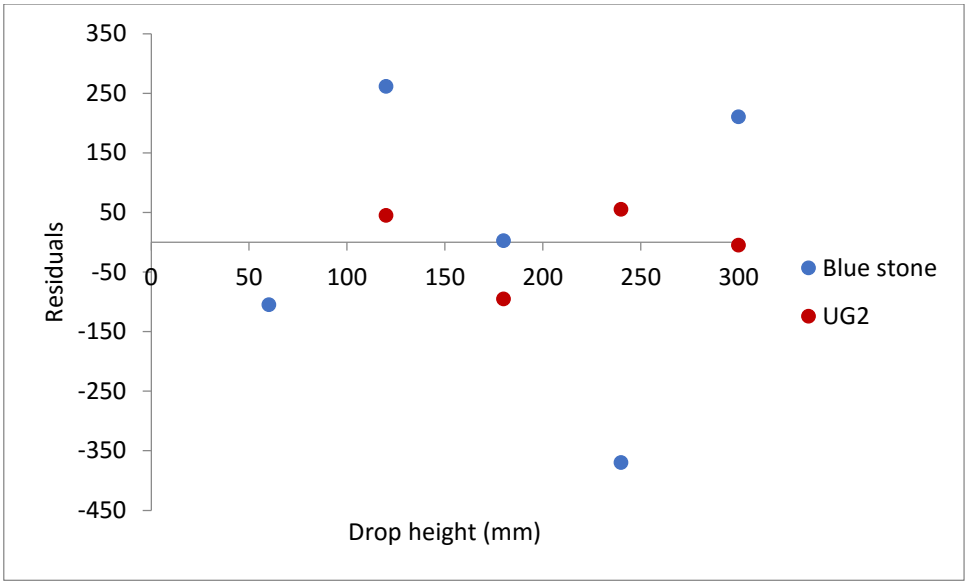

Figure 6.8: Residuals obtained for increasing drop height for both blue stone and UG2

From Figure 6.8 it is seen that the plotted data shows a random pattern of residuals around the x-axis for both ores. This is an indication that the data is a good fit for a linear model; hence the peak force and drop height have been described as linearly related.

Figure 6.9 shows the effect of increasing drop height on the peak forces obtained at a constant steel ball mass of 510 g for tests conducted on blue stone. Plots are presented with increasing bed depth for one, five and nine layers. Figure 6.10 shows the effect of increasing drop height on the peak forces obtained at a constant steel ball mass of 510 g for tests conducted on UG2. The data is plotted for increasing bed depth for one, three and seven layers.

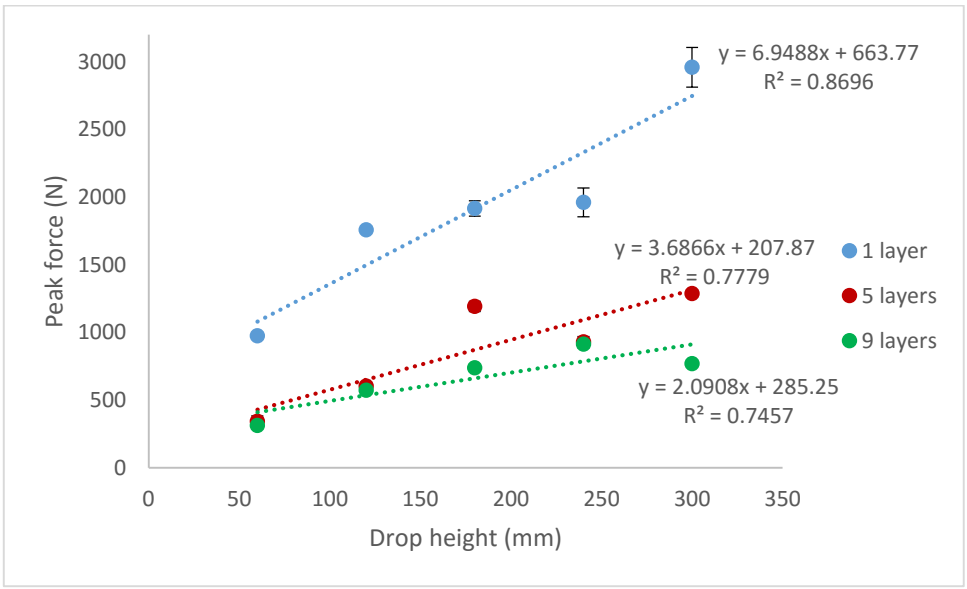

Figure 6.9: Peak force as a function of drop height with increasing bed depth for tests conducted on blue stone

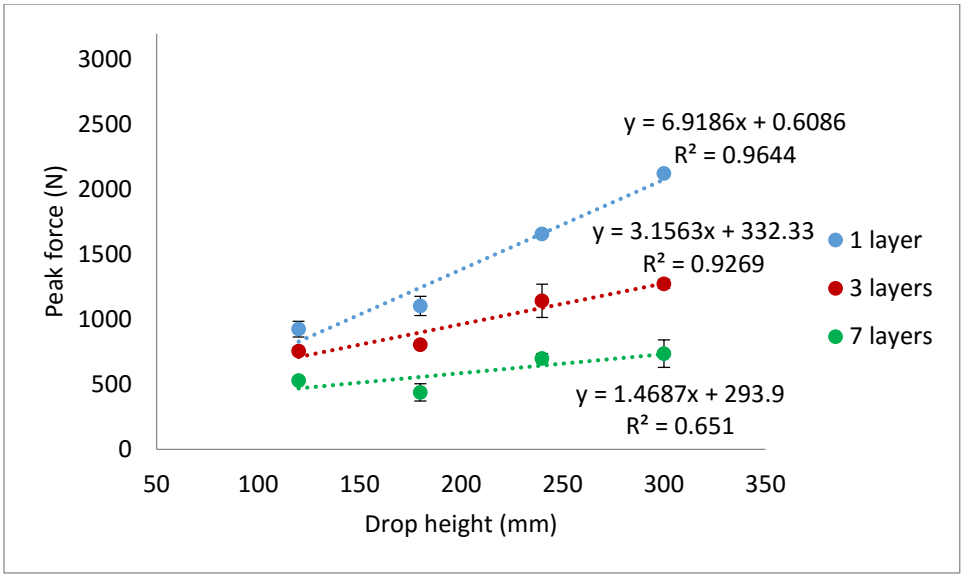

Figure 6.10: Peak force as a function of drop height with increasing bed depth for tests conducted on UG2

Figure 6.9 and Figure 6.10 show that the steepest regression lines were obtained when tests were conducted on one layer of particles and the slope of the regression lines decreased with increasing bed depth. This indicates that for each drop height, a bed depth of one layer had the largest influence on the peak force and there was a reduced effect on the peak force obtained as the bed depth was increased. This result is similar to that obtained for increasing steel ball mass (Section 6.1.1).

From Figure 6.4, Figure 6.5, Figure 6.9 and Figure 6.10 it is seen that for both blue stone and UG2, the drop height had a greater effect on the peak force obtained than the steel ball mass. This was seen from comparison of the slopes of the regression lines at the same bed depth (one layer was used for comparison). The regression lines obtained for increasing drop height had larger slopes than those for increasing ball mass.

Comparison of the peak forces obtained for blue stone (Section 4.1) with those for UG2 (Section 5.1) showed that the results for blue stone were generally higher than those for UG2 at the same drop heights. As mentioned in Section 6.1.1 the dissimilarities in the peak forces obtained for the two ores can be attributed to the differences in elastic constants and hardness of each ore (Section 2.6 and Section 3.3.1).

6.1.3. Effect of increasing the bed depth

From the breakage tests conducted, it was predicted that there would be a reduction in peak force with an increase in the number of layers due to a decreasing fraction of the impact force being distributed across each layer.

Linear and exponential trend lines were fitted to the data and were compared in order to determine the most suitable trend line relating the peak force to the bed depth. The two different trend lines were fitted to the data obtained for tests conducted using the largest steel ball mass of 510 g and the highest drop height of 300 mm for both blue stone and UG2. For each ore, the two trend lines, their respective R^2 values and equations are shown in Figure 6.11 and Figure 6.12.

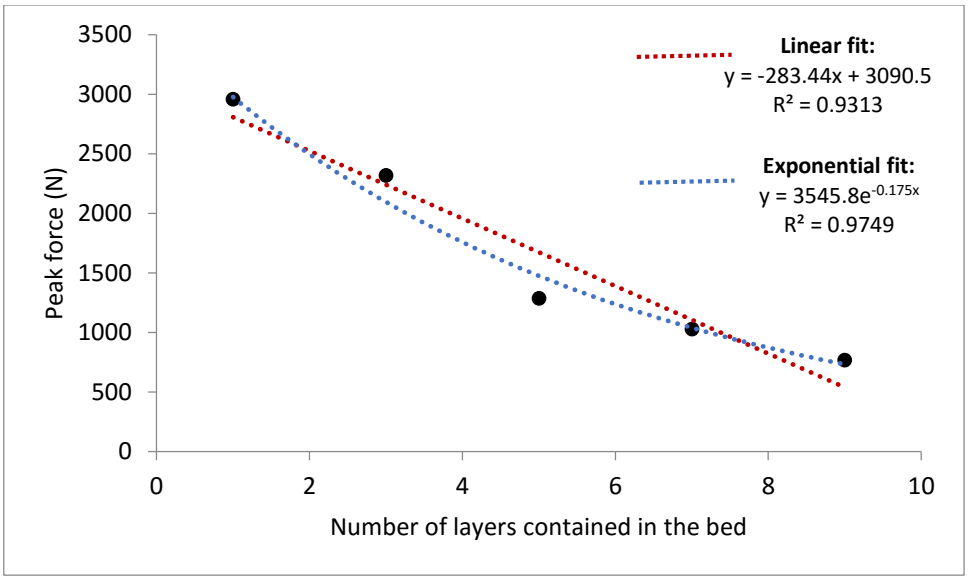

Figure 6.11: Peak force vs bed depth data fitted to linear and exponential trend lines for tests conducted on blue stone using the 510 g ball and 300 mm drop height

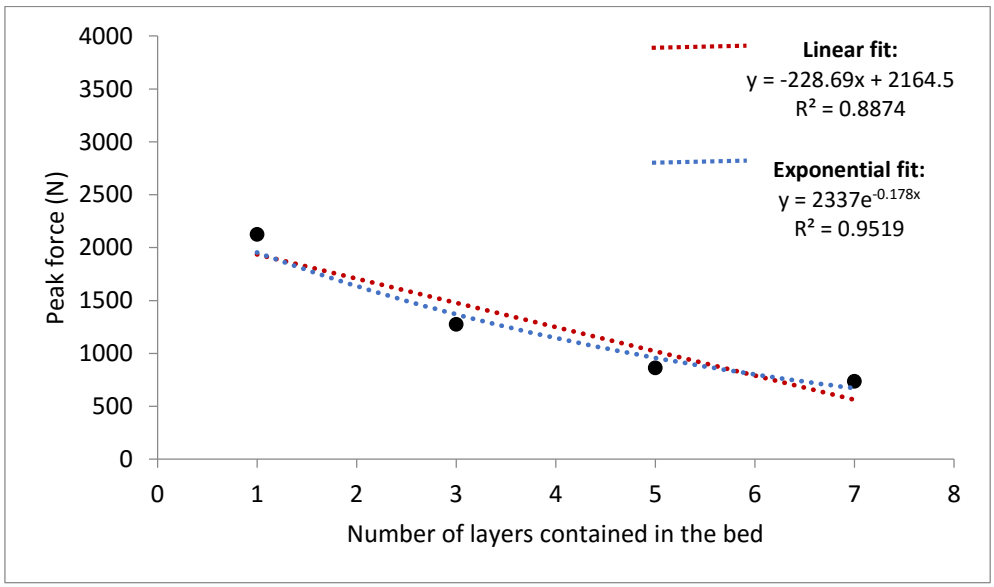

Figure 6.12: Peak force vs bed depth data fitted to linear and exponential trend lines for tests conducted on UG2 using the 510 g ball and 300 mm drop height

Figure 6.11 and Figure 6.12 show that show that the peak force decreases with an increase in the number of layers contained in the bed. The linear and exponential fits were used to highlight the trends for interpolation, rather than for extrapolation. This is because extrapolation for the peak force at zero layers would have not have yielded any meaningful breakage data for the study. At larger bed depths, the trend suggested by the exponential fit shows that the peak force follows an asymptotic decrease towards zero. This result is expected but have to would be verified through experiments rather than by extrapolation of the plots shown in Figure 6.11 and Figure 6.12.

From both figures it is seen that the R^2 values obtained for both the linear and exponential trend lines were close to 1. However, for both ores the R^2 values obtained for the exponential trend lines were much close to unity than those for the linear trend lines. This indicates that although the linear trend lines were a good fit to the data, the exponential trend lines were a better fit. Therefore, the peak force and bed depth have been described as having an exponential relationship.

Figure 6.13 and Figure 6.14 show the effect of increasing the bed depth on the peak forces obtained for tests conducted on blue stone and UG2. The results are presented for increasing steel ball mass for 110, 357 and 510 g at a constant drop height of 300 mm.

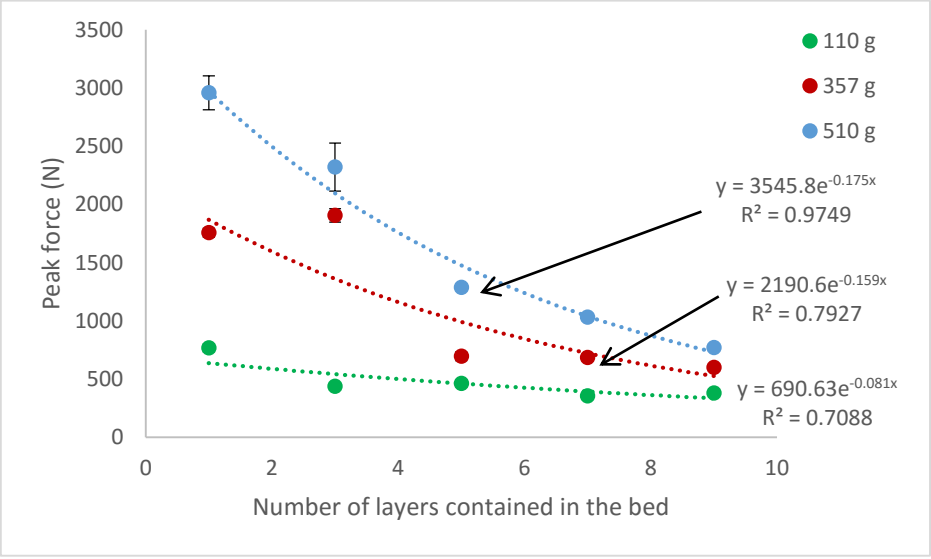

Figure 6.13: Peak force as a function of bed depth with increasing steel ball mass for tests conducted on blue stone

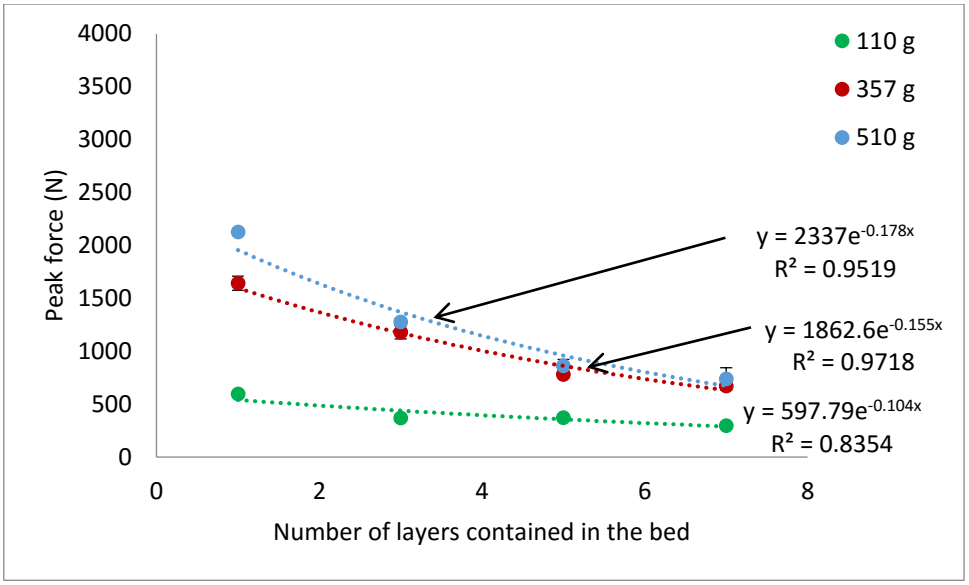

Figure 6.14: Peak force as a function of bed depth with increasing steel ball mass for tests conducted on UG2

From Figure 6.13 and Figure 6.14 it is seen that the steepness of the exponential trend lines increased with increasing steel ball mass, indicating that higher input energies had a greater effect on the peak forces obtained. The figures also show that for each input energy, the difference in peak forces obtained between adjacent bed depths decreased with increasing bed depth. This illustrates that smaller bed depths had a larger impact on the peak force, and the increased number of layers at larger bed depths resulted in a reduced effect on the peak force.

From the results presented in Section 4.1 and Section 5.1 it was found that for both ores, some tests conducted using the same steel ball showed a trend in which statistically equal results were obtained at adjacent bed depths. For some tests anomalies in which the peak force at a larger bed depth was greater than that at a smaller one for the same input energy were observed. The discrepancies from the predicted trend can be attributed to the distinct grain and flaw structure of each particle which led to variances in the force distribution through the bed (Vervoorn & Austin, 1990; Tavares & King, 1998).

6.2. Discussion of the fracture energy results

The effects of varying the steel ball mass, drop height and bed depth of particles on the fracture energy are discussed in this section. Results are only discussed for UG2 as blue stone particles did not break at the range of input energies used in this work.

6.2.1. Effect of increasing the steel ball mass

From the UG2 results shown in Section 5.2 it was seen that the energy used for particle fracture for all the steel balls was low and below 3 %. Schonert (1996) and Gutsche & Fuerstenau (1999) proposed that when stress is applied to a bed of particles, a fraction of the input energy is used to rearrange the particles within the bed, resulting in less energy being available to cause breakage (Section 2.7.3). This is a contributing factor to the low values of energy used to cause fracture for all the steel balls.

Figure 6.15 shows the effect of increasing the steel ball mass on the fracture energy at a constant drop height of 300 mm. The results are presented for increasing number of layers contained in the bed.

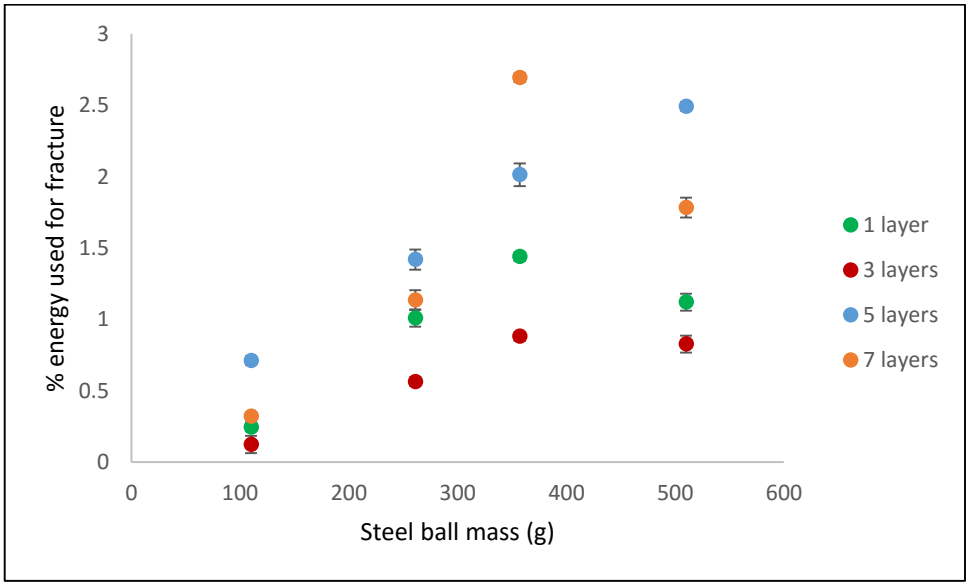

Figure 6.15: Fracture energy as a function of increasing input energy and increasing bed depth for tests conducted on UG2

From Figure 6.15 it is seen that for the different bed depths the results did not show the same trend and there was no direct correlation between the % energy utilized for fracture and the steel ball mass. This result was unexpected as it was anticipated that an increase in the ball mass would result in a greater amount of energy used for particle fracture due to an increasing surface area of impact. This finding suggests that there is a more complex relationship at play, which is worth investigating in future work.

The greatest amount of energy used for fracture was generally obtained at the largest input energies of 2.9×10^{-7} and 4.2×10^{-7} kWh using the 357 and 510 g balls respectively. For some adjacent bed depths, the fracture energy obtained using the 357 ball was greater than or equal to that obtained using the 510 g ball. This suggests that there is a maximum amount of energy

that can be used for particle fracture regardless of an increase in the magnitude of the input energy.

From Figure 6.15 it is seen that the fracture energy generally increased with increasing steel ball mass from 110 - 357 g and increasing bed depth from 3 – 5 layers. A three-dimensional (3D) surface plot was used to compare the effect of the steel ball mass and bed depth on the fracture energy in the ranges in which increasing these variables resulted in an increase in the fracture energy. The surface plot made is presented in Figure 6.16.

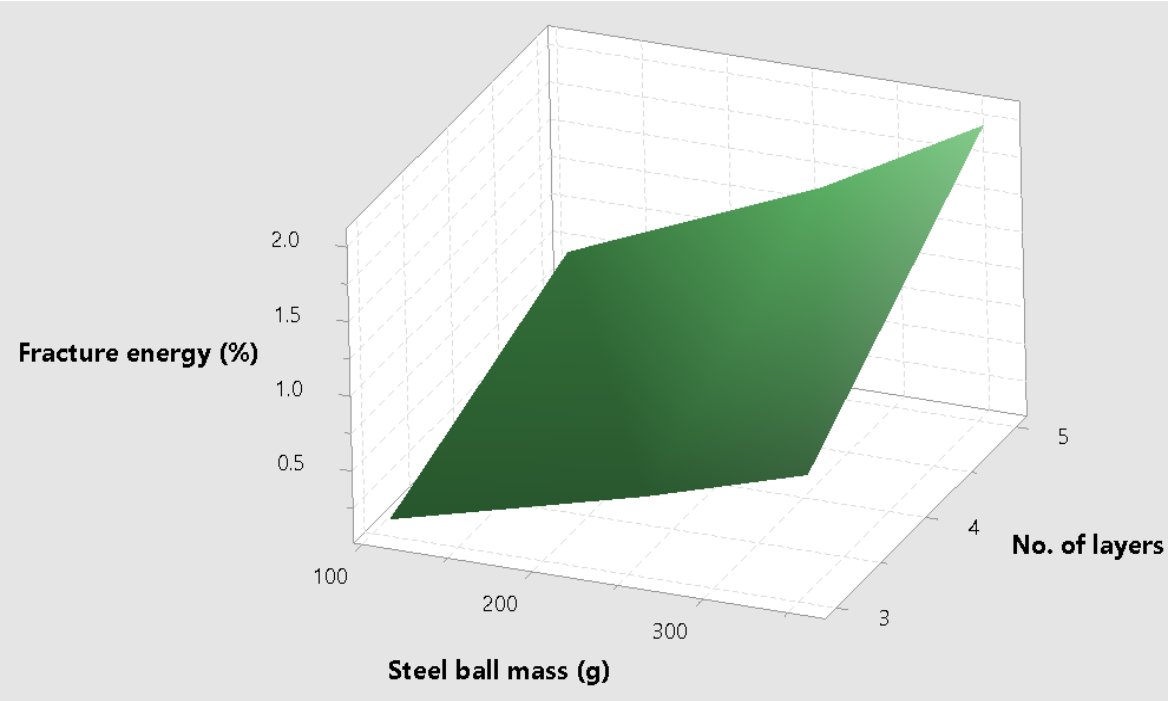

Figure 6.16: 3D surface plot showing the effect of increasing the steel ball mass and the bed depth on the fracture energy for tests conducted at a constant drop height of 300 mm

From Figure 6.16 it is seen that the plot showed a larger slope for an increase in the number of layers contained in the bed compared to an increase in the steel ball mass. This indicates that for the range of these two variables considered, the fracture energy was more reliant on the number of layers contained in the bed compared to the magnitude of the input energy.

6.2.2. Effect of increasing the drop height

Figure 6.17 shows the effect of increasing drop height on the energy available for particle fracture at a constant steel ball mass of 510 g. The results are presented for increasing bed depth.

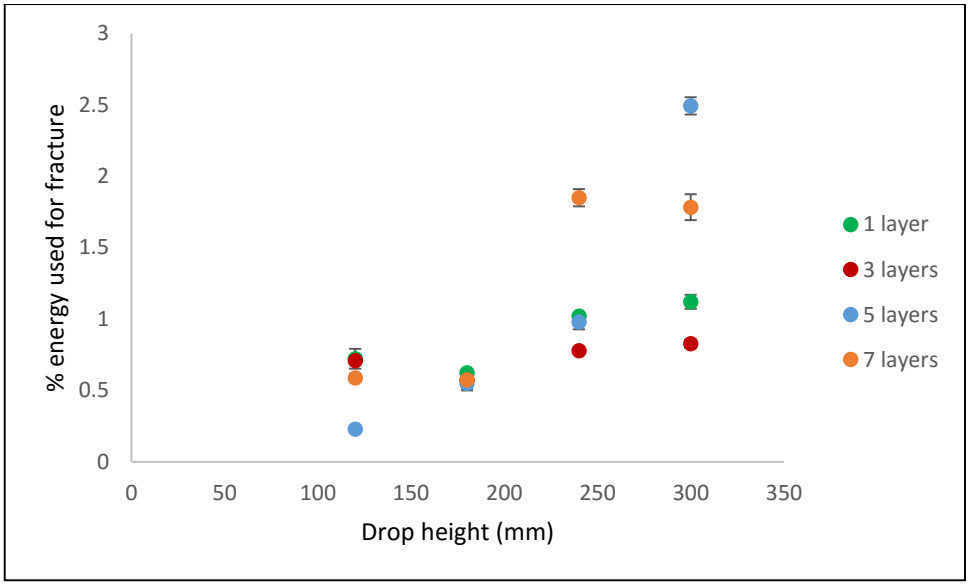

Figure 6.17: Fracture energy as a function of the drop height with increasing bed depth for tests conducted on UG2

Figure 6.17 shows that for the different bed depths, the fracture energy was not directly related to the drop height. It was typically found that the fracture energy obtained at a drop height of 240 mm was greater than or equal to that obtained at 300 mm. As mentioned in Section 6.2.1, this indicates that the greatest amount of energy that can be utilized for particle fracture can be attained without using the highest input energy.

From Figure 6.17 it is seen that the fracture energy generally increased with increasing drop height from 180 – 240 mm and increasing bed depth from 3 – 5 layers. A three-dimensional (3D) surface plot was used to compare the effect of the drop height and bed depth on the fracture energy in the ranges in which increasing these variables resulted in an increase in the fracture energy. The surface plot made is presented in Figure 6.18

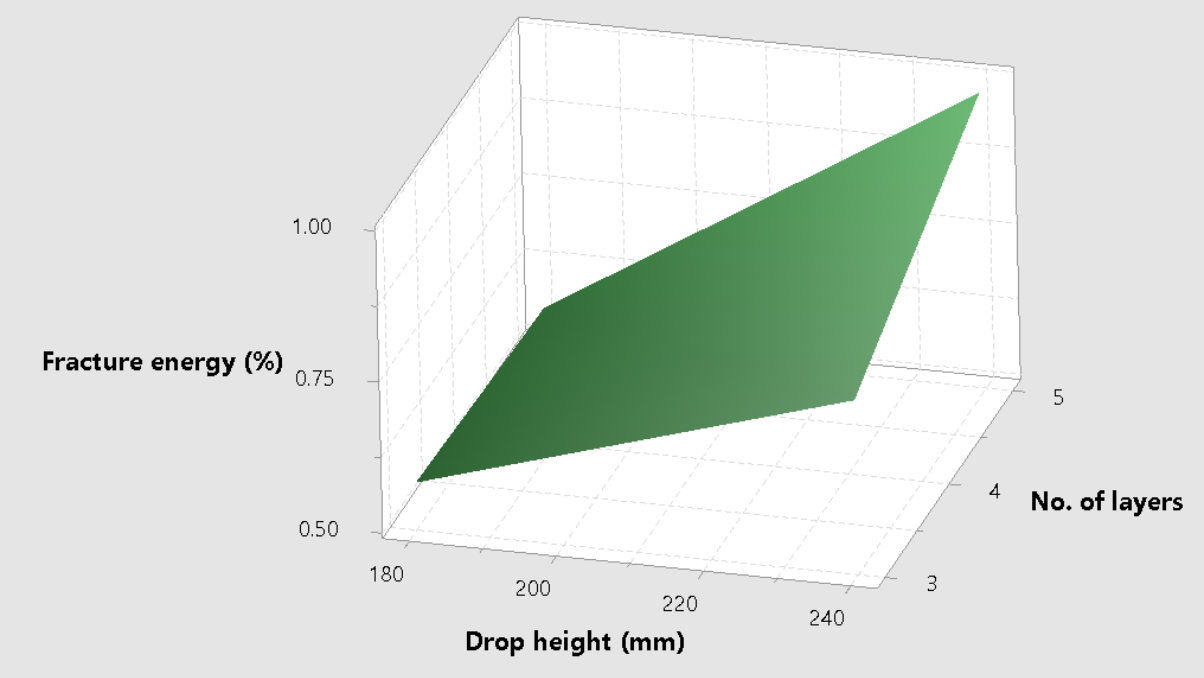

Figure 6.18: 3D surface plot showing the effect of increasing the drop height and the bed depth on the fracture energy for tests conducted at a constant steel ball mass of 510 g

From Figure 6.18 it is seen that for both ores, the plots showed a larger slope for increasing the number of layers in comparison to increasing the drop height. This confirms the findings stated in Section 6.2.1, that for the range of these variables considered, the particle fracture energy was more dependent on the bed depth than the input energy.

6.2.3. Effect of increasing the bed depth

Khanal et al. (2007) proposed that for bed breakage, a greater fraction of the input energy is used to reposition particles within the bed as more particles are added, resulting in less energy being used to cause fracture (Section 2.7.3).

From the UG2 results presented in Section 5.2 it was found that the results obtained did not show the exact findings made by Khanal et al. (2007). This is because none of the tests conducted consistently showed the expected trend which was a continuous decrease in the fracture energy with increasing bed depth for the same input energies.

Figure 6.19 shows the effect of increasing bed depth on the fracture energy at a constant drop height of 300 mm for tests conducted on UG2. The results are presented for increasing steel ball mass from 110 to 510 g.

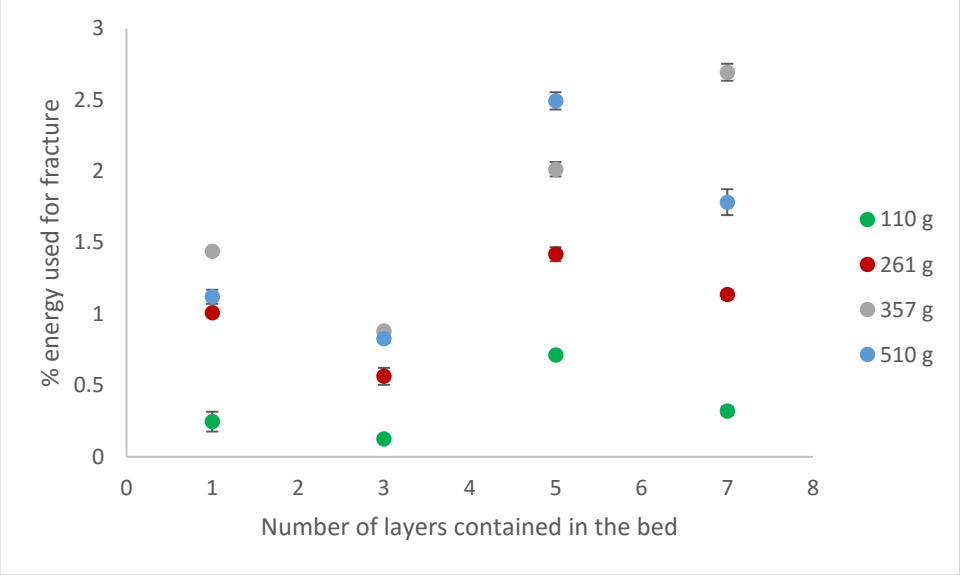

Figure 6.19: The effect of increasing bed depth on the fracture energy with increasing input energy for tests conducted on UG2

From Figure 6.19 it is seen that the fraction of input energy used for breakage and the bed depth were not directly related. The % energy utilized for particle breakage decreased when the number of layers was increased from one to three. However, an increase in the fracture energy was observed when the bed depth was increased from three to five layers, where the maximum fracture energy was typically obtained at this bed depth. This suggests that five layers was the optimum bed depth that allowed for the highest amount of energy to be used for particle fracture. It is postulated that at lower bed depths the number of layers in the bed was too low to absorb a large amount of energy to use for particle fracture; hence a great fraction of the input energy was transmitted through the bed and was lost to the surroundings. At five layers the increased thickness of the bed allowed for a greater fraction of the input energy to be used for breakage instead of being lost to the surroundings.

Increasing the bed depth from five layers generally resulted in a reduction in the energy used for fracture. The decrease in the fracture energy can be attributed to a higher fraction of the input energy being used to rearrange the increased number of particles within the bed, resulting in less energy being available to cause particle fracture (Khanal et al., 2007).

In work done by Barrios et al. (2013), breakage tests were conducted on four different materials of varying hardness: copper ore, quartz, granulite and limestone, where copper ore was the hardest and limestone the softest material tested. For the harder materials: copper ore, quartz and granulite it was found that the breakage obtained remained constant or reduced when the number of layers contained in the bed was increased. This was due to the loss of kinetic energy as a result of the transfer of momentum of the falling ball to the particles that were projected away during impact. This in turn caused less energy available to be used

for breakage of the particles with an increase in the number of layers in the bed. However, for the softest material, limestone, it was found that the breakage increased with an increase in the number of layers. This was a result of the stressing energies involved between the falling ball and the ejected particles which were high enough to cause breakage as a result of the low particle strengths. The results found in this work are consistent with those found by Barrios et al. (2013) for copper ore, quartz and granulite, where the energy available for breakage decreased with an increase in the bed depth for the hard UG2 ore.

6.3. Discussion of the breakage results

In this section the breakage results are discussed. The lack of breakage of blue stone particles is discussed in Section 6.3.1. The effect of increasing the input energy on the breakage of UG2 particles is discussed in Section 6.3.2. The discussion of the effect which varying the bed depth had on the breakage attained is given in Section 6.3.3 and the effect of the fracture energy on the breakage obtained is presented in Section 6.3.4.

6.3.1. Explanation for the lack of breakage of blue stone particles

From the blue stone and UG2 results presented in Section 4 and Section 5, it was seen that no breakage of blue stone particles occurred; however there was breakage of UG2 particles.

Figure 6.20 and Figure 6.21 show the Force-time profiles obtained for breakage tests conducted using all the steel balls on one layer of blue stone and UG2 particles.

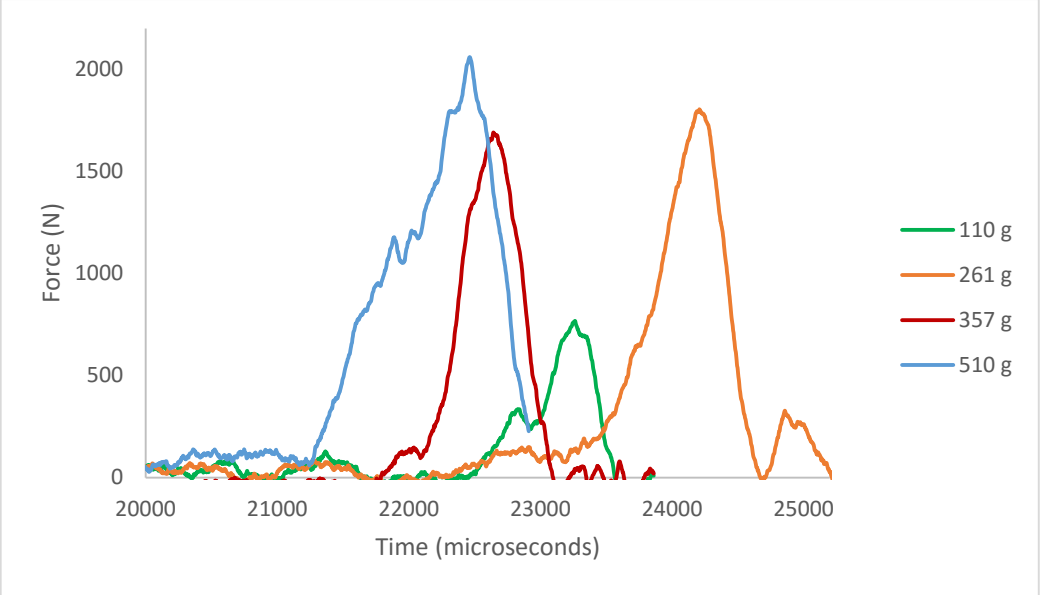

Figure 6.20: Force-time profiles obtained for breakage tests conducted on one layer of blue stone particles using all the steel balls

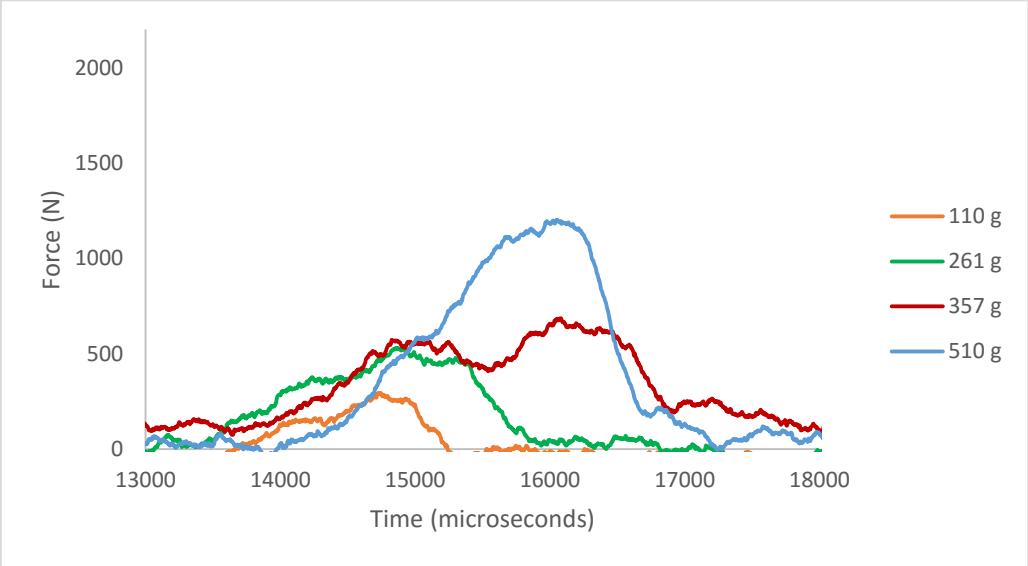

Figure 6.21: Force-time profiles obtained for breakage tests conducted on one layer of UG2 particles using all the steel balls

From the work done by Tavares & King (2004) it was found that materials with a higher modulus of elasticity and stiffness had the shortest impact duration (time taken from the beginning to the end of impact). From Figure 6.20 and Figure 6.21 it is seen that for blue stone particles the rise time (time taken to reach the peak force) was shorter and the Force-time peaks tapered off quickly after the peak force was reached. The impact duration was shorter for tests conducted on the stiffer blue stone particles than for tests done on UG2. This finding is in line with that made by Tavares & King (2004). The broader Force-time profiles obtained for UG2 indicate that the force propagated through the particles for a longer time. As a result,

the UG2 particles had more energy available for breakage, whereas the blue stone particles had less energy and did not break.

The peak forces obtained for blue stone were larger than those for UG2, which suggests that the UG2 particles yielded at lower fracture forces. The breakage of UG2 at lower fracture forces was expected, as UG2 is a softer ore than blue stone (Section 3.3.1). At the input energies used, blue stone particles did not break due to the ore's hardness. Higher input energies could not be used to investigate the breakage of blue stone particles as the SILC used for experiments only allowed for a maximum ball mass and drop height of 510 g and 300 mm respectively.

6.3.2. Effect of increasing the input energy on the degree of breakage obtained

Stamboliadis (2002), Morrison & Cleary (2004) and Shi & Kojovic (2007) found that the breakage obtained initially increases with increasing specific input energy; however, as the specific input energy is increased further, the breakage reaches a constant value (Section 2.7.1). Based on the findings made by the researchers, a similar result was expected for the tests conducted in this work.

The UG2 results presented in Section 5.3 showed that the breakage results obtained for the tests were low, and were all below 35 % passing. This can be attributed to the low values of input energies used, where the maximum input energy was 4.2×10^{-7} kWh.

Tests conducted at the same bed depth generally showed the trend observed by Stamboliadis (2002), Morrison & Cleary (2004) and Shi & Kojovic (2007). It was found that the breakage initially increased greatly with increasing input energy; however at larger input energies the breakage obtained plateaued towards a constant value. For all tests, the least breakage was found at the lowest input energies as expected. From all the tests conducted, the maximum breakage of 31.7 % passing was obtained at one layer of particles using the 357 g ball and 240 mm drop height. This finding illustrates that it is possible to obtain a greater amount of breakage at lower input energies, as the maximum breakage was not obtained at the largest input energy.

A 3D surface plot, shown in Figure 6.22, was used to compare the effect of increasing the input energy by varying the steel ball mass compared to the drop height on the breakage obtained.

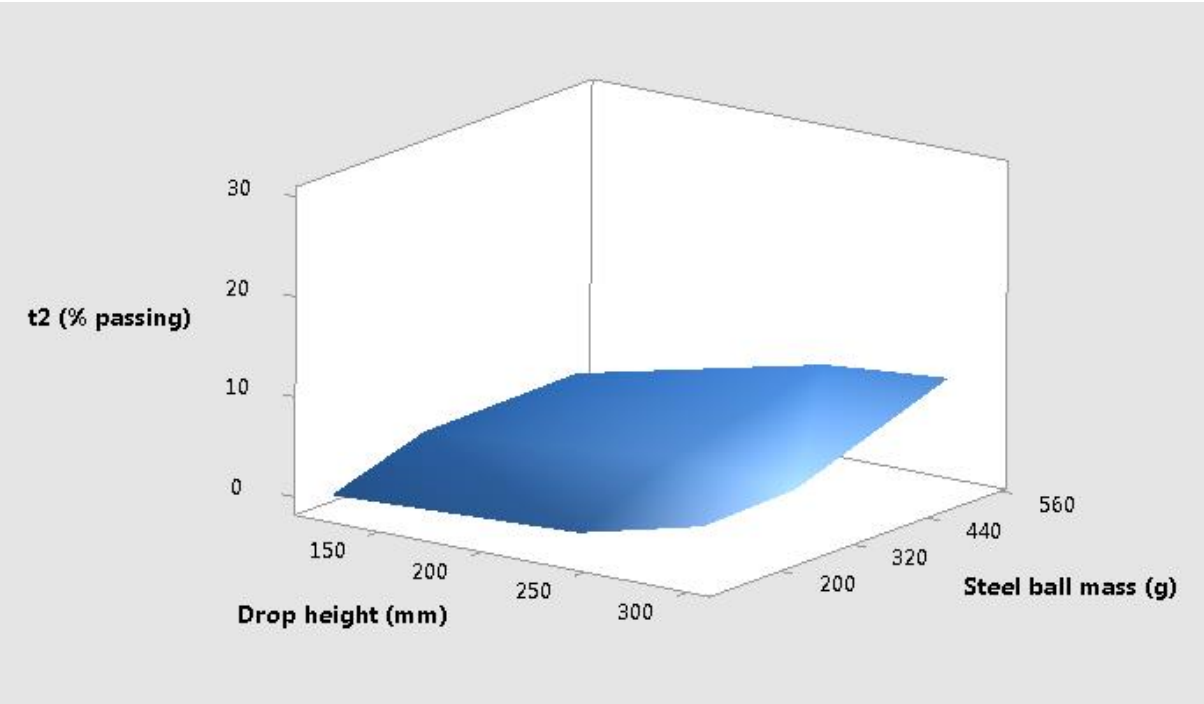

Figure 6.22: 3D surface plot showing the effect of increasing the steel ball mass versus the drop height on the breakage obtained

Figure 6.22 shows that the slope for an increase in the steel ball mass was larger than that for an increase in the drop height. This illustrates that for the range of these two variables used, the steel ball mass had a greater effect on the breakage obtained compared to the drop height.

6.3.3. Effect of increasing the bed depth on the degree of breakage obtained

From studies conducted by Schonert (1996) and Barrios et al. (2013) it was found that there was a decrease in the breakage obtained with increasing bed depth due to a reducing amount of energy per unit mass being available to cause breakage.

The results presented in Section 5.3 showed that the highest degree of breakage was attained at one layer and it decreased with increasing bed depth. These results were in line with the findings made by Schonert (1996) and Barrios et al. (2013). A negligible amount of breakage was obtained at the largest bed depths of five and seven layers which can be attributed to the low input energies used.

For several tests it was found that the fracture energy was the highest at five and seven layers; however the least breakage was obtained at these bed depths. This finding suggests that at the largest bed depths a higher fraction of the input energy was required to cause particle fracture due to the increased thickness of the bed.

6.3.4. Effect of the fracture energy on the breakage obtained

From the results presented in Section 5.3 it was observed that the breakage obtained and the fracture energy were not directly related. For each bed depth, the general trend was a large increase in the breakage attained with a small increase in the fracture energy at lower fracture energy values. A further increase in the fracture energy led to a negligible change in the breakage values obtained. This finding indicates that there is an optimum amount of energy required that leads to the greatest breakage, where an in increase in the energy beyond the optimum point does not significantly affect the breakage obtained.

7. CONCLUSIONS AND RECOMMENDATIONS

Overview

This chapter provides the conclusions made from the work done in this study, along with recommendations for future work.

7.1. Observations made from experimental work

The study was aimed at investigating the effect of three variables: steel ball mass, drop height and bed depth on the breakage behaviour of particles in partially confined conditions. This was done by conducting bed breakage tests on blue stone and UG2 and investigating the effect of the three variables on the peak forces obtained, the fracture energy and the degree of particle breakage attained. The relationship between the fracture energy and degree of breakage was also evaluated.

It was found that the peak forces for blue stone were larger because it is harder and has a larger stiffness compared to UG2. For both ores it was found that the peak force increased linearly with increasing steel ball mass and drop height. The drop height was found to have a greater effect on the peak force obtained compared to the steel ball mass. For each steel ball and drop height, one layer of particles had the greatest impact on the peak force and increasing the bed depth resulted in a reduced effect on the peak forces obtained. An exponential relationship was found between the peak force and bed depth, where the peak force decreased with increasing bed depth.

It was found that the blue stone particles did not break at the range of input energies used in this work, therefore no fracture energy results were reported for blue stone. The fracture energy values for UG2 were low, where for all tests conducted the maximum energy used for particle fracture was 2.7 % of the input energy. It was found that the greatest amount of energy used for fracture was generally obtained at the largest input energies using the 357 and 510 g balls. In some cases it was found that the fracture energy obtained using the 357 ball was greater than or equal to that obtained using the 510 g ball, suggesting that there is a maximum amount of energy that can be used for particle fracture regardless of an increase in the magnitude of the input energy.

It was found that the optimum drop height which resulted in the highest fracture energy was generally either 240 or 300 mm. The fracture energy obtained at 240 mm was generally equal to or greater than that obtained at the maximum drop height of 300 mm, also indicating that

the greatest amount of energy that can be utilized for particle fracture can be attained without using the highest input energy

The experimental results showed that the fracture energy and the bed depth were not directly related. A bed depth of five layers was found to be the optimum bed depth that allowed for the highest fraction of input energy to be utilized for fracture. Increasing the bed depth from five layers generally resulted in a reduction in the fracture energy. It was found that the bed depth had a larger effect on the fracture energy compared to both the steel ball mass and drop height.

For the tests conducted, the degree of breakage was quantified using the t_2 parameter. At the range of input energies used to conduct breakage tests, no breakage results were obtained for blue stone due to the hardness and stiffness of the ore. For UG2, tests conducted at the same bed depth showed a trend in which the breakage initially increased greatly with increasing input energy; however at larger input energies the breakage obtained approached a constant value. Although the input energy was varied by changing both the steel ball mass and the drop height, the results showed that the degree of breakage was more dependent on the steel ball mass compared to the drop height. For all tests conducted, the maximum breakage was obtained at one layer of particles and increasing the bed depth led to a decrease in the breakage obtained. The results showed that the fracture energy and the degree of breakage were not directly related. It was found that there is an optimum amount of energy utilized for particle fracture that leads to the greatest breakage, where an in increase in the energy beyond the optimum point does not significantly affect the breakage obtained.

7.2. Conclusions

Based on the objectives and hypotheses of the study, the following conclusions were made:

- The peak force is linearly related to the steel ball mass and drop height (and therefore the input energy) where increasing each of these variables resulted in an increase in the peak force. An exponential relationship was found between the peak force and bed depth, where the peak force decreased with increasing bed depth.

- There is no direct correlation between the fracture energy and the steel ball mass and drop height (and therefore the input energy). There is also no direct correlation between the fracture energy and the particle bed depth. The greatest amount of energy utilized for breakage was generally obtained at the largest input energies using the 357 and 510 g balls. The optimum drop height which resulted in the highest amount of

energy used for breakage was generally found to be either 240 or 300 mm. A bed depth of five layers was found to be the optimum bed depth that allowed for the highest amount of energy to be used for breakage.

- The degree of breakage initially increases with increasing input energy (dependent on the steel ball mass and the drop height) however at larger input energies the breakage obtained approached a constant value. The maximum breakage was obtained at one layer of particles and increasing the bed depth led to a decrease in the breakage obtained.

- The degree of breakage obtained is not directly related to the fracture energy. It was found that there was an optimum amount of energy used for particle fracture that led to the greatest breakage, where an in increase in the energy beyond the optimum point did not significantly affect the breakage obtained.

This work was done to test the two hypotheses presented in Section 2.9. The first hypothesis put forward was found to be true as it was shown that the bed depth has a greater effect on the proportion of input energy used for fracture compared to both the steel ball mass and drop height. This indicates that the energy used for fracture is more dependent on the thickness of the bed compared to the input energy.

The second hypothesis put forward was also proven to be true as it was shown that although the input energy is dependent on both the steel ball mass and the drop height, the steel ball mass has a greater effect on the breakage obtained compared to the drop height. This is because the steel ball affects the contact surface area for balls of the same material density, where increasing the ball mass exposes more particles to impact, resulting in higher breakage.

7.3. Recommendations for future work

Several limitations prevented some investigations from being carried out. Firstly, it was not possible to quantify the amount of force that was transmitted through each layer in the bed and the breakage that occurred in each respective layer. Also, the maximum input energy used for tests was found at a ball mass of 510 g and 300 mm as the Short Impact Load Cell did not allow for ball masses and drop heights larger than these to be used. As a result of the low input energies used, the blue stone particles did not break due to the ore's hardness.

In light of the findings made in the study, the following recommendations for further studies are made:

- Numerical methods such as Discrete Element Method (DEM) simulations should be employed to quantify the distribution of the applied force across the bed of particles. The Discrete Element Method is a technique used to model the behaviour of discrete interacting bodies (Agrawala et al., 1997). Discrete element simulations have been used by a number of researchers to get an in-depth understanding of the breakage behaviour of particles (Cleary, 1998; Mishra, 2003; Khanal et al, 2004; Antonyuk et al., 2006)

- DEM simulations should be used to evaluate the amount of breakage which occurs in each layer of particles contained in the bed

- For a more rigorous SILC calibration procedure, a more detailed methodology such as removing the instrumented bar and calibrating it on a different test bed can be used

- Due to the low input energies that the Short Impact Load Cell allows for, an ore softer than blue stone (such as another platinum bearing ore) should be used to conduct tests in order to obtain breakage results

- A full energy balance of the system should be determined for better accuracy in isolating the energy used for fracture from that lost to other forms such as friction, kinetic energy and the energy lost by the rebound velocity of the ball

- To further investigate the breakage behaviour of various ores, future work should consider the effect of ore type, hardness and toughness

- A larger impact load cell that can accommodate larger beds should be used for experiments to compare the results obtained in this work to those attained with larger particle beds

8. REFERENCES

Agrawala, S., Rajamani, R., Songfack, P. & Mishra, B. 1997. Mechanics of media motion in tumbling mills with 3D discrete element method. *Minerals Engineering.* 10(2):215-227.

Al-Mousawi, M., Reid, S. & Deans, W. 1997. The use of the split Hopkinson pressure bar techniques in high strain rate materials testing. *Proceedings of the Institution of Mechanical Engineers, Part C: Journal of Mechanical Engineering Science.* 211(4):273-292.

Anderson, T.L. 2005. *Fracture mechanics: fundamentals and applications.* CRC press.

Antonyuk, S., Khanal, M., Tomas, J., Heinrich, S. & Mörl, L. 2006. Impact breakage of spherical granules: experimental study and DEM simulation. *Chemical Engineering and Processing: Process Intensification.* 45(10):838-856.

Austin, L.G. 2002. A treatment of impact breakage of particles. *Powder Technology.* 126(1):85-90.

Barrios, G.K., de Carvalho, R.M. & Tavares, L.M. 2011. Modeling breakage of monodispersed particles in unconfined beds. *Minerals Engineering.* 24(3):308-318.

Barrios, G.K., de Carvalho, R.M. & Tavares, L.M. 2013. Breakage of Particles by Impact in Unconfined Beds with Multiple Layers. Proceedings of the 13th European Symposium on Comminution & Classification. 9-12 September 2013, Braunschweig, Germany.

Bbosa, L., Powell, M. & Cloete, T. 2006. An investigation of impact breakage of rocks using the split Hopkinson pressure bar. *Journal of the South African Institute of Mining and Metallurgy.* 106(4):291-296.

Bbosa, L.S. 2007. Measurement of impact breakage properties of ore particles using a series of devices. MSc thesis. University of Cape Town.

Bernotat, S. & Schönert, K. 1988. Size reduction. *Ullmann's Encyclopedia of Industrial Chemistry.*

Bond, F.C. 1952. The third theory of comminution. *AIME Transactions. 193: 484-494.*

Bourgeois, F. & Banini, G. 2002. A portable load cell for in-situ ore impact breakage testing. *International Journal of Mineral Processing.* 65(1):31-54.

Broek, D. 1986. *Elementary engineering fracture mechanics.* Springer.

Brown, G., Miles, N. & Jones, T. 1996. A fractal description of the progeny of single impact single particle breakage. *Minerals Engineering.* 9(7):715-726.

Brown, G. & Reddish, D. 1997. Experimental relations between rock fracture toughness and density. *International Journal of Rock Mechanics and Mining Sciences.* 34(1):153-155.

Chaboche, J. 1988. Continuum damage mechanics: Part II—Damage growth, crack initiation, and crack growth. *Journal of Applied Mechanics.* 55(1):65-72.

Cleary, P.W. 1998. Predicting charge motion, power draw, segregation and wear in ball mills using discrete element methods. *Minerals Engineering.* 11(11):1061-1080.

Courtney, T.H. 2005. *Mechanical behavior of materials.* Waveland Press.

Cramer, L.A. 2001. The extractive metallurgy of South Africa's platinum ores. *Jom.* 53(10):14-18.

Dai, F., Huang, S., Xia, K. & Tan, Z. 2010. Some fundamental issues in dynamic compression and tension tests of rocks using split Hopkinson pressure bar. *Rock Mechanics and Rock Engineering.* 43(6):657-666.

Darling, P. 2011. *SME mining engineering handbook.* SME.

Erdogan, F. 2000. Fracture mechanics. *International journal of solids and structures*. 37(1-2):171-183.

Frew, D., Forrestal, M.J. & Chen, W. 2001. A split Hopkinson pressure bar technique to determine compressive stress-strain data for rock materials. *Experimental Mechanics.* 41(1):40-46.

Fuerstenau, D. & Abouzeid, A. 2002. The energy efficiency of ball milling in comminution. *International Journal of Mineral Processing.* 67(1):161-185.

Fuerstenau, D., Lutch, J. & De, A. 1999. The effect of ball size on the energy efficiency of hybrid high-pressure roll mill/ball mill grinding. *Powder Technology.* 105(1):199-204.

Gama, B.A., Lopatnikov, S.L. & Gillespie, J.W. 2004. Hopkinson bar experimental technique: a critical review. *Applied Mechanics Reviews.* 57(4):223-250.

Genc, O., Ergon, L. & Benzer, H. 2004. Single particle impact breakage characterization of materials by drop weight testing. *Fizykochemiczne Problemy Mineralurgii/Physicochemical Problems of Mineral Processing.* (38):241-255.

Gray III, G. & Blumenthal, W.R. 2000. Split-Hopkinson pressure bar testing of soft materials. *ASM Handbook.* 8:488-496.

Gupta, C.K. & Suri, A. 1993. *Extractive metallurgy of niobium.* CRC press.

Gutsche, O. & Fuerstenau, D. 1999. Fracture kinetics of particle bed comminution—ramifications for fines production and mill optimization. *Powder Technology.* 105(1):113-118.

Harrison, J.P. & Hudson, J.A. 2000. *Engineering rock mechanics-an introduction to the principles.* Elsevier.

Hogg, R. 1999. Breakage mechanisms and mill performance in ultrafine grinding. *Powder Technology.* 105(1):135-140.

Jaeger, J.C., Cook, N.G. & Zimmerman, R. 2009. *Fundamentals of rock mechanics.* John Wiley & Sons.

JKTech. n.d. *Laboratory Services: JK Drop weight test. Machine manual.* Available:

http://www.jktech.com.au/sites/default/files/brochures/LabServices_DWTest_Indetail.pdf [2015, April 30]

Johnson, K. L. 1987. *Contact Mechanics.* Cambridge University Press.

Kachanov, L. 1986. *Introduction to continuum damage mechanics.* Springer.

Kapur, P., Pande, D. & Fuerstenau, D. 1997. Analysis of single-particle breakage by impact grinding. *International Journal of Mineral Processing.* 49(3):223-236.

Kawatra, S.K. 2006. *Advances in comminution.* SME.

Khanal, M., Schubert, W. & Tomas, J. 2004. Ball impact and crack propagation–simulations of particle compound material. *Granular Matter.* 5(4):177-184.

Khanal, M., Schubert, W. & Tomas, J. 2007. Discrete element method simulation of bed comminution. *Minerals Engineering.* 20(2):179-187.

King, R.P. & Bourgeois, F. 1993. Measurement of fracture energy during single-particle fracture. *Minerals Engineering.* 6(4):353-367.

Kojovic, T., Shi, F.N., Larbi-Bram, S. & Manlapig, E. 2010. Validation of the JKMRC rotary breakage tester (JKRBT) ore breakage characterisation device. *International Mineral Processing Congress 2010.* Australasian Institute of Mining and Metallurgy. 901.

Kolsky, H., 1949. An investigation of the mechanical properties of materials at very high rates of loading. Proceedings of the Physical Society. Section B, 62(11): 676.

Krajcinovic, D. & Mastilovic, S. 1995. Some fundamental issues of damage mechanics. *Mechanics of Materials.* 21(3):217-230.

Landis, E.N. 1999. Micro–macro fracture relationships and acoustic emissions in concrete. *Construction and Building Materials.* 13(1):65-72.

Larbi-Bram, S. 2009. A Study of Ore Breakage Characterization for AG/SAG Mill Modelling. PhD thesis. University of Queensland.

Lynch, A.J. & Rowland, C.A. 2005. *The history of grinding.* SME.

McLaren, C.H. & De Villiers, J.P. 1982. The platinum-group chemistry and mineralogy of the UG-2 chromitite layer of the Bushveld Complex. *Economic Geology.* 77(6):1348-1366.

Mishra, B. 2003. A review of computer simulation of tumbling mills by the discrete element method: part I—contact mechanics. *International Journal of Mineral Processing.* 71(1):73-93.

Mishra, B. & Rajamani, R.K. 1992. The discrete element method for the simulation of ball mills. *Applied Mathematical Modelling.* 16(11):598-604.

Mishra, B. & Thornton, C. 2001. Impact breakage of particle agglomerates. *International Journal of Mineral Processing.* 61(4):225-239.

Moothedath, S.K. & Ahluwalia, S. 1992. Mechanism of action of grinding aids in comminution. *Powder Technology.* 71(3):229-237.

Morrell, S. 2015. Global trends in ore hardness. Proceedings of the 6th International Conference on Semi-Autogenous and High Pressure Grinding Technology. 20–24 September 2015, Vancouver, British Columbia, Canada.

Morrison, R. & Cleary, P. 2004. Using DEM to model ore breakage within a pilot scale SAG mill. *Minerals Engineering.* 17(11):1117-1124.

Napier-Munn, T.J., Morrell, S., Morrison, R.D. & Kojovic, T. 1996. *Mineral comminution circuits: their operation and optimisation.* Julius Kruttschnitt Mineral Research Centre, University of Queensland.

Narayanan, S. 1987. Modelling the performance of industrial ball mills using single particle breakage data. *International Journal of Mineral Processing.* 20(3):211-228.

Narayanan, S. & Whiten, W. 1988. Determination of comminution characteristics from single-particle breakage tests and its application to ball-mill scale-up. *Transactions of the Institution of Mining and Metallurgy Section c-Mineral Processing and Extractive Metallurgy.* 97:C115-C124.

Nguyen, A., Husemann, K. & Oettel, W. 2002. Comminution behaviour of an unconfined particle bed. *Minerals Engineering.* 15(1):65-74.

Nikolov, S. 2004. Modelling and simulation of particle breakage in impact crushers. *International Journal of Mineral Processing.* 74:S219-S225.

Oettel, W. & Husemann, K. 2004. The effect of a grinding aid on comminution of fine limestone particle beds with single compressive load. *International Journal of Mineral Processing.* 74:S239-S248.

Ozkahraman, H. 2005. A meaningful expression between bond work index, grindability index and friability value. *Minerals Engineering.* 18(10):1057-1059.

Pauw, O. & Maré, M. 1988. The determination of optimum impact-breakage routes for an ore. *Powder Technology.* 54(1):3-13.

Pharr, G., Oliver, W. & Brotzen, F. 1992. On the generality of the relationship among contact stiffness, contact area, and elastic modulus during indentation. *Journal of Materials Research.* 7(03):613-617.

Potapov, A.V. & Campbell, C.S. 2001. Parametric dependence of particle breakage mechanisms. *Powder Technology.* 120(3):164-174.

Prokajcic, Z. 2008. Energy efficient comminution circuits-A modified grinding strategy and the selection of a target product size. Proceedings of the 2nd annual Centre for Sustainable Resource Processing conference 18-19 November 2008. Brisbane, Queensland.

Radziszewski, P. 2000. Developing an experimental procedure for charge media wear prediction. *Minerals Engineering.* 13(8):949-961.

Ramesh, K. & Narasimhan, S. 1996. Finite deformations and the dynamic measurement of radial strains in compression Kolsky bar experiments. *International Journal of Solids and Structures.* 33(25):3723-3738.

Rocco, C., Guinea, G., Planas, J. & Elices, M. 1999. Size effect and boundary conditions in the Brazilian test: theoretical analysis. *Materials and Structures.* 32(6):437-444.

Runge, K., Tabosa, E. & Jankovic, A. 2013. Particle Size Distribution Effects that Should be Considered when Performing Flotation Geometallurgical Testing. *GeoMet 2013: The Second AusIMM International Geometallurgy Conference.* The Australasian Institute of Mining and Metallurgy (AusIMM). 335.

Sadrai, S., Meech, J., Ghomshei, M., Sassani, F. & Tromans, D. 2006. Influence of impact velocity on fragmentation and the energy efficiency of comminution. *International Journal of Impact Engineering.* 33(1):723-734.

Salman, A., Gorham, D. & Verba, A. 1995. A study of solid particle failure under normal and oblique impact. *Wear.* 186:92-98.

Salman, A.D., Ghadiri, M. & Hounslow, M. 2007. *Particle breakage.* Elsevier.

Schönert, K. 1991. Advances in comminution fundamentals and impacts on technology. *Aufbereitungs-Technik.* 32(9):487-494.

Schönert, K. 1996. The influence of particle bed configurations and confinements on particle breakage. *International Journal of Mineral Processing.* 44:1-16.

Schouwstra, R., Kinloch, E. & Lee, C. 2000. A short geological review of the Bushveld Complex. *Platinum Metals Review.* 44(1):33-39.

Schultz, R. 1995. Limits on strength and deformation properties of jointed basaltic rock masses. *Rock Mechanics and Rock Engineering.* 28(1):1-15.

Shi, F. & Kojovic, T. 2007. Validation of a model for impact breakage incorporating particle size effect. *International Journal of Mineral Processing.* 82(3):156-163.

Shi, F., Kojovic, T., Larbi-Bram, S. & Manlapig, E. 2009. Development of a rapid particle breakage characterisation device–The JKRBT. *Minerals Engineering.* 22(7):602-612.

Sikong, L., Hashimoto, H. & Yashima, S. 1990. Breakage behavior of fine particles of brittle minerals and coals. *Powder Technology.* 61(1):51-57.

SILC Data Acquisition Module- Operation and Design. 2002. Machine manual. 409: 6-14.

Published by De Beers.

Singh, N., Urcan, H., Naidoo, K., Ryder, J., Watson, B., Milev, A. & Roberts, M. 2005. The influence of pillars on the Merensky Reef horizon on stoping operations on the underlying UG2 Reef horizon. *Journal-South African Institute of Mining and Metallurgy.* 105(6):427

Song, B. & Chen, W. 2005. Split Hopkinson pressure bar techniques for characterizing soft materials. *Latin American Journal of Solids and Structures.* 2(2):113-152.

Stamboliadis, E.T. 2002. A contribution to the relationship of energy and particle size in the comminution of brittle particulate materials. *Minerals Engineering.* 15(10):707-713.

Tang, C., Xu, X., Kou, S., Lindqvist, P. & Liu, H. 2001. Numerical investigation of particle breakage as applied to mechanical crushing—Part I: Single-particle breakage. *International Journal of Rock Mechanics and Mining Sciences.* 38(8):1147-1162.

Tavares, L. 1999. Energy absorbed in breakage of single particles in drop weight testing. *Minerals Engineering.* 12(1):43-50.

Tavares, L. & King, R. 1998. Single-particle fracture under impact loading. *International Journal of Mineral Processing.* 54(1):1-28.

Tavares, L. & King, R. 2004. Measurement of the load–deformation response from impact-breakage of particles. *International Journal of Mineral Processing.* 74:S267-S277.

Tavares, L.M. 2007. Breakage of single particles: quasi-static. *Handbook of Powder Technology.* 12:3-68.

Thornton, C., Ciomocos, M. & Adams, M. 1999. Numerical simulations of agglomerate impact breakage. *Powder Technology.* 105(1):74-82.

Towler, G.P. & Sinnott, R.K. 2013. *Chemical engineering design: principles, practice, and economics of plant and process design.* Elsevier.

Tromans, D. 2008. Mineral comminution: energy efficiency considerations. *Minerals Engineering.* 21(8):613-620.

Vervoorn, P. & Austin, L. 1990. The analysis of repeated breakage events as an equivalent rate process. *Powder Technology.* 63(2):141-147

Wang, E., Shi, F. & Manlapig, E. 2011. Pre-weakening of mineral ores by high voltage pulses. *Minerals Engineering.* 24(5):455-462.

Wang, L. 2011. *Foundations of stress waves.* Elsevier.

Weedon, D. & Wilson, F. 2000. Modelling iron ore degradation using a twin pendulum breakage device. *International Journal of Mineral Processing.* 59(3):195-213.

Wills, B.A. 2011. *Wills' mineral processing technology: an introduction to the practical aspects of ore treatment and mineral recovery.* Butterworth-Heinemann.

Young, W.C. & Budynas, R.G. 2002. *Roark's formulas for stress and strain.* McGraw-Hill New York.

.

9. APPENDICES

10.1 Appendix A: Sample calculations

10.2 Appendix B: Voltage-time signals obtained for SILC calibration

10.3 Appendix C: Experimental values used to conduct breakage tests on blue stone

10.4 Appendix D: Experimental values used to conduct bed breakage tests on UG2

10.5 Appendix E: Particle size distributions obtained for tests conducted on UG2

9.1. Appendix A: Sample calculations

9.1.1. Determination of the experimental and theoretical calibration factors

A. Calculation of the experimental calibration factor

Sample calculations are based on the largest steel ball of 510 g released from the greatest height of 300 mm.

Values used to calculate the experimental calibration factor

Steel ball mass (g)	510
Drop height (mm)	300
Ball diameter (mm)	50.0
Rod diameter (mm)	20.0
Acceleration due to gravity (m/s^2)	9.81
Rod density (kg/m^3)	7820
Rod length (m)	1.50

The velocity of the steel ball is determined from conservation of mechanical energy:

$$\mathrm{mgh_0} = \frac{1}{2}\mathrm{mv_b}^2$$

Where:

m: Mass of the steel ball (kg)

g: Acceleration due to gravity (m/s^2)

h_0: Initial height of the steel ball before it released (m)

v_b: Velocity of the steel ball just before impact (m/s)

Therefore, $v_{ball} = \sqrt{2gh} = 2.43$ m/s

The velocity of the rod upon impact is found by elastic contact theory and is given by:

$$v_{rod} = v_{ball}\left(\frac{A_{ball}}{A_{ball} + A_{rod}}\right)$$

Where:

V_{rod}: Rod velocity (m/s)

V_b: Ball velocity (m/s)

A_{ball}: Effective area of the ball (m^2)

A_{rod}: Cross-sectional area of the rod (m^2)

Note: A_{ball} is calculated as 10% of the ball's surface area.

$A_{ball} = 10\ \% \times \frac{\pi \times \text{ball diameter}^2}{4} = 0.0002\ m^2$

$A_{rod} = \frac{\pi \times \text{rod diameter}^2}{4} = 0.0003\ m^2$

Then $v_{rod} = 0.93$ m/s

One dimensional stress wave theory is used to evaluate the stress applied to the steel rod:

$$\sigma = Cv_{rod}\rho$$

Where:

σ: Stress applied to the steel rod (N/m^2)

C: Pulse speed (m/s)

V_{rod}: Rod velocity (m/s)

ρ: Steel rod density (kg/m^3)

The pulse speed through the rod, C, is determined as:

$$C = \frac{2 \times Length\ of\ rod}{pulse\ time}$$

$C = \frac{2\ x\ 1.5}{317 \mu s} = 9464$ m/s

Then σ = 9464 m/s x 0.93 m/s x 7814.5 kg/m^3

= 69.0 MPa

The calibration factor is given as a ratio of the stress per unit voltage and is determined as:

$K = \frac{\sigma}{Vavg} = \frac{69.0}{1.8}$

Therefore experimental calibration factor K = 38.2 MPa/V

Note: An average value of the calibration factors determined at the four drop heights was used for calculations. The calibration constants found for the 120, 180 and 240 mm drop heights are shown in the table below.

Calibration constants obtained at the 120, 180 and 240 mm drop heights

Drop height (mm)	Calibration constant
120	36.94
180	36.93
240	37.58

B. Calculation of the theoretical calibration factor

Values of the parameters used to calculate the theoretical calibration factor

Parameter	Value
Young's modulus	2.11 x 10^{11}
Amplifier gain	1000
Bridge factor	2.0
Bridge excitation voltage	5.0
Gauge factor	2.0

The theoretical calibration constant is given by:

$$K_{theoretical} = \frac{4E}{ABvF}$$

Where:

E: Young's modulus of the rod

A: Amplifier gain

B: Bridge factor

V: Bridge excitation voltage

F: Gauge factor

Therefore theoretical calibration factor $K_{theoretical}$ = 40.4 MPa/V

9.1.2. Determination of the peak force obtained for a breakage test

For a breakage test, the stress applied to the steel rod corresponding to each voltage recorded during the breakage event is determined as:

$$\sigma = \mathrm{KV}$$

Where:

σ: Stress applied to the steel rod (N/m^2)

K: Calibration constant used to relate the measured voltage to the stress (N/Vm^2)

V: Measured voltage (V)

The force applied to the bed of particles for each voltage recorded is determined using the stress as follows:

$$F = \sigma A_{rod}$$

Where:

F: Force applied to the particle sample (N)

σ: Stress applied to the steel rod (N/m^2)

A_{rod}: Cross sectional area of the steel rod (m^2)

The peak force is determined as the maximum force obtained from the breakage event. A force-time curve obtained using the 510 g ball released from a height of 300 mm onto one layer of blue stone particles is shown in the figure below. The peak force of approximately 2300 N is indicated by the dotted line.

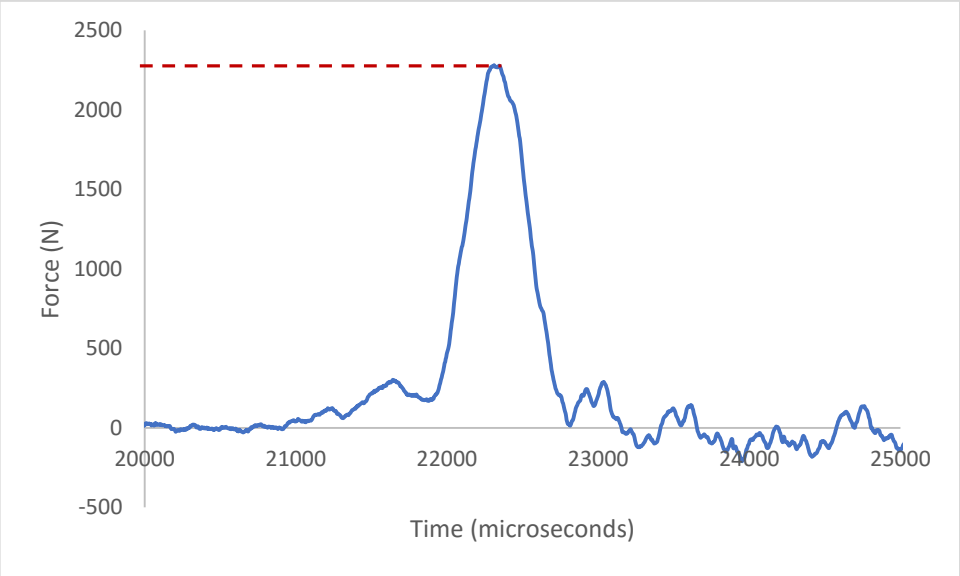

Peak force obtained for breakage test conducted on one layer of blue stone particles at the greatest input energy

9.1.3. Determination of the energy particle fracture energy for a breakage test

To evaluate the strain energy on the rod, the work done in discrete time steps is accumulated to give the squared integral of the wave. By conservation of energy, the fracture energy (strain energy absorbed by the particle up to the point of failure) is assumed to be equal to the strain energy on the rod when the breakage event occurs. The strain energy transferred to the rod is calculation as:

$$E_{strain} = \sum_{t0}^{t_{final}} \left(\frac{\left(\frac{\sigma(t_{n+1})+\sigma(t_n)}{2}\right)^2 (t_{n+1} - t_n)(A_{rod})}{C\rho} \right)$$

Where:

t_0: Initial contact time between falling ball and SILC steel rod (s)

t_{final}: Time at which particle fracture occurs (s)

σ: Stress applied to the rod (N/m^2)

t_{n+1}: Final time recorded for each time step (s)

t_n: Initial time recorded for each time step (s)

A_{rod}: Surface area of the rod (m^2)

C: Pulse speed through the rod (m/s)

ρ: Density of the rod (kg/m^3)

The particle fracture energy is determined from accumulating the strain energy in discrete time steps from the instant when the breakage event is initially recorded to the instant of particle fracture.

9.1.4. Determination of the degree of breakage obtained for tests conducted on UG2

The particle size distributions obtained from screening the sample collected when a breakage test was conducted were used to determine the t_2 breakage indicator which was used to quantify the degree of breakage obtained.

$t_{2\text{-size}} = \frac{1}{2}\sqrt{6.7 \text{ x } 3.35}$ mm

$t_{2\text{-size}}$ = 2.37 mm

To determine the t_2 % passing, given as the percentage of the material passing through a screen of aperture size 2.37 mm, interpolation between the screen sizes of 2 and 2.8 mm was done. Sample calculations are shown for the breakage test conducted on one layer of UG2 particles using the largest input energy:

% material passing through the 2.8 mm screen: 30.79 %

% material passing through the 2 mm screen: 23.84 %

% material passing 2.37 mm = 30.79 % + $\frac{2.37-2 \text{ mm}}{2.8-2 \text{ mm}}$ (23.84 % - 30.79 %)

$\therefore$ t_2 (% passing) = 27.5 %

9.2. Appendix B: Voltage-time signals obtained for SILC calibration

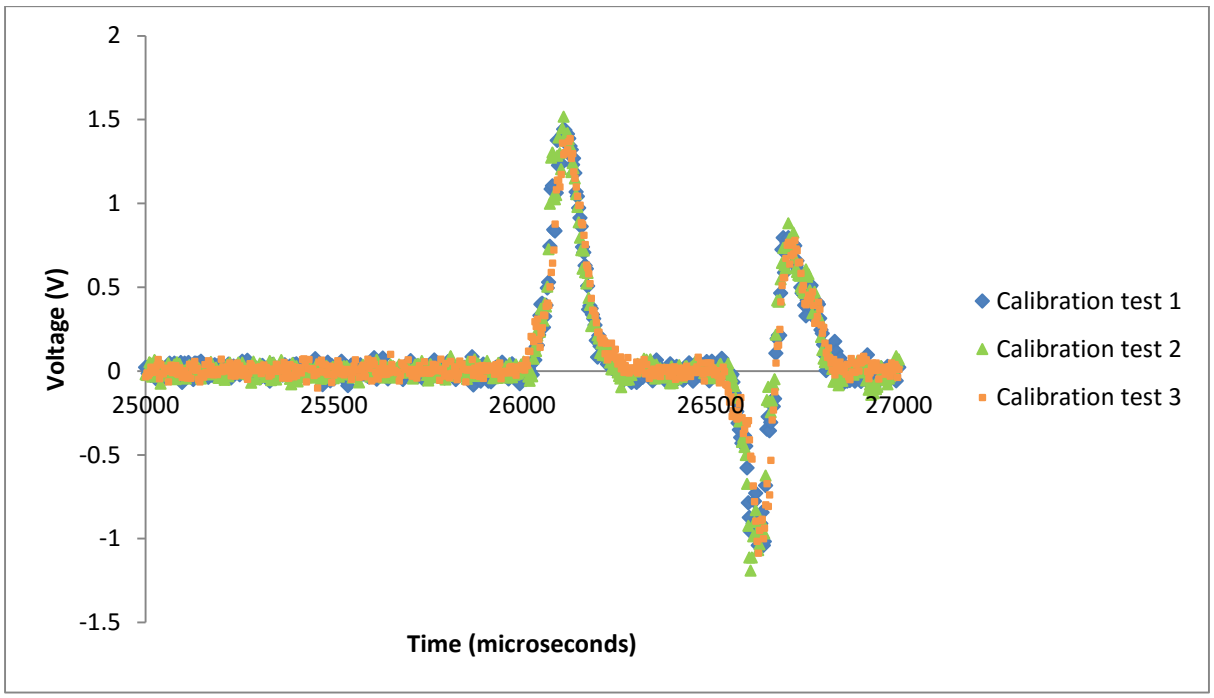

Plot of three steel-on-steel calibration tests conducted for the 510 g ball dropped at a height of 240 mm

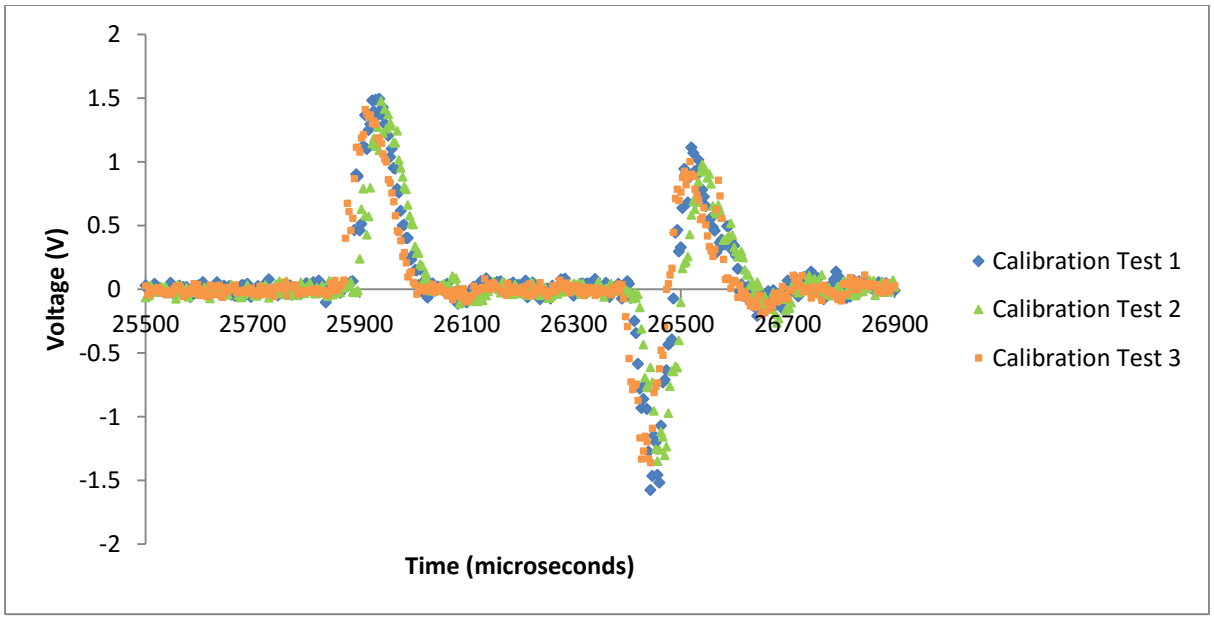

Plot of three steel-on-steel calibration tests conducted for the 510 g ball dropped at a height of 180 mm

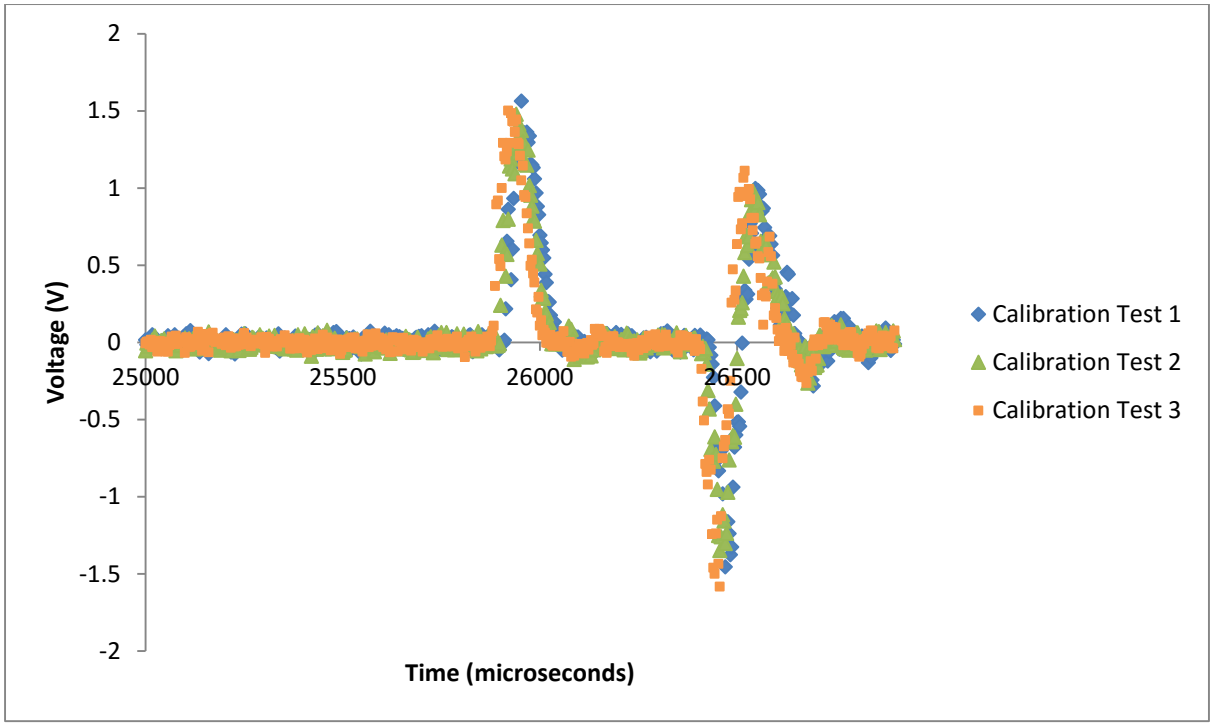

Plot of three steel-on-steel calibration tests conducted for the 510 g ball dropped at a height of 120 mm

9.3. Appendix C: Experimental values for breakage tests on blue stone

9.3.1. Breakage tests conducted on blue stone using the 510 g ball

Run 1 of tests conducted on blue stone using the 510 g ball

Test number	Drop height (mm)	Bed depth (layers of particles)	Sample mass (g)
1	60	1	2.0
2	60	3	5.3
3	60	5	10.0
4	60	7	12.6
5	60	9	16.9
6	120	1	1.7
7	120	3	5.6
8	120	5	11.9
9	120	7	15.5
10	120	9	18.5
11	180	1	2.6
12	180	3	6.2
13	180	5	10.9
14	180	7	15.0
15	180	9	17.9
16	240	1	2.1
17	240	3	5.9
18	240	5	12.6
19	240	7	13.6
20	240	9	18.0
21	300	1	2.0
22	300	3	6.1
23	300	5	11.8
24	300	7	15.0
25	300	9	17.1

Repeat 1 of tests conducted on blue stone using the 510 g ball

Test number	Drop height (mm)	Bed depth (layers of particles)	Sample mass (g)
1 R1	60	1	1.8
2 R1	60	3	5.6
3 R1	60	5	9.8
4 R1	60	7	13.9
5 R1	60	9	18.2
6 R1	120	1	1.8
7 R1	120	3	6.4
8 R1	120	5	9.8
9 R1	120	7	13.4
10 R1	120	9	17.9
11 R1	180	1	2.2
12 R1	180	3	5.7
13 R1	180	5	9.5
14 R1	180	7	12.9
15 R1	180	9	17.8
16 R1	240	1	2.4
17 R1	240	3	6.1
18 R1	240	5	9.1
19 R1	240	7	13.2
20 R1	240	9	16.1
21 R1	300	1	1.9
22 R1	300	3	6.3
23 R1	300	5	10.0
24 R1	300	7	13.8
25 R1	300	9	16.5

Note: ‘R1’ refers to Repeat 1

Repeat 2 of breakage tests conducted on blue stone using the 510 g ball

Test number	Drop height (mm)	Bed depth (layers of particles)	Sample mass (g)
1 R2	60	1	2.2
2 R2	60	3	5.5
3 R2	60	5	9.34
4 R2	60	7	13.29
5 R2	60	9	18.05
6 R2	120	1	2.3
7 R2	120	3	5.55
8 R2	120	5	9.33
9 R2	120	7	13.09
10 R2	120	9	17.02
11 R2	180	1	2.4
12 R2	180	3	6.1
13 R2	180	5	9.25
14 R2	180	7	13.8
15 R2	180	9	16.96
16 R2	240	1	2.0
17 R2	240	3	5.8
18 R2	240	5	10.19
19 R2	240	7	13.46
20 R2	240	9	16.63
21 R2	300	1	1.8
22 R2	300	3	5.7
23 R2	300	5	10.1
24 R2	300	7	15.4
25 R2	300	9	16.53

Note: ‘R2’ refers to Repeat 2

9.3.2. Breakage tests conducted on blue stone using the 357 g ball

Run 1 of tests conducted on blue stone using the 357 g ball

Test number	Drop height (mm)	Bed depth (layers of particles)	Sample mass (g)
26	60	1	2.0
27	60	3	5.4
28	60	5	9.1
29	60	7	13.0
30	60	9	16.2
31	120	1	1.8
32	120	3	6.0
33	120	5	9.9
34	120	7	13.3
35	120	9	16.7
36	180	1	1.8
37	180	3	5.6
38	180	5	8.4
39	180	7	13.7
40	180	9	15.6
41	240	1	2.2
42	240	3	5.7
43	240	5	9.9
44	240	7	12.2
45	240	9	16.4
46	300	1	2.4
47	300	3	5.7
48	300	5	9.2
49	300	7	13.8
50	300	9	16.7

Repeat 1 of tests conducted on blue stone using the 357 g ball

Test number	Drop height (mm)	Bed depth (layers of particles)	Sample mass (g)
26 R1	60	1	1.9
27 R1	60	3	5.8
28 R1	60	5	8.1
29 R1	60	7	13.6
30 R1	60	9	15.9
31 R1	120	1	2.2
32 R1	120	3	5.4
33 R1	120	5	8.4
34 R1	120	7	12.2
35 R1	120	9	16.8
36 R1	180	1	2.0
37 R1	180	3	5.5
38 R1	180	5	8.4
39 R1	180	7	13.2
40 R1	180	9	16.5
41 R1	240	1	2.3
42 R1	240	3	5.8
43 R1	240	5	8.5
44 R1	240	7	13.6
45 R1	240	9	16.0
46 R1	300	1	2.6
47 R1	300	3	6.1
48 R1	300	5	9.2
49 R1	300	7	13.3
50 R1	300	9	16.8

Note: ‘R1’ refers to Repeat 1

Repeat 2 of tests conducted on blue stone using the 357 g ball

Test number	Drop height (mm)	Bed depth (layers of particles)	Sample mass (g)
26 R2	60	1	2.2
27 R2	60	3	6.0
28 R2	60	5	9.3
29 R2	60	7	11.0
30 R2	60	9	16.1
31 R2	120	1	2.4
32 R2	120	3	5.7
33 R2	120	5	9.2
34 R2	120	7	11.8
35 R2	120	9	14.5
36 R2	180	1	2.3
37 R2	180	3	6.1
38 R2	180	5	9.8
39 R2	180	7	13.8
40 R2	180	9	16.5
41 R2	240	1	1.9
42 R2	240	3	5.6
43 R2	240	5	9.6
44 R2	240	7	11.9
45 R2	240	9	16.9
46 R2	300	1	2.1
47 R2	300	3	5.3
48 R2	300	5	9.3
49 R2	300	7	12.5
50 R2	300	9	15.5

Note: ‘R2’ refers to Repeat 2

9.3.3. Breakage tests conducted on blue stone using the 261 g ball

Run 1 of tests conducted on blue stone using the 261 g ball

Test number	Drop height (mm)	Bed depth (layers of particles)	Sample mass (g)
51	60	1	1.8
52	60	3	5.6
53	60	5	8.7
54	60	7	12.6
55	60	9	17.8
56	120	1	1.9
57	120	3	5.6
58	120	5	9.5
59	120	7	14.0
60	120	9	16.7
61	180	1	2.2
62	180	3	6.6
63	180	5	9.3
64	180	7	13.7
65	180	9	17.0
66	240	1	2.3
67	240	3	5.4
68	240	5	9.3
69	240	7	13.6
70	240	9	17.3
71	300	1	2.0
72	300	3	6.0
73	300	5	9.9
74	300	7	13.4
75	300	9	16.6

Repeat 1 of tests conducted on blue stone using the 261 g ball

Test number	Drop height (mm)	Bed depth (layers of particles)	Sample mass (g)
51 R1	60	1	2.0
52 R1	60	3	5.0
53 R1	60	5	8.9
54 R1	60	7	13.5
55 R1	60	9	18.3
56 R1	120	1	2.1
57 R1	120	3	6.1
58 R1	120	5	9.3
59 R1	120	7	11.0
60 R1	120	9	16.1
61 R1	180	1	2.0
62 R1	180	3	7.5
63 R1	180	5	10.1
64 R1	180	7	12.9
65 R1	180	9	16.9
66 R1	240	1	1.9
67 R1	240	3	7.7
68 R1	240	5	10.1
69 R1	240	7	13.4
70 R1	240	9	15.2
71 R1	300	1	1.7
72 R1	300	3	5.5
73 R1	300	5	9.9
74 R1	300	7	12.8
75 R1	300	9	16.2

Note: ‘R1’ refers to Repeat 1

Repeat 2 of tests conducted on blue stone using the 261 g ball

Test number	Drop height (mm)	Bed depth (layers of particles)	Sample mass (g)
51 R2	60	1	2.3
52 R2	60	3	6.1
53 R2	60	5	9.1
54 R2	60	7	12.9
55 R2	60	9	17.9
56 R2	120	1	2.3
57 R2	120	3	6.4
58 R2	120	5	10.0
59 R2	120	7	13.8
60 R2	120	9	16.5
61 R2	180	1	1.9
62 R2	180	3	6.0
63 R2	180	5	9.5
64 R2	180	7	13.3
65 R2	180	9	17.8
66 R2	240	1	1.9
67 R2	240	3	6.0
68 R2	240	5	9.4
69 R2	240	7	13.2
70 R2	240	9	17.0
71 R2	300	1	2.0
72 R2	300	3	5.7
73 R2	300	5	10.3
74 R2	300	7	14.2
75 R2	300	9	17.3

Note: ‘R2’ refers to Repeat 2

9.3.4. Breakage tests conducted on blue stone using the 110 g ball

Run 1 of tests conducted on blue stone using the 110 g ball

Test number	Drop height (mm)	Bed depth (layers of particles)	Sample mass (g)
76	60	1	1.7
77	60	3	5.9
78	60	5	10.1
79	60	7	14.0
80	60	9	16.6
81	120	1	2.0
82	120	3	6.2
83	120	5	9.9
84	120	7	13.1
85	120	9	17.5
86	180	1	2.2
87	180	3	5.8
88	180	5	9.9
89	180	7	14.3
90	180	9	17.4
91	240	1	2.2
92	240	3	6.1
93	240	5	10.6
94	240	7	13.6
95	240	9	16.4
96	300	1	2.0
97	300	3	5.9
98	300	5	9.9
99	300	7	14.1
100	300	9	18.6

Repeat 1 of tests conducted on blue stone using the 110 g ball

Test number	Drop height (mm)	Bed depth (layers of particles)	Sample mass (g)
76 R1	60	1	2.3
77 R1	60	3	6.2
78 R1	60	5	9.6
79 R1	60	7	13.3
80 R1	60	9	17.1
81 R1	120	1	1.9
82 R1	120	3	5.9
83 R1	120	5	10.2
84 R1	120	7	14.0
85 R1	120	9	17.8
86 R1	180	1	2.1
87 R1	180	3	5.7
88 R1	180	5	8.9
89 R1	180	7	13.5
90 R1	180	9	16.8
91 R1	240	1	2.0
92 R1	240	3	5.9
93 R1	240	5	10.9
94 R1	240	7	14.2
95 R1	240	9	18.2
96 R1	300	1	2.0
97 R1	300	3	5.8
98 R1	300	5	9.4
99 R1	300	7	13.8
100 R1	300	9	17.7

Note: ‘R1’ refers to Repeat 1

Repeat 2 of tests conducted on blue stone using the 110 g ball

Test number	Drop height (mm)	Bed depth (layers of particles)	Sample mass (g)
76 R2	60	1	2.2
77 R2	60	3	6.5
78 R2	60	5	9.7
79 R2	60	7	13.9
80 R2	60	9	18.1
81 R2	120	1	1.9
82 R2	120	3	5.8
83 R2	120	5	10.0
84 R2	120	7	13.4
85 R2	120	9	17.1
86 R2	180	1	1.8
87 R2	180	3	6.1
88 R2	180	5	9.5
89 R2	180	7	13.9
90 R2	180	9	17.9
91 R2	240	1	1.8
92 R2	240	3	6.7
93 R2	240	5	9.8
94 R2	240	7	13.5
95 R2	240	9	17.8
96 R2	300	1	1.7
97 R2	300	3	6.4
98 R2	300	5	8.9
99 R2	300	7	14.5
100 R2	300	9	18.2

Note: ‘R2’ refers to Repeat 2

9.4. Appendix D: Experimental values used for breakage tests on UG2

9.4.1. Breakage tests conducted on UG2 using the 510 g ball

Run 1 of tests conducted on UG2 using the 510 g ball

Test number	Drop height (mm)	Bed depth (layers of particles)	Sample mass (g)
1	120	1	2.2
2	120	3	5.7
3	120	5	12.4
4	120	7	13.5
5	180	1	2.4
6	180	3	6.5
7	180	5	11.0
8	180	7	15.3
9	240	1	2.1
10	240	3	6.6
11	240	5	10.9
12	240	7	16.8
13	300	1	3.0
14	300	3	6.9
15	300	5	10.8
16	300	7	14.9

Repeat 1 of test conducted on UG2 using the 510 g ball

Test number	Drop height (mm)	Bed depth (layers of particles)	Sample mass (g)
1 R1	120	1	2.4
2 R1	120	3	12.6
3 R1	120	5	12.6
4 R1	120	7	17.9
5 R1	180	1	2.6
6 R1	180	3	7.1
7 R1	180	5	12.1
8 R1	180	7	18.0
9 R1	240	1	2.5
10 R1	240	3	7.3
11 R1	240	5	11.4
12 R1	240	7	12.5
13 R1	300	1	2.7
14 R1	300	3	7.1
15 R1	300	5	12.3
16 R1	300	7	16.9

Note: ‘R1’ refers to Repeat 1

Repeat 2 of tests conducted on UG2 using the 510 g ball

Test number	Drop height (mm)	Bed depth (layers of particles)	Sample mass (g)
1 R2	120	1	3.8
2 R2	120	3	9.5
3 R2	120	5	14.8
4 R2	120	7	22.1
5 R2	180	1	3.8
6 R2	180	3	8.1
7 R2	180	5	14.1
8 R2	180	7	22.0
9 R2	240	1	3.2
10 R2	240	3	7.7
11 R2	240	5	14.7
12 R2	240	7	24.3
13 R2	300	1	2.4
14 R2	300	3	7.4
15 R2	300	5	12.7
16 R2	300	7	17.5

Note: ‘R2’ refers to Repeat 2

9.4.2. Breakage tests conducted on UG2 using the 357 g ball

Run 1 of tests conducted on UG2 using the 357 g ball

Test number	Drop height (mm)	Bed depth (layers of particles)	Sample mass (g)
17	120	1	2.08
18	120	3	6.45
19	120	5	11.15
20	120	7	16.51
21	180	1	2.46
22	180	3	6.96
23	180	5	10.72
24	180	7	16.57
25	240	1	2.37
26	240	3	6.75
27	240	5	10.43
28	240	7	15.07
29	300	1	2.15
30	300	3	7.78
31	300	5	10.36
32	300	7	15.37

Repeat 1 of tests conducted on UG2 using the 357 g ball

Test number	Drop height (mm)	Bed depth (layers of particles)	Sample mass (g)
17 R1	120	1	2.7
18 R1	120	3	7.7
19 R1	120	5	14.1
20 R1	120	7	19.4
21 R1	180	1	3.0
22 R1	180	3	8.3
23 R1	180	5	14.9
24 R1	180	7	20.9
25 R1	240	1	3.2
26 R1	240	3	8.0
27 R1	240	5	13.5
28 R1	240	7	18.3
29 R1	300	1	2.1
30 R1	300	3	6.8
31 R1	300	5	13.0
32 R1	300	7	17.6

Note: ‘R1’ refers to Repeat 1

Repeat 2 of tests conducted on UG2 using the 357 g ball

Test number	Drop height (mm)	Bed depth (layers of particles)	Sample mass (g)
17 R2	120	1	2.9
18 R2	120	3	8.8
19 R2	120	5	14.6
20 R2	120	7	23.2
21 R2	180	1	2.7
22 R2	180	3	9.9
23 R2	180	5	14.8
24 R2	180	7	20.4
25 R2	240	1	3.4
26 R2	240	3	8.8
27 R2	240	5	12.1
28 R2	240	7	18.6
29 R2	300	1	2.1
30 R2	300	3	6.8
31 R2	300	5	14.4
32 R2	300	7	20.3

Note: ‘R2’ refers to Repeat 2

9.4.3. Breakage tests conducted on UG2 using the 261 g ball

Run 1 of tests conducted on UG2 using the 261 g ball

Test number	Drop height (mm)	Bed depth (layers of particles)	Sample mass (g)
33	120	1	2.6
34	120	3	7.7
35	120	5	11.8
36	120	7	16.9
37	180	1	2.6
38	180	3	6.7
39	180	5	12.7
40	180	7	18.3
41	240	1	2.6
42	240	3	8.0
43	240	5	12.8
44	240	7	16.5
45	300	1	7.8
46	300	3	7.8
47	300	5	13.8
48	300	7	16.0

Repeat 1 of tests conducted on UG2 using the 261 g ball

Test number	Drop height (mm)	Bed depth (layers of particles)	Sample mass (g)
33 R1	120	1	2.7
34 R1	120	3	9.3
35 R1	120	5	14.6
36 R1	120	7	19.6
37 R1	180	1	3.2
38 R1	180	3	7.8
39 R1	180	5	13.6
40 R1	180	7	21.0
41 R1	240	1	2.3
42 R1	240	3	7.4
43 R1	240	5	12.7
44 R1	240	7	19.6
45 R1	300	1	2.9
46 R1	300	3	7.9
47 R1	300	5	13.6
48 R1	300	7	21.6

Note: ‘R1’ refers to Repeat 1

Repeat 2 of tests conducted on UG2 using the 261 g ball

Test number	Drop height (mm)	Bed depth (layers of particles)	Sample mass (g)
33 R2	120	1	3.1
34 R2	120	3	7.8
35 R2	120	5	14.2
36 R2	120	7	20.3
37 R2	180	1	2.7
38 R2	180	3	7.4
39 R2	180	5	14.4
40 R2	180	7	18.6
41 R2	240	1	2.8
42 R2	240	3	7.8
43 R2	240	5	11.6
44 R2	240	7	20.9
45 R2	300	1	2.6
46 R2	300	3	8.1
47 R2	300	5	14.8
48 R2	300	7	20.5

Note: ‘R2’ refers to Repeat 2

9.4.4. Breakage tests conducted on UG2 using the 110 g ball

Run 1 of tests conducted on UG2 using the 110 g ball

Test number	Drop height (mm)	Bed depth (layers of particles)	Sample mass (g)
49	120	1	2.0
50	120	3	7.1
51	120	5	12.8
52	120	7	17.2
53	180	1	2.8
54	180	3	7.2
55	180	5	13.1
56	180	7	16.0
57	240	1	2.5
58	240	3	7.1
59	240	5	12.5
60	240	7	17.0
61	300	1	2.5
62	300	3	7.9
63	300	5	11.9
64	300	7	19.3

Repeat 1 of tests conducted on UG2 using the 110 g ball

Test number	Drop height (mm)	Bed depth (layers of particles)	Sample mass (g)
49 R1	120	1	2.3
50 R1	120	3	6.9
51 R1	120	5	11.6
52 R1	120	7	17.6
53 R1	180	1	2.2
54 R1	180	3	8.1
55 R1	180	5	11.6
56 R1	180	7	17.1
57 R1	240	1	2.1
58 R1	240	3	7.4
59 R1	240	5	11.9
60 R1	240	7	16.3
61 R1	300	1	1.9
62 R1	300	3	6.9
63 R1	300	5	10.3
64 R1	300	7	15.3

Note: ‘R1’ refers to Repeat 1

Repeat 2 of tests conducted on UG2 using the 110 g ball

Test number	Drop height (mm)	Bed depth (layers of particles)	Sample mass (g)
49 R2	120	1	1.9
50 R2	120	3	6.5
51 R2	120	5	12.1
52 R2	120	7	16.9
53 R2	180	1	1.7
54 R2	180	3	7.6
55 R2	180	5	12.2
56 R2	180	7	16.6
57 R2	240	1	2.0
58 R2	240	3	6.7
59 R2	240	5	11.1
60 R2	240	7	17.4
61 R2	300	1	2.2
62 R2	300	3	7.5
63 R2	300	5	9.8
64 R2	300	7	15.9

Note: ‘R2’ refers to Repeat 2

9.5. Appendix E: Particle size distributions obtained for UG2

9.5.1. Tests conducted using the 510 g ball

Particle size distributions for Run 1 of tests conducted on UG2 using the 510 g ball

	Mass retained (g)															
Sieve size (mm)	Test 1	Test 2	Test 3	Test 4	Test 5	Test 6	Test 7	Test 8	Test 9	Test 10	Test 11	Test 12	Test 13	Test 14	Test 15	Test 16
8.0	0	0.00	0.00	0.00	0.00	0.00	0.00	0.00	0.00	0.00	0.00	0.00	0.00	0.00	0.00	0.00
5.6	0	1.25	5.76	2.18	0.44	2.11	1.91	6.76	0.98	1.49	5.20	8.07	0.47	1.55	4.37	6.12
4.0	1.43	3.42	5.08	9.27	1.19	3.22	7.03	6.23	0.00	3.26	3.88	6.20	1.43	3.90	4.68	6.73
2.8	0.54	0.68	1.51	1.96	0.56	0.78	1.90	2.24	0.61	1.01	1.46	2.28	0.19	0.63	0.99	1.78
2.0	0.04	0.18	0.02	0.00	0.07	0.13	0.02	0.05	0.14	0.24	0.05	0.08	0.21	0.23	0.29	0.03
1.4	0	0.05	0.03	0.01	0.05	0.02	0.04	0.04	0.09	0.29	0.08	0.02	0.13	0.18	0.06	0.07
Pan	0.16	0.11	0.01	0.08	0.08	0.22	0.07	0.02	0.32	0.35	0.21	0.15	0.59	0.45	0.37	0.15
Total mass (g)	2.17	5.69	12.41	13.50	2.39	6.48	10.97	15.34	2.14	6.64	10.88	16.80	3.02	6.94	10.76	14.88

Particle size distributions for Repeat 1 of tests conducted on UG2 using the 510 g ball

	Mass retained (g)															
Sieve size (mm)	Test 1 R1	Test 2 R1	Test 3 R1	Test 4 R1	Test 5 R1	Test 6 R1	Test 7 R1	Test 8 R1	Test 9 R1	Test 10 R1	Test 11 R1	Test 12 R1	Test 13 R1	Test 14 R1	Test 15 R1	Test 16 R1
8.0	0.00	0.00	0.00	0.00	0.00	0.00	0.00	0.00	0.00	0.00	0.00	0.00	0.00	0.00	0.00	0.00
5.6	1.14	3.64	5.24	6.82	0.51	3.02	6.78	8.88	0.00	2.10	3.50	10.38	0.78	1.03	4.64	3.85
4.0	0.95	3.92	7.17	10.29	1.15	2.92	4.52	8.52	0.91	4.06	6.38	0.92	0.44	4.30	7.28	11.95
2.8	0.21	0.18	0.05	0.75	0.34	0.72	0.62	0.42	0.61	0.48	1.25	1.07	0.66	0.99	0.17	0.98
2.0	0.02	0.06	0.00	0.00	0.09	0.11	0.07	0.09	0.47	0.23	0.09	0.00	0.14	0.23	0.06	0.05
1.4	0.00	0.00	0.07	0.00	0.13	0.08	0.01	0.00	0.19	0.12	0.04	0.00	0.16	0.15	0.07	0.02
Pan	0.10	0.10	0.04	0.03	0.35	0.29	0.06	0.04	0.36	0.35	0.15	0.13	0.49	0.41	0.12	0.08
Total mass (g)	2.42	7.90	12.57	17.89	2.57	7.14	12.06	17.95	2.54	7.34	11.41	12.50	2.67	7.11	12.34	16.93

Note: ‘R1’ refers to Repeat 1

Particle size distributions for Repeat 2 of tests conducted on UG2 using the 510 g ball

	Mass retained (g)															
Sieve size (mm)	Test 1 R2	Test 2 R2	Test 3 R2	Test 4 R2	Test 5 R2	Test 6 R2	Test 7 R2	Test 8 R2	Test 9 R2	Test 10 R2	Test 11 R2	Test 12 R2	Test 13 R2	Test 14 R2	Test 15 R2	Test 16 R2
8.0	0.00	0.00	0.00	0.00	0.00	0.00	0.00	0.00	0.00	0.00	0.00	0.00	0.00	0.00	0.00	0.00
5.6	0.73	3.13	6.29	9.52	0.81	0.44	3.28	8.64	0.35	1.35	3.68	10.52	0.28	0.99	4.84	5.89
4.0	1.98	5.90	8.09	11.39	1.48	5.83	7.92	12.56	0.60	5.38	9.30	12.09	0.33	5.09	6.79	10.46
2.8	0.69	0.30	0.36	0.96	0.67	1.49	2.49	0.75	1.27	0.56	1.47	1.52	0.63	0.77	0.54	0.49
2.0	0.03	0.03	0.00	0.03	0.09	0.13	0.13	0.00	0.28	0.06	0.09	0.07	0.16	0.14	0.24	0.11
1.4	0.09	0.05	0.00	0.04	0.40	0.00	0.06	0.02	0.08	0.06	0.03	0.02	0.19	0.11	0.05	0.04
Pan	0.23	0.09	0.01	0.14	0.32	0.19	0.24	0.07	0.58	0.29	0.12	0.11	0.79	0.34	0.20	0.46
Total mass (g)	3.75	9.50	14.75	22.08	3.77	8.08	14.12	22.04	3.16	7.70	14.69	24.33	2.38	7.44	12.66	17.45

Note: ‘R2’ refers to Repeat 2

9.5.2. Tests conducted using the 357 g ball

Particle size distributions for Run 1 of tests conducted on UG2 using the 357 g ball

	Mass retained (g)															
Sieve size (mm)	Test 17	Test 18	Test 19	Test 20	Test 21	Test 22	Test 23	Test 24	Test 25	Test 26	Test 27	Test 28	Test 29	Test 30	Test 31	Test 32
8.0	0.00	0.00	0.00	0.00	0.00	0.00	0.00	0.00	0.00	0.00	0.00	0.00	0.00	0.00	0.00	0.00
5.6	0.45	1.25	2.90	5.21	0.87	1.81	1.83	7.07	0.00	1.66	1.54	4.09	0.69	1.54	3.52	3.53
4.0	0.97	3.61	5.23	9.18	0.33	3.38	5.88	7.32	1.00	3.82	6.76	6.87	0.34	4.01	5.00	7.58
2.8	0.38	1.37	2.73	2.09	0.74	1.04	2.81	2.05	0.47	0.61	1.94	3.72	0.53	1.89	1.38	4.08
2.0	0.12	0.08	0.06	0.02	0.13	0.30	0.06	0.00	0.13	0.20	0.05	0.19	0.19	0.10	0.16	0.02
1.4	0.02	0.04	0.04	0.00	0.12	0.07	0.05	0.09	0.17	0.09	0.04	0.04	0.10	0.04	0.06	0.06
Pan	0.14	0.10	0.19	0.01	0.27	0.36	0.09	0.04	0.60	0.37	0.10	0.16	0.30	0.20	0.24	0.10
Total mass (g)	2.08	6.45	11.15	16.51	2.46	6.96	10.72	16.57	2.37	6.75	10.43	15.07	2.15	7.78	10.36	15.37

Particle size distributions for Repeat 1 of tests conducted on UG2 using the 357 g ball

	Mass retained (g)															
Sieve size (mm)	Test 17 R1	Test 18 R1	Test 19 R1	Test 20 R1	Test 21 R1	Test 22 R1	Test 23 R1	Test 24 R1	Test 25 R1	Test 26 R1	Test 27 R1	Test 28 R1	Test 29 R1	Test 30 R1	Test 31 R1	Test 32 R1
8.0	0.00	0.00	0.00	0.00	0.00	0.00	0.00	0.00	0.00	0.00	0.00	0.00	0.00	0.00	0.00	0.00
5.6	0.00	1.20	6.90	8.01	0.38	2.65	5.06	7.50	1.33	1.16	4.32	8.68	0.00	1.36	5.44	8.76
4.0	2.52	5.94	7.22	11.05	1.23	4.23	9.40	12.98	0.64	4.72	8.10	9.54	1.08	2.97	5.33	7.79
2.8	0.12	0.41	0.00	0.16	0.84	1.20	0.22	0.41	0.23	1.32	0.91	0.00	0.68	1.75	1.74	0.78
2.0	0.05	0.05	0.00	0.09	0.11	0.09	0.13	0.00	0.17	0.37	0.03	0.04	0.07	0.20	0.24	0.05
1.4	0.00	0.03	0.00	0.01	0.03	0.03	0.00	0.00	0.14	0.09	0.07	0.00	0.07	0.17	0.00	0.07
Pan	0.01	0.07	0.01	0.03	0.41	0.11	0.10	0.05	0.69	0.33	0.08	0.03	0.16	0.39	0.20	0.12
Total mass (g)	2.70	7.70	14.13	19.35	3.00	8.31	14.91	20.94	3.20	7.99	13.51	18.29	2.06	6.84	12.95	17.57

Note: ‘R1’ refers to Repeat 1

Particle size distributions for Repeat 2 of tests conducted on UG2 using the 357 g ball

	Mass retained (g)															
Sieve size (mm)	Test 17 R2	Test 18 R2	Test 19 R2	Test 20 R2	Test 21 R2	Test 22 R2	Test 23 R2	Test 24 R2	Test 25 R2	Test 26 R2	Test 27 R2	Test 28 R2	Test 29 R2	Test 30 R2	Test 31 R2	Test 32 R2
8.0	0.00	0.00	0.00	0.00	0.00	0.00	0.00	0.00	0.00	0.00	0.00	0.00	0.00	0.00	0.00	0.00
5.6	0.29	0.52	4.89	11.51	0.38	3.90	4.70	6.34	0.35	3.27	3.00	10.88	0.00	0.45	6.57	11.06
4.0	2.45	7.24	8.95	11.05	1.48	5.44	9.57	13.14	1.04	4.82	8.42	7.58	0.82	4.22	7.37	8.09
2.8	0.00	0.72	0.45	0.59	0.43	0.32	0.44	0.85	1.35	0.31	0.57	0.15	0.63	1.22	0.34	0.90
2.0	0.08	0.15	0.17	0.00	0.08	0.17	0.00	0.01	0.12	0.07	0.00	0.00	0.14	0.35	0.00	0.11
1.4	0.00	0.06	0.00	0.00	0.00	0.02	0.01	0.00	0.05	0.04	0.01	0.00	0.06	0.16	0.00	0.03
Pan	0.08	0.08	0.18	0.03	0.29	0.08	0.03	0.05	0.44	0.30	0.13	0.02	0.43	0.37	0.12	0.06
Total mass (g)	2.90	8.77	14.64	23.18	2.66	9.93	14.75	20.39	3.35	8.81	12.13	18.63	2.08	6.77	14.40	20.25

Note: ‘R2’ refers to Repeat 2

9.5.3. Tests conducted using the 261 g ball

Particle size distributions for Run 1 of tests conducted on UG2 using the 261 g ball

	Mass retained (g)															
Sieve size (mm)	Test 33	Test 34	Test 35	Test 36	Test 37	Test 38	Test 39	Test 40	Test 41	Test 42	Test 43	Test 44	Test 45	Test 46	Test 47	Test 48
8.0	0.00	0.00	0.00	0.00	0.00	0.00	0.00	0.00	0.00	0.00	0.00	0.00	0.00	0.00	0.00	0.00
5.6	0.39	3.14	5.43	8.08	0.89	2.73	3.26	8.42	0.38	3.19	6.82	7.37	1.71	1.99	5.00	4.81
4.0	1.14	3.80	5.28	7.53	1.19	3.13	8.48	9.01	1.06	3.37	4.81	8.76	0.23	3.47	7.54	9.61
2.8	0.54	0.49	1.10	1.26	0.05	0.58	0.79	0.82	0.78	1.26	0.98	0.24	0.22	1.97	0.99	1.45
2.0	0.15	0.10	0.00	0.00	0.17	0.08	0.07	0.00	0.14	0.08	0.10	0.04	0.00	0.16	0.13	0.03
1.4	0.14	0.00	0.00	0.00	0.05	0.08	0.02	0.00	0.01	0.00	0.02	0.03	0.07	0.09	0.01	0.06
Pan	0.25	0.13	0.00	0.06	0.27	0.13	0.06	0.06	0.19	0.07	0.08	0.08	0.28	0.12	0.08	0.07
Total mass (g)	2.61	7.66	11.81	16.93	2.62	6.73	12.68	18.31	2.56	7.97	12.81	16.52	2.51	7.80	13.75	16.03

Particle size distributions for Repeat 1 of tests conducted on UG2 using the 261 g ball

	Mass retained (g)															
Sieve size (mm)	Test 33 R1	Test 34 R1	Test 35 R1	Test 36 R1	Test 37 R1	Test 38 R1	Test 39 R1	Test 40 R1	Test 41 R1	Test 42 R1	Test 43 R1	Test 44 R1	Test 45 R1	Test 46 R1	Test 47 R1	Test 48 R1
8.0	0.00	0.00	0.00	0.00	0.00	0.00	0.00	0.00	0.00	0.00	0.00	0.00	0.00	0.00	0.00	0.00
5.6	0.83	1.11	2.28	3.10	1.46	0.80	1.52	4.40	0.00	1.08	2.31	6.79	0.97	0.35	3.52	7.62
4.0	1.28	6.81	11.12	15.78	0.81	5.52	10.72	15.84	0.91	4.84	9.18	12.45	0.65	6.47	9.25	12.80
2.8	0.25	1.16	1.11	0.65	0.48	0.99	1.35	0.66	0.68	1.06	1.06	0.33	0.40	0.93	0.61	1.06
2.0	0.15	0.13	0.06	0.00	0.09	0.26	0.00	0.05	0.25	0.15	0.07	0.00	0.16	0.04	0.09	0.06
1.4	0.03	0.05	0.02	0.03	0.11	0.00	0.00	0.00	0.14	0.07	0.00	0.00	0.06	0.04	0.05	0.01
Pan	0.16	0.05	0.00	0.01	0.21	0.19	0.03	0.02	0.35	0.24	0.09	0.00	0.63	0.11	0.06	0.03
Total mass (g)	2.70	9.31	14.59	19.57	3.16	7.76	13.62	20.97	2.33	7.44	12.71	19.57	2.87	7.94	13.58	21.58

Note: ‘R1’ refers to Repeat 1

Particle size distributions for Repeat 2 of tests conducted on UG2 using the 261 g ball

	Mass retained (g)															
Sieve size (mm)	Test 33 R2	Test 34 R2	Test 35 R2	Test 36 R2	Test 37 R2	Test 38 R2	Test 39 R2	Test 40 R2	Test 41 R2	Test 42 R2	Test 43 R2	Test 44 R2	Test 45 R2	Test 46 R2	Test 47 R2	Test 48 R2
8.0	0.00	0.00	0.00	0.00	0.00	0.00	0.00	0.00	0.00	0.00	0.00	0.00	0.00	0.00	0.00	0.00
5.6	0.36	0.00	1.83	6.99	0.25	1.56	4.94	7.82	0.00	2.57	3.34	7.85	0.34	2.79	5.94	9.26
4.0	2.27	6.30	11.41	11.95	1.76	4.76	8.78	9.87	1.55	4.16	7.10	12.04	1.08	4.37	8.36	10.49
2.8	0.18	1.43	0.98	1.23	0.52	0.75	0.53	0.94	0.58	0.92	1.09	0.92	0.80	0.50	0.36	0.67
2.0	0.12	0.00	0.00	0.05	0.02	0.12	0.09	0.00	0.25	0.04	0.08	0.00	0.15	0.13	0.05	0.03
1.4	0.05	0.01	0.00	0.00	0.06	0.07	0.00	0.00	0.18	0.02	0.00	0.04	0.04	0.06	0.01	0.00
Pan	0.13	0.02	0.00	0.07	0.12	0.09	0.03	0.01	0.22	0.13	0.03	0.00	0.16	0.21	0.04	0.03
Total mass (g)	3.11	7.76	14.22	20.29	2.73	7.35	14.37	18.64	2.78	7.84	11.64	20.85	2.57	8.06	14.76	20.48

Note: ‘R2’ refers to Repeat 2

9.5.4. Tests conducted using the 110 g ball

Particle size distributions for Run 1 of tests conducted on UG2 using the 110 g ball

	Mass retained (g)															
Sieve size (mm)	Test 49	Test 50	Test 51	Test 52	Test 53	Test 54	Test 55	Test 56	Test 57	Test 58	Test 59	Test 60	Test 61	Test 62	Test 63	Test 64
8.0	0.00	0.00	0.00	0.00	0.00	0.00	0.00	0.00	0.00	0.00	0.00	0.00	0.00	0.00	0.00	0.00
5.6	1.30	3.40	8.74	11.54	1.27	4.71	7.76	8.36	1.31	2.04	7.73	10.77	0.82	4.09	6.32	12.03
4.0	0.69	3.73	3.88	5.59	0.94	2.16	5.11	7.18	0.73	4.67	4.78	5.91	0.86	2.97	4.39	6.91
2.8	0.00	0.00	0.12	0.11	0.22	0.24	0.18	0.37	0.35	0.31	0.00	0.20	0.42	0.60	1.04	0.28
2.0	0.00	0.00	0.00	0.00	0.09	0.03	0.00	0.00	0.06	0.00	0.00	0.00	0.13	0.00	0.00	0.00
1.4	0.00	0.00	0.00	0.00	0.09	0.05	0.00	0.04	0.00	0.06	0.00	0.03	0.02	0.04	0.00	0.04
Pan	0.00	0.00	0.02	0.00	0.16	0.03	0.00	0.04	0.04	0.01	0.02	0.06	0.20	0.20	0.10	0.02
Total mass (g)	1.99	7.13	12.76	17.24	2.77	7.22	13.05	15.99	2.49	7.09	12.53	16.97	2.45	7.90	11.85	19.28

Particle size distributions for Repeat 1 of tests conducted on UG2 using the 110 g ball

	Mass retained (g)															
Sieve size (mm)	Test 49 R1	Test 50 R1	Test 51 R1	Test 52 R1	Test 53 R1	Test 54 R1	Test 55 R1	Test 56 R1	Test 57 R1	Test 58 R1	Test 59 R1	Test 60 R1	Test 61 R1	Test 62 R1	Test 63 R1	Test 64 R1
8.0	0.00	0.00	0.00	0.00	0.00	0.00	0.00	0.00	0.00	0.00	0.00	0.00	0.00	0.00	0.00	0.00
5.6	0.22	1.56	3.20	8.78	0.98	2.55	3.30	8.18	0.00	1.08	2.85	3.82	0.00	1.39	1.83	3.53
4.0	0.33	3.90	5.23	7.79	0.00	4.13	7.13	7.59	1.38	4.84	5.85	11.35	1.08	2.97	5.48	7.54
2.8	0.63	0.63	2.88	0.78	0.64	1.20	1.09	1.29	0.52	1.06	2.93	0.98	0.58	1.79	2.81	4.08
2.0	0.16	0.23	0.06	0.05	0.20	0.09	0.08	0.00	0.04	0.15	0.06	0.06	0.05	0.20	0.06	0.02
1.4	0.19	0.18	0.04	0.07	0.09	0.03	0.00	0.00	0.00	0.07	0.04	0.02	0.07	0.17	0.05	0.06
Pan	0.79	0.41	0.19	0.15	0.32	0.11	0.03	0.06	0.16	0.24	0.19	0.08	0.16	0.39	0.09	0.10
Total mass (g)	2.32	6.91	11.60	17.62	2.23	8.11	11.63	17.12	2.10	7.44	11.92	16.31	1.94	6.91	10.32	15.33

Note: ‘R1’ refers to Repeat 1

Particle size distributions for Repeat 2 of tests conducted on UG2 using the 110 g ball

	Mass retained (g)															
Sieve size (mm)	Test 49 R2	Test 50 R2	Test 51 R2	Test 52 R2	Test 53 R2	Test 54 R2	Test 55 R2	Test 56 R2	Test 57 R2	Test 58 R2	Test 59 R2	Test 60 R2	Test 61 R2	Test 62 R2	Test 63 R2	Test 64 R2
8.0	0.00	0.00	0.00	0.00	0.00	0.00	0.00	0.00	0.00	0.00	0.00	0.00	0.00	0.00	0.00	0.00
5.6	0.00	1.61	3.90	6.82	1.10	0.80	5.56	7.47	0.88	0.45	1.93	8.73	0.22	1.37	3.43	6.76
4.0	0.72	3.08	5.21	9.29	0.64	5.42	5.08	8.76	0.00	4.22	7.13	7.69	0.33	5.18	5.90	6.63
2.8	0.61	1.04	2.73	0.75	0.00	0.99	1.51	0.24	0.51	1.22	1.90	0.78	0.53	0.56	0.30	2.44
2.0	0.14	0.30	0.06	0.00	0.00	0.23	0.02	0.04	0.20	0.32	0.02	0.05	0.16	0.06	0.03	0.05
1.4	0.06	0.07	0.04	0.00	0.00	0.00	0.03	0.03	0.09	0.16	0.04	0.07	0.19	0.06	0.05	0.04
Pan	0.41	0.36	0.19	0.03	0.00	0.19	0.01	0.08	0.32	0.37	0.07	0.12	0.78	0.29	0.09	0.02
Total mass (g)	1.94	6.46	12.13	16.89	1.74	7.63	12.21	16.62	2.00	6.74	11.09	17.44	2.21	7.52	9.80	15.94

Note: ‘R2’ refers to Repeat 2